Energy performance analysis through the ongoing commissioning of houses in northern Canada

Behrad Bezyan

A Thesis

In the Department

Of

Building, Civil and Environmental Engineering

Presented in Partial Fulfilment of the Requirements

for the Degree of

Master of Applied Science (Building Engineering) at

Concordia University

Montreal, Quebec, Canada

April 2018

CONCORDIA UNIVERSITY

School of Graduate Studies

This is to certify that the thesis prepared

By: Behrad Bezyan

Entitled: Energy performance analysis through the ongoing commissioning of houses in northern Canada

and submitted in partial fulfillment of the requirements for the degree of

Master of Applied Science (Building Engineering)

complies with the regulations of the University and meets the accepted standards with respect to originality and quality.

Signed by the final Examining Committee:

————————————————— Chair, Examiner
Dr. A. Athienitis

————————————————— Examiner
Dr. F. Haghighat

————————————————— External Examiner
Dr. R. Sedaghati

————————————————— Supervisor
Dr. R. Zmeureanu

Approved by _____
Chair of Department of Graduate Program Director

April 10th, 2018   _____
Dean of Faculty

ABSTRACT

Energy performance analysis through the ongoing commissioning of houses in northern Canada

Behrad Bezyan

Ongoing commissioning of buildings is used for the analysis the energy performance and operation of the heating ventilating and air conditioning (HVAC) systems, based on the measurements of physical variables in an existing building. Prediction of heating energy demand, detection of abnormal energy performance and operation conditions, identifications of variables that affect the normal operation and performance are the goals of ongoing commissioning of buildings, as covered in this thesis.

This thesis proposes the development of benchmarking models to be used for the ongoing commissioning of the energy performance of heating system in two semi-detached houses of Inuvik, NWT, Canada. The scope is the comparison of the recorded measurements with the benchmarking models` predictions to detect changes in the energy performance. This is the first step in the ongoing commissioning, which is normally followed up by the identification of causes of such a change. This study compares the quality of predictions when the benchmarking model uses the static and augmented window techniques for retraining. On the average, over a longer prediction time interval, the measurements of total heating energy demand are close with the predictions of the benchmarking model that uses the static window technique. When the benchmarking models are retrained by using the augmented window technique, their predictions are useful for the comparison with measurements over shorter time intervals. The comparison between measurements and predictions as well as the analysis of information extracted from the

daily signature of heating energy demand reveal more significant changes in the operation of heating system of house A compared with house B.

Another section of this thesis presents the application of the Principal Component Analysis (PCA) for the definition of the threshold of normal operation of the heating system in two houses, the detection of outliers in the PC-based space of the heating system operation, and the identification of those system variables which are the source of outliers. This case study uses measurements collected in December 2014 as the training data set, which is then applied to measurements of February 2015 as the application data set. The temperature of supply and return water temperature for heating one house are the major sources of outliers identified from data of February 2015. The identification by the PCA of variables with abnormal values is validated by using of a modified data set.

ACKNOWLEDGEMENTS

TABLE OF CONTENTS

LIST OF FIGURES

LIST OF TABLES

LIST OF ACRONYMS

Name	Definition
ANN	Artificial Neural Network
BAS	Building Automation System
CPR	Change-Point Regression
CV(RMSE)	Coefficient of Variance of Root-Mean-Square-Error
DHW	Domestic Hot Water
FDD	Fault Detection and Diagnosis
GMR	Gaussian Mixture Regression
GPR	Gaussian Process Regression
HVAC	Heating, Ventilating and Air Conditioning
IDUs	Indoor Units
PC	Principle Component
PCA	Principal Component Analysis
RMSE	Root-Mean-Square-Error
SPM	Statistical Process Monitoring
VRF	Variable Refrigerant Flow

NOMENCLATURE

$\hat{y}_i$	The predicted value	-
F_{tr}	The projection of original measurements in the PC-based space, called scores	-
$X_{j,tr}$	The j-column of the original training data set	-
$X_{j.ap}$	The j-column of the new data set	-
f_{ij}	the score of the i-observation along the j-principal direction	-
sx_j	$2.\sigma_{j,tr}$	-
sx_j	The ellipsoid semi-axis along the j-principal direction	-
x_C	The coordinates of the projection of outlier S on the zero-value axis of variable	-
x_P	The coordinates of point P from the Q matrix	-
x_S	The coordinates of the outlier S in the PC#1 - PC#2 space	-
y_C	The coordinates of the projection of outlier S on the zero-value axis of variable	-
y_P	The coordinates of point P from the Q matrix	-
y_S	The coordinates of the outlier S in the PC#1 - PC#2 space	-
y_i	The measured value	-
$zX_{j,tr}$	The j-column of the normalized training data set	-
$zX_{j.ap}$	The j-column of the normalized application data set	-

$\mu_{j,tr}$	The average value of the j-column of the original training data set	-
$\sigma_{j,tr}$	The standard deviation of the j-column of the original training data	-
a	The slope of the weather-dependent energy demand	MJ/(m² ºC)
b	The intersect of the non-weather dependent energy demand	MJ/(m²)
BIN(T$_o$)	The number of days of occurrence of the outdoor air temperature bin having T_O as centre	-
c	The specific heat of water (4.18)	kJ/kg·ºC
E	Energy demand	MJ/(m²)
E$_P$	The predicted total energy demand based on the benchmarking model	MJ/(m²)
F_{hA}	Water flow rate for space heating (House A)	L/min
F_{hB}	Water flow rate for space heating (House B)	L/min
F$_{wA}$	Water flow rate for DHW (House A)	L/min
F$_{wA}$	Water flow rate for DHW (House B)	L/min
ṁ$_{DHW}$	Domestic hot water flow rate	kg/min
ṁ$_H$	The heating water flow rate	kg/min
Q	The matrix of coefficients	-
Q $_{DHW}$	The heat flow rate of domestic hot water	kJ
Q $_{solar\ hot\ water}$	Heat flow rate added to the pre-heating DHW tank by the solar loop	kJ
Q $_{space\ heating\ demand}$	The heat flow rate of space heating demand	kJ

Q_h	The matrix of coefficients for space heating	-
Q_w	The matrix of coefficients for Domestic Hot Water	-
R^2	Coefficient of determination	-
T_1	The air temperature that enters the heat recovery ventilator; in the absence of pre-heating process $T_1 = T_O$ (outdoor air temperature)	°C
T_2	The supply air temperature leaving heat recovery ventilator and entering the space (°C)	°C
T_3	the exhaust air temperature leaving the space and entering the heat recovery ventilator (°C)	°C
T_4	Supply water temperature from the boiler	°C
T_5	Return water temperature to the boiler	°C
T_6	The cold-water temperature from the city main	°C
T_7	The pre-heated domestic water temperature in pre-heating water tank	
T_8	The heated domestic water temperature from storage water tank to houses A and B	°C
T_o	The daily average outdoor temperature	°C
$T_{returnA}$	Return water temperature for space heating (House A)	°C
$T_{returnB}$	Return water temperature for space heating (House B)	°C
$T_{supplyA}$	Supply water temperature for space heating (House A)	°C
$T_{supplyB}$	Supply water temperature for space heating (House B)	°C
$T_{w\_returnA}$	Return water temperature for DHW (House A)	°C

$T_{w\_returnB}$	Return water temperature for DHW (House B)	ºC
$T_{w\_supplyA}$	Supply water temperature for DHW (House A)	ºC
$T_{w\_supplyB}$	Supply water temperature for DHW (House B)	ºC
ε	The sensible thermal effectiveness of the heat recovery ventilator (HRV)	-
ȳ	The average measured values	-
SC	The Euclidean distance	-

1. INTRODUCTION

Energy performance analysis of the buildings is an important issue for monitoring energy use and identifications of the malfunctions in the system.

For analysis the energy performance of the buildings, two approaches are commonly used; (1) forward modeling, and (2) inverse modeling. Forward modeling is simulation and can be conducted by various software, and inverse modeling is data mining, which monitored values within a period of time are deployed for analysis.

Energy performance analysis of the ongoing commissioning houses in this study is conducted using data inverse modeling. This study presents the analysis of energy performance of two units of a semi-detached houses located in Inuvik, Northwest Territories, Canada, from the measurements carried out from October 1, 2014 to September 30, 2015. Measurements at one-minute time interval of the water and air temperatures, the water and air flow rates, and the monthly natural-gas usage were available from the Arctic Energy Alliance. The outdoor air temperatures were obtained from Environment Canada at 60 minutes time interval.

The analysis is based only on the available measurements, without any additional inquiries or short-term measurements about the change in people's energy-related behavior, the change in controls of heating and ventilation systems, or the integrity and accuracy of monitoring system.

The remarkable scopes of analysis of the monitored data are; (1) development of benchmarking models using linear regression for prediction of heating energy demand, and (2) detection of variables which are the major sources of outliers, with application of PCA method.

Results are presented at different levels of time integration by using annual, monthly, daily and hourly values.

This thesis proposes an approach for using the measurements recorded in these two houses for the ongoing commissioning process that consists in the comparison of measured data with predictions from benchmarking models as discussed in section 5. As an example, the daily signatures of space heating energy demand for houses A and B are developed using data in December 2014. Over the time period of January 1 to March 31, 2015 the house A has 7.8% less daily space heating energy demand than the predicted daily values. On the contrary, the house B has 3.6% more daily space heating energy demand than the predicted daily values.

Another section of this thesis which is discussed in section 6 is application of Principal Component Analysis (PCA) method for outliers` detection and identification of the variables which are the main sources of outliers for space heating system. An ellipsoid threshold model in December 2014 is developed and it is applied in another data set in order to detect the outliers and variables in the data set. It was concluded that, supply and return temperature of water for space heating for house B, are the main sources of outliers in application data set (February 2015).

2. LITERATURE REVIEW

Building sector is one of the principle source of energy consumption, approximately 30% of the total energy use of the world according to the key world statistics of 2017 [1]. Therefore, it is really important to analyze the energy performance of the buildings in order to save a great deal of energy and make them more efficient, and furthermore, schedule a suitable maintenance plan for equipment of the heating, ventilating and air conditioning (HVAC) systems.

Energy performance analysis of the buildings are introduced in two approaches: (1) Forward modeling, and (2) Inverse modeling. Simulation using various simulation programs, such as e-QUEST [2], EnergyPlus [3], TRNSYS [4] etc. is forward modeling. In forward modeling, description characteristics of the building, such as geometry, roof, walls and windows specifications, spec of the HVAC system equipment and etc. are defined in the simulation program. Inverse modeling is analysis of energy performance of the building on the basis of monitored historical data, such as energy consumption of building and climatic data, such as outdoor air temperature. Energy signature and energy benchmarking models are the inverse modellings. In this thesis, inverse modeling using monitored values is studied.

2.1. Benchmarking models

The comparison of measurements in buildings and HVAC systems with the predictions of benchmarking models should be applied in all possible situations to detect deterioration of performance or unusual operation conditions. This comparison should be an integral part of the ongoing commissioning process. The benchmarking models can be developed from the measurements of existing systems in operation by using inverse or data driven models such as the black box or gray box. These models are easy to develop, train and retrain if sufficient data of good

quality are available, and then to apply for the prediction of target variables of interest [5]. Every building has a unique benchmarking model, and it cannot be applied for evaluation of the energy performance of other buildings [6].

The systematic development of whole-building energy performance models as benchmarking model was conducted for the building retrofitting [7]. Application of fuzzy linear regression technique in developing benchmarking models was proposed in [8]. The accuracy of predictions is decreased if the benchmarking models are used over the period with different weather conditions from training and testing data sets [9]. A benchmarking model was used for the ongoing commissioning of the refrigeration system of an indoor ice rink [10]. Multivariate linear regression analysis with principle component analysis to consider the multicollinearity risk with high dimensional dataset was applied for developing a benchmarking model in [11]. A benchmarking model was developed for heat recovery unit in a central plant [12].

Fumo and Biswas [13] concluded that simple and multiple linear regression models for the prediction of energy consumption of single family houses, by using hourly or daily data, are preferred compared to other statistical models. Multilinear regression models were used for the development of benchmarking models for the heating and cooling energy consumption of residential and commercial buildings [14-18]. The comparison of models` predictions with measurements indicated acceptable difference [19-21].

Liu et al. [22] proposed the development of a dynamic energy benchmarks for office buildings with limited data available. Zhang et al. [23] studied various benchmarking models for prediction of hot water energy consumption in office building, by using the change-point regression model (CPR), the Gaussian process regression model (GPR), the Gaussian mixture

regression model (GMR), and the Artificial Neural Network model (ANN) with hourly and daily data.

Abushakra and Paulus [24-26] concluded that hourly monitored data of two weeks in swinging season is sufficient for developing a benchmarking model of whole building energy use. The model predictions might become poorer if more data from extreme climate are added. Optimum length of the observation period, time or season of the observation, required variables and the technique which is effective and acceptable for the user, should be considered in order to predict long term energy use based on the short-term measurements.

In this study, the benchmarking models of daily space heating energy demand of two semi-detached houses of Inuvik, NWT, Canada, are developed by using the measurements of December 2014, as the reference or initial training data set. The benchmarking models are the employed for the prediction of daily heating demand over the next three months from January 1 to March 31, 2015. This study compares the quality of predictions of two retraining techniques, the static window and the augmented window. The difference between the predictions and measurements of the application time interval reveal changes in the heating energy demand.

Li et al. [5] presented a review regarding different methods which are used in benchmarking building energy consumption as presented in Table 2.1.

Table 2.1: Energy benchmarking models

Method		Input	Time resolution level	Application
Black box	Bin method	Day of the week, hour of the day, weather data	Multiple resolution	Fault detection
	Linear regression	Day type, weather data, historical data	Multiple resolution	Fault detection, load prediction
	Support vector regression	Weather data	Multiple resolution	Prediction of cooling load, monthly utility bill split
	Gaussian process regression	Weather data, other selected explanatory variables	Multiple resolution	Retrofit analysis, replacement of detailed simulation
	Artificial neural network	Weather data, time, DHW/heating system and equipment properties, energy consumption patterns, dwelling characteristics	Hourly	Prediction of cooling load, hot water heating load, space heating load, total energy consumption, fault detection
	Decision tree	Weather data, building type, ownership of electric appliance, building area	Annually	Electricity prediction, total energy prediction
Gray box	Bayesian network	Weather data, known parameters, prior distribution of unknown parameters, historical energy consumption data	Daily	Energy consumption estimation
	RC network	Weather data, historical energy consumption data	Hourly	Building heating/cooling load prediction, demand control
White box	Normative	Weather data, simplified building design parameters	Hourly, monthly	Energy source planning, energy policy analysis, retrofit analysis
	Idealized model based	Weather data, simplified building design parameters	Hourly	Energy consumption benchmark, optimal control
	Modified bin method	Weather data, simplified building design parameters	Hourly	Fault detection
	Detailed simulation	Weather data, simplified building design parameters	Sub-hourly	Monthly utility bill split, fault detection, retrofit analysis, load prediction

In this study, simple linear regression technique from black box method for developing the benchmarking models with application of static and augmented window methods are deployed for analysis of daily heating energy demand of semi-detached houses, located in Inuvik, NWT. Predicted values which are acquired by trained models in the benchmarking models are compared with the actual measurements in the prediction data sets and the accuracies of the models are

evaluated with Coefficient of determination (R^2), application of Root-mean-square-error (RMSE) and coefficient of variance for root-mean-square-error CV(RMSE).

Coefficient of determination (R^2) is a measure for presentation the correlation of two variables to each other and evaluate the benchmarking model with using Equation 2.1 from reference [27]. Root-mean-square-error (RMSE) which quantifies the typical size of errors in prediction, and Coefficient of variance of the root-mean-square-error (CV(RMSE)) are the other parameters which are used in order to evaluate the quality of the fitting and prediction accuracy versus real measurements and calculated with Equations 2.2 and 2.3 from reference [27].

$$R^2 = \left[1 - \frac{\sum_{i=1}^{n}(y_i - \hat{y}_i)^2}{\sum_{i=1}^{n}(y_i - \bar{y}_i)^2}\right] \cdot 100 \qquad\qquad 2.1$$

$$RMSE = \sqrt{\frac{\sum_{i=1}^{n}(\hat{y}_i - y_i)^2}{n-1}} \qquad\qquad 2.2$$

$$CV\,(RMSE) = \frac{\sqrt{\frac{\sum_{i=1}^{n}(\hat{y}_i - y_i)^2}{n-1}}}{\bar{y}} \cdot 100 \qquad\qquad 2.3$$

where: y_i = the measured value

             $\hat{y}_i$ = the predicted value

             $\bar{y}_i$ = the average measured values

             n = the number of data which are used for the development of the benchmarking model

R^2 value varies between 0 and 100%. If R^2 is zero, the variation of the variables has no impact on the predicted variables. If R^2 is 100%, the model explains that, variation in variable has the highest impact on the predictions. R^2 bigger that 75% has an acceptable relationship between energy demand and considered variable [9].

According to [28], the model predictions of the whole building energy consumption, when using hourly data, is acceptable if CV(RMSE) is less than 30%; and the model using monthly data is acceptable if CV(RMSE) is between 5 to 15%. Since the ASHRAE guideline 14 does not specify the acceptance criterion for the models using daily data, the maximum value of CV(RMSE) of 30% is used in this study.

2.2. Energy signature

Energy signature is a graphical linear regression method which presents the actual energy performance of the building which is correlated with climatic variables [29-33]. Energy signature is used for comparison of actual consumption of a building with other results such as predictions or consumptions previous years, in order to compare the energy consumption calculations with actual performance. Also, it can be used as a pre-energy audit to remark the malfunctions or problems in energy consumption, which can be a suitable method for the customer awareness. Energy signature is made on a Cartesian plane, which x-axis represents external climatic parameter and y-axis presents energy performance. The weather-dependent energy signature is shown in Equation 2.4;

$$E = a \cdot T_O + b \qquad\qquad 2.4$$

where: $E =$ is the energy use (demand) in MJ/m^2 or kWh/m^2 per unit or time, which can be per month, day or hour

$a =$ the slope, in MJ/m^2 or kWh/m^2 per unit of temperature

$T_O =$ the average outdoor temperature in ${}^\circ C$

$b =$ the intersect in MJ/m^2 or kWh/m^2

There are three energy signature curves: (1) real energy signature, (2) design energy signature, (3) energy signature by law [31]. Real energy signature presents the real measured consumption or building energy performance over a period of time, and it is a linear regression of data, which, energy consumption is increased when outdoor air temperature is dropped. Analysis of energy consumption via energy signature, provides a determination of a design reference curve which is named design energy signature. As a case in point weekly data is compared with the developed curve to detect abnormal performances. Another proposed type of energy signature is called energy signature by law. If the building has a good thermal insulation, energy signature slope presents that, lower slope has lower heat loss. Belussi et al. [31] discussed that, with comparison of real energy signature with energy signature by law, energy consumption reduction regarding thermal resistance is compiled law. Moreover, the potential of enhancing houses envelop for energy consumption reduction, and cost effectiveness is determined via this comparison.

A building energy performance is provided via comparison of design energy signature and real energy signature. If these two curves overlap, it shows that building performance meets the design stage analysis, and if they do not overlap and they have two different slopes, it is concluded that energy performance of the building varies from the design model. So, in this case, real energy signature will provide some signs of the reason for abnormal energy performance of heating system. Also, based on energy signature slope and heat transfer coefficient, response of the building envelop to climate change can be detected [34].

According to the energy signature, space heating energy consumption is increased as outdoor air temperature is dropped below a balance-point temperature. Heating balance-point temperature is a temperature at which, the heat is gained from internal occupants and equipment balance heat loss through the building envelope. Therefore, except the energy consumption for hot

water, no space heating is needed when outdoor air temperature is higher than balance-point temperature [35].

2.3. Principal component analysis (PCA)-based method

Building commissioning is a process of measuring and evaluation of the energy performance of a building and HVAC system with respect to the design intent and standard performance [36]. Katipamula and Brambley [37] showed that 15% to 30% of the energy use in buildings is wasted due to the degradation of HVAC equipment, unsuitable scheduled maintenance and systems control. A high proportion of the energy waste can be avoided with proper maintenance by using automated fault detection and diagnosis (FDD). Several studies focused on the FDD of HVAC equipment by using different data driven models [38]. One practical problem related to the use of accurate and time-efficient FDD techniques comes from the large number of measurements of several variables over extended intervals of time, many of those variables being correlated.

Principal Component Analysis (PCA) method is a multivariate technique, used in other fields [39, 40], that can mitigate this problem by transforming the original data set of j inter-correlated variables into a smaller data set of k independent new variables, where k < j, known as Principal Components (PCs).

The literature review of [6], which used PCA for FDDs applications, is expanded with the papers presented in this study. Xu et al. [41] concluded that the PCA gives useful residuals for sensor-fault detection, diagnosis, and estimation. However, the conventional PCA-based strategy that directly employs raw measurements is less efficient because of noises and dynamics embodied in the data, than the proposed strategy using wavelet analysis and PCA.

Hu et al. [42] developed a self-Adaptive Principal Component Analysis (APCA) method that can remove erroneous temperature measurements with absolute magnitude less than 1ºC, which increases the efficiency of fault detection.

Cotrufo and Zmeureanu [43] proposed the use of PCA method for the fault detection of sensors and degradation in equipment performance of a system.

Gajjar et al. [44] recognized that the PCA was widely used for process fault detection, however, the interpretation of the principal components (PCs) is a challenging task since each PC is a linear combination of the original variables. They applied the sparse-PCA by restricting some PC loadings to zero, which results in a clearer interpretation of results.

Beghi et al. [45] used the PCA to identify anomalies from normal operation variability and isolated variables related to faults, without having any prior knowledge about abnormal measurements. They used Statistical Process Monitoring (SPM) approach to monitor the behavior of the system, and a simple diagnosis table, based on experts' diagnosis rules, to identify the shifts from the nominal working conditions.

Hu et al. [46] estimated the undetectable boundary of each sensor assigned in PCA model, and the fault detection efficiency of eight sensors installed in a chiller, for different severe levels of faults. Hu et al. [47] started from the observation that the results of any data-driven method are highly dependent on the quality of the training data. They developed a statistical training data cleaning strategy for PCA-based for FDD & Reconstruction method for chiller sensors. The method called SPCA uses the Euclidean distance to find out outliers in the measurement data set.

Guo et al. [48] developed an enhanced sensor fault detection and diagnosis method for the variable refrigerant flow (VRF) system based on Savitzky-Golay (SG) method of the PCA. The SG method is used for data smoothing. They concluded that the SG-PCA method is efficient and

reliable for FDD under large fluctuations in the VRF operation. Guo et al. [49] proposed a modularized PCA method for FDD of the VRF system with different numbers of indoor units (IDUs), and which identifies which IDU is faulty.

The previous studies concluded that different PCA-based methods can detect faulty measurements or performance degradation of the HVAC system. The identification of faulty sensors, however, still requires additional research.

This study expands the approach of Cotrufo and Zmeureanu [43] for the use of PCA-based method for the identifications of the variables which cause the abnormal performance of space heating. The case study uses measurements of two houses, recently built in Inuvik, NWT, Canada. In the context of this paper, the term "abnormal performance" is not limited to faults; it might be the result of changes of the operation conditions.

3. DATA/INFORMATION PROVIDED BY THE ARCTIC ENERGY ALLIANCE

This study presents the energy performance of two units of the Northern Sustainable Housing (NSH), House A and House B, located on Reliance Street, Inuvik, NWT, Canada. Inuvik is situated at 68.3°N latitude. The detailed description is available in [50]:

The design thermal resistances of houses A and B are presented in Table 3.1, and exceeds the minimum requirement of the Model National Energy Code of Canada for Houses (MNECH-1997) [51]. Thermal resistance of exterior walls in these houses is 8.1 m^2K/W compared with 4.75 m^2K/W in MNECH, 14.1 m^2K/W for roof compared with 10.6 m^2K/W in MNECH and 9.3 m^2K/W for floor compared with 8.1 m^2K/W in MNECH. The air infiltration rate at 50 Pa pressure difference is about 50% of the maximum value of 4.55 ACH required by MNECH.

Two houses are supported by space frame foundations which are proved to work well in permafrost conditions. Therefore, the floors are exposed to the outdoor air.

Table 3.1: Design thermal resistance (m^2K/W) of house envelope

Component	Inuvik house	MNECH (1997) [51]
Exterior walls	8.1	4.75
Roof	14.1	10.6
Floor	9.3	8.1
Windows	0.97 (rear windows); 2 % of window-wall ratio (WWR) 0.74 (front windows); 5.6 % of WWR	-
Doors	0.98	-

Figure 3.1 shows the schematic configuration of the total HVAC system of houses A and B. There is One gas-fired high efficiency condensing boiler of 141,000 Btu/h (41.3 kW), with a manufacturer rated AFUE efficiency of 96%, serves both houses A and B. The hot water is

supposed to be used for space heating through radiators, the pre-heating of outdoor air before entering the Heat Recovery Ventilator (HRV), and for the domestic hot water. Each house has a separate ventilation system that is composed of a pre-heating coil and a Heat Recovery Ventilator (HRV). The HRV is ENERGY STAR® rated with an apparent sensible effectiveness of 0.83 at 0ºC and 0.89 at -25ºC.

Figure 3.1: Schematic configuration of the HVAC system

Two storage tanks connected in series are used for the preparation of the domestic hot water for both houses. The cold water from the city main enters first the pre-heating tank of 119 US gal (450 L), where the water is pre-heated by the solar energy captured by thermal solar collectors (four Enerworks TL glazed flat-plate of 11.5 m^2). The pre-heated water enters the main storage

tank, where the water is heated by the hot water from the boiler. The cold water can also enter directly the main storage tank.

The simulation with RETScreen predicted that two solar collectors per unit would save annual natural gas about 12.6 GJ per unit.

The electricity use on each circuit in the house was monitored by Site Sages (formerly emonitor).

Electricity is used for appliances, lights, plugs, fans of heat recovery ventilator, pump for heating system and furnace of hot water ant etc.

Each house has eight 224 W Sharp photovoltaic modules oriented 35º east of south, installed on the roof at 75º tilt angle, for a total nameplate of 1,792 W per house. The photovoltaic panels are monitored using the Sunnyportal website. The electricity generated by the PV panels is supposed to be first used by loads within the house, and the excess generation sent into the grid.

Measurements recorded in these two houses at 1-min time interval were made available to the authors for the processing and analysis of energy performance. The thermal energy demand for space heating and domestic hot water are calculated by using measurements from the temperature sensors and the water flow meters (Appendix A). The heat recovered through the Heat Recovery Ventilators is calculated by using the temperature sensors and air flow meters. The outdoor air temperature recorded at 1-hour time interval were obtained from Environment Canada's weather file (climate.weather.gc.ca). The monthly recorded natural gas use was also available.

From the measurements recorded at 1-min time over one year, from October 1, 2014 to September 30, 2015, the hourly, daily, monthly and annual values of the variables of interest are calculated, analyzed and presented in the thesis.

The preliminary analysis of measurements revealed:

1. Missing data, and erroneous data from the pre-heating coils and the heat recovery ventilator of unit A. The HRV of house A was mostly unused, for the purpose of assessing the difference in energy usage between one house with HRV (house B) and one without HRV (house A).

2. The solar energy was captured in the pre-heating tank, which increased the water temperature by a few degrees only. However, the pre-heated water was not transferred to the main domestic hot water tank. That storage tank heated the cold water from the city main up to the desired domestic hot water temperature by using the hot water loop from the boiler.

4. ANALYSIS OF MEASUREMENTS

4.1. Annual energy demand, use and production

The analysis is based on measurements from October 1, 2014 to September 30, 2015. The formulas used for the calculation of energy demand for space heating and domestic hot water, and of heat recovered from the solar loop are presented in Equations 4.1, 4.2 and 4.3.

$$Q_{\text{space heating demand}} = \Sigma\ \dot{m}_H \cdot c \cdot (T_4 - T_5) \qquad\qquad\qquad 4.1$$

where: Q = the heat flow rate of space heating demand (kJ)

$\dot{m}_H$ = the heating water flow rate (kg/min)

c = the specific heat of water (kJ/kg·°C)

T_4 = supply water temperature from the boiler (°C) (Figure 3.1)

T_5 = return water temperature to the boiler (°C) (Figure 3.1)

$$Q_{\text{DHW}} = \Sigma\ \dot{m}_{\text{DHW}} \cdot c \cdot (T_8 - T_6) \qquad\qquad\qquad 4.2$$

where: Q = the heat flow rate of domestic hot water (kJ)

$\dot{m}_{\text{DHW}}$ = domestic hot water flow rate (kg/min)

T_6 = the cold-water temperature from the city main (°C), since the pre-heated water is used in the DHW storage tank (Figure 3.1)

T_8 = the heated domestic water temperature from storage water tank to houses A and B (°C) (Figure 3.1)

$Q_{\text{solar hot water}} = \Sigma\ \dot{m}_{DHW} \cdot c \cdot (T_7 - T_6)$ <div align="right">*4.3*</div>

where: Q = heat flow rate added to the pre-heating DHW tank by the solar loop (kJ)

T_6 = the cold-water temperature from the city main to the pre-heating water tank (Figure 3.1)

T_7 = the pre-heated domestic water temperature in pre-heating water tank (Figure 3.1)

The houses A and B have almost the same annual heating energy demand that must be delivered by the boiler: 98.1 kWh/(m^2 year) for house A, and 101.7 kWh/(m^2 year) for house B (Table 4.1); for a difference of about 3.7%. The total heating energy demand of these two houses is 99.9 kWh/(m^2 year), where the floor area corresponds to both houses. Since the energy demand of pre-heating coils is zero, the heating energy demand corresponds only to the space heating by radiators.

The total energy demand for space heating and domestic hot water is 122.4 kWh/(m^2 year), with the space heating energy demand representing 81.6% of the total.

The annual measured natural gas energy use, for both heating the space and domestic hot water, is 178.2 kWh/(m^2 year). By assuming the ratio of 81.6% (calculated above for the space heating energy demand), the gas energy use for heating is estimated at 0.816·178.2 = 145.5 kWh/(m^2 year). The annual average thermal efficiency of the gas-fired boiler is estimated as 122.4/178.2 = 0.69.

The electricity use in house A (81 kWh/(m^2 year)) is 2.7 higher than in house B (30 kWh/(m^2 year)), for the total of 101 kWh/(m^2 year) for both houses A and B. That difference might be due to the difference in people's energy-related behavior in those two houses.

Total annual electricity produced by the PV panels of 10.5 kWh/(m^2 year) is 19% of the annual electricity us of 55.5 kWh/(m^2 year) (Table 4.1).

Total annual solar hot water production of 1.7 kWh/(m^2 year) is negligible (7.5%) compared with the annual domestic hot water energy demand of 22.6 kWh/(m^2 year).

Table 4.1: Annual energy demand, use, and production of the two houses A and B

	Unit	House A	House B	Houses A+B[1]
Thermal energy demand				
Heating energy demand	MJ/m^2 year (kWh/m^2 year)	353 (98.1)	366 (101.7)	360 (99.9)
Domestic hot water energy demand	MJ/m^2 year (kWh/m^2 year)	70 (19.4)	93 (25.8)	82 (22.6)
Total energy demand: heating and domestic hot water	MJ/m^2 year (kWh/m^2 year)	423 (117.5)	459 (127.5)	441 (122.4)
Total natural gas energy use for space heating and DHW				
Natural gas energy use	MJ/m^2 year (kWh/m^2 year)	-		641.4 (178.2)
Electricity use				
Total electricity use	kWh/m^2 year	81	30	55.5
Total energy use: natural gas and electricity				
Total energy use	kWh/m^2 year			233.7
Electricity and thermal energy production				
Total photovoltaic (PV) production	kWh/m^2 year	10	11	10.5
Solar hot water production A+B	MJ/m^2 year (kWh/m^2 year)	-		6 (1.7)
Total energy production[1]	MJ/m^2 year (kWh/m^2 year)	-		81.6 (12.2)

---

[1] The energy demand, use and production of each house is calculated with reference to floor area of each house; while the total energy demand, use and production of the two houses A and B is calculated with reference to the total floor area on those two houses.

4.2. Comparison between the measured annual energy demand and simulated energy demand

The annual measured gas energy use of 178.2 kWh/(m² year) exceeds the expected annual energy use of 121.7 kWh/(m² year), according to the simulation with HOT2000 program in [50].

The simulated value for annual electricity use is 67.1 kWh/(m² year) which exceeds the measured value of 55.5 kWh/(m² year). Such differences might come from differences between the as-built/as-operated house characteristics and the corresponding inputs in HOT2000 program. It is beyond the scope of this thesis to discuss the source of differences between the measured and simulated energy use.

However, it was noticed that the heating setpoint temperature input in the HOT2000 program was 21ºC, while the measured average indoor air temperature in the winter season (October to March) was 28ºC in house A and 24.6ºC in house B. Those significantly higher indoor air temperatures led to higher energy use for space heating.

4.3. Comparison with energy performance of other houses from publications

For comparison purposes, Table 4.2 shows that the two houses A and B in Inuvik with 9,769 HDD (ºC-day) that use 145.5 kWh/(m² year) of natural gas for space heating perform better than the two low-energy houses in Greenland with 8,276 HDD (ºC-day), which use 90 and 140 kWh/(m² year), respectively. Those two houses in Greenland are in a "warmer" weather, with about 1,000 HDD (ºC-day) lower than in Inuvik.

Table 4.3 shows that the two houses in Inuvik, with the measured space heating energy use of 145.5 kWh/(m² year), perform better than some houses at warmer locations and lower latitudes;

for instance #4 (Vienna), #8 (Warsaw), #10-12 (Toronto, Fredericton, Montreal), #15 (Oulu), #16-17 (Regina, Winnipeg).

Figure 4.1, shows the annual heating energy demand of Inuvik houses, the measured heating energy demand of passive and low-energy houses, and average heating energy use of conventional houses in different locations around the world versus heating degree days (HDD).

Table 4.2: Measured annual space heating energy use of passive and low-energy houses in cold climate regions

	Country	City	Year of measurement	HDD (ºC-day)	Latitude (ºN)	Space heating energy use kWh/m^2 yr (MJ/m^2 yr)	House type
1	Latvia	Riga [52]	2010	4,193	56.97	26 (93.6)	Passive
2	Norway	Oslo [52]	2010	4,344	59.9	18 (64.8)	Passive
3	Lithuania	Vilnius [52]	2010	4,361	54.63	25 (90)	Passive
4	Sweden	Stockholm [52]	2010	4,409	59.65	21 (75.6)	Passive
5	Finland	Hyvinkää [52]	2010	4,560	60.6	18 (64.8)	Passive
6	Estonia	Tallinn [52]	2010	4,649	59.47	25 (90)	Passive
7	Canada	Fredericton, New Brunswick [53]	2013	4,692	45.87	4.3 (15.48)	Passive
8	Norway	Tromso [52]	2010	5,567	69.68	38 (136.8)	Passive
9	Finland	Jyväskylä [52]	2010	5,621	62.4	38 (136.8)	Passive
10	Finland	Sodankylä [52]	2010	6,955	67.37	53 (190.8)	Passive
11	Greenland	Sismiut [54]	2010	8,276	66.92	90 (324)	Low-energy
12	Greenland	Sismiut [55]	2006	8,276	66.92	140 (504)	Low-energy
13	Finland	Tapanila [56]	2000	8,740	60.32	76 (273.6)	Low-energy
14	**Canada**	**Inuvik**	**2014-2015**	**9,769**	**68.3**	**145.5 (A+B)**	

Table 4.3: Average annual space heating energy use of houses in different regions

	Country	City	Year of measurement	HDD (ºC-day)	Lat (ºN)	Space heating energy use kWh/m² yr (MJ/m² yr)
1	Italy	Rome [57]	2004	1,525	41.8	86.7 (312.12)
2	Denmark	Karup [57]	2003	2,430	56.3	37.5 (135)
3	France	Bourges [57]	2004	2,550	47.06	130.5 (469.8)
4	Austria	Vienna [57]	2004	2,752	48.2	185.2 (666.72)
5	Canada	Vancouver [58]	2011	2,932	49.2	141.67 (510)
6	Germany	Kassel [57]	2003	3,070	51.4	150 (540)
7	UK	Newcastle [57]	-	3,244	55.04	100 (360)
8	Poland	Warsaw [57]	2004	3,539	51.1	190 (684)
9	Norway	Namsos [57]	2005	3,570	64.5	97.9 (352.44)
10	Canada	Toronto [58]	2011	4,108	43.86	147.2 (529.92)
11	Canada	Fredericton [58]	2011	4,692	45.87	155.6 (560.16)
12	Canada	Montreal [58]	2011	4,849	45.67	169.4 (609.84)
13	Sweden	Ostersund [57]	2003	5,050	63.2	37.5 (135)
14	Canada	Calgary [58]	2011	5,086	51.11	177.8 (640)
15	Finland	Oulu [57]	2005	5,130	65	176.5 (635.4)
16	Canada	Regina [58]	2011	5,707	50.43	163.9 (590)
17	Canada	Winnipeg [58]	2011	5,750	49.92	163.9 (590)
18	**Canada**	**Inuvik**	**2014-2015**	**9,769**	**68.3**	**145.5 (A+B)**
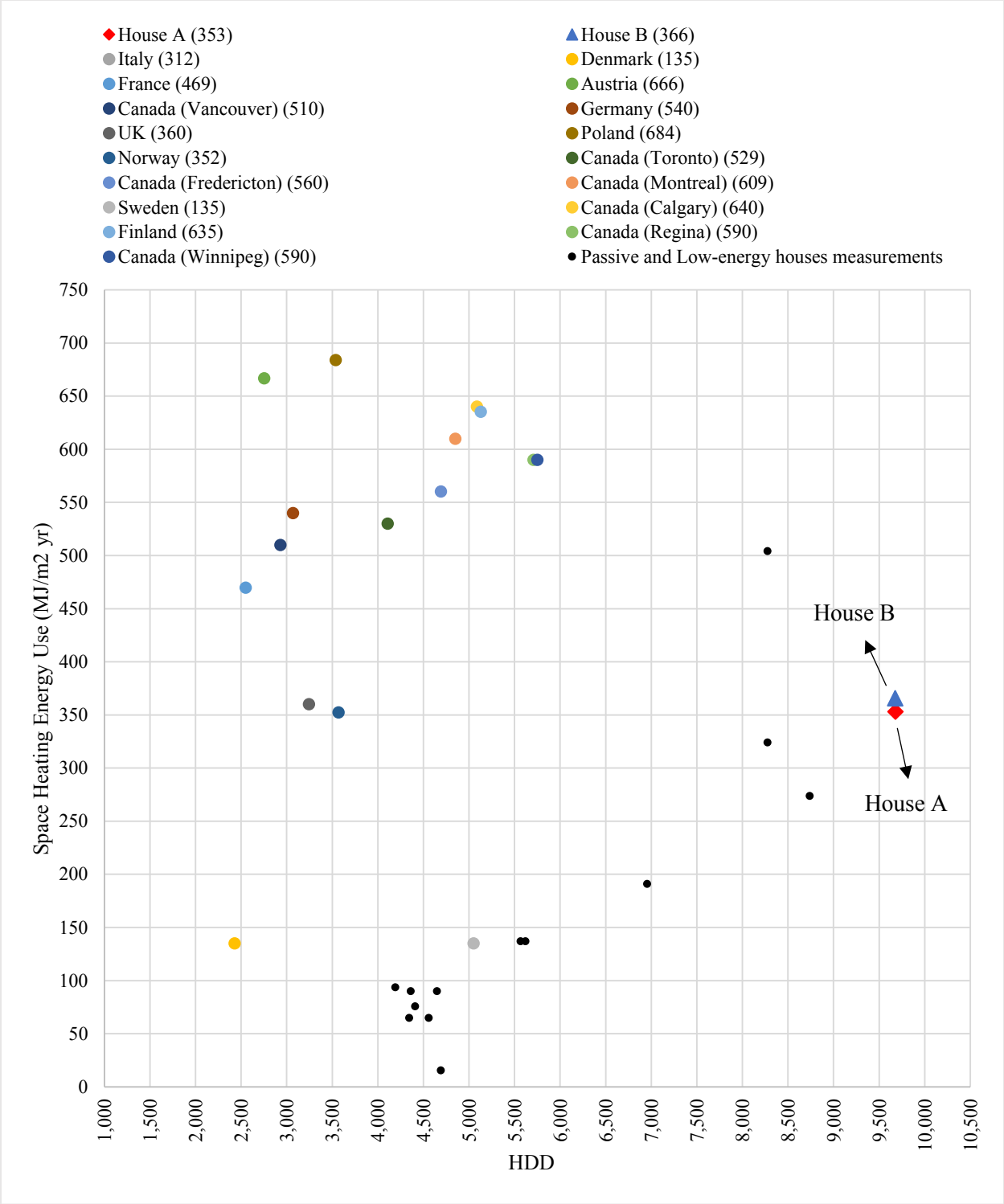
Figure 4.1: Comparison of measured space heating energy demand of Inuvik houses (A and B) with passive and low-energy houses measurements and average energy demand of houses in different locations around the world

4.4. Monthly energy demand, use and production

The monthly thermal efficiency of the gas-fired boiler varies between 0.77 in March 2015 and 0.43 in July 2015 (Table 4.4). The PV production of electricity is negligible in the winter months; it varies between 0 and 5% of the total electricity use between October 2014 and February 2015, and is about 7% in September 2015.

Table 4.4: Monthly energy demand, use, and productions in the two houses A and B from October 1, 2014 to September 30, 2015

Month	House	Heating demand	Hot water demand	Total energy demand: heating and hot water	Natural gas use	Boiler efficiency	Total electricity use	Total photovoltaic (PV) production A+B
		MJ/m² month	MJ/m² month	MJ/m² month	MJ/m² month	(-)	kWh/m² month	kWh/m² month
October 2014	A	25.58	6.88	37.5	56	0.67	10.8	0.4
	B	31.39	11.1					
November 2014	A	58.17	8.16	63.3	85.3	0.74	13.8	0
	B	52.34	7.88					
December 2014	A	55.14	6.42	62.5	94.3	0.66	14.7	0
	B	54.84	8.6					
January 2015	A	64.32	2.46	69.3	99.4	0.70	9.5	0
	B	64.67	7.14					
February 2015	A	46.06	5.63	57.4	91.0	0.63	10.5	0.5
	B	56.46	6.58					
March 2015	A	37.23	7.93	52.3	67.8	0.77	10.7	2.6
	B	46.57	12.91					
April 2015	A	25.25	6.83	34.4	45.3	0.76	5.5	4.2
	B	28.09	8.54					
May 2015	A	10.67	8.64	17.0	27.8	0.61	6.3	5.1
	B	6.41	8.25					
June 2015	A	3.53	3.95	8.2	13.1	0.63	13.9	3.6
	B	1.26	7.66					
July 2015	A	0.98	4.09	4.3	9.9	0.43	7.0	2.7
	B	0	3.5					
August 2015	A	5.76	4.37	10.4	17.6	0.59	7.6	1.6
	B	6.03	4.69					
September 2015	A	20.27	4.34	24.2	33.7	0.72	8.9	0.6
	B	17.61	6.08					

4.5. Monthly energy signature

The energy signature is commonly used to relate the energy demand with the outdoor air temperature as explained in section 2.2 (Equation 2.4):

$$E = a \cdot T_O + b$$

<div align="right">*2.4*</div>

where: E = energy demand in MJ/(m^2 month);

a = The slope of the weather-dependent energy demand, in MJ/(m^2 °C month)

b = The intersect in MJ/(m^2 month)

T_O = Monthly average outdoor temperature in °C.

The coefficients a and b are identified through the least-square method applied to the monthly data. The coefficient a represents the house effective heat loss through the envelope, including the air infiltration, and the efficiency of the heating system. The coefficient a indicates the sensitivity of the energy demand to the weather conditions, represented in this method by the outdoor air temperature. Higher is the coefficient a, higher is the sensitivity of the energy demand to the outdoor air temperature.

The slopes a of energy signatures of houses A and B are almost equal, i.e., 1.56 MJ/(m^2 month) for house A, and 1.72 MJ/(m^2 month), which indicate that the effectiveness of thermal envelopes, and of the heating systems of both houses are almost equal (Figure 4.2).

The intersects b of the two houses A and B are almost equal, i.e., 20.48 MJ/(m^2 month) and 20.66 MJ/(m^2 month), respectively, which indicates that at 0 ºC outdoor air temperature, the space heating energy demands of those houses are almost equal.

The intersection of the energy signature with the OX axis indicates the value of the reference temperature at which the heating system turns on. The monthly signature shows that in both houses A and B, the heating system starts when the outdoor air temperature is around 12-13ºC.
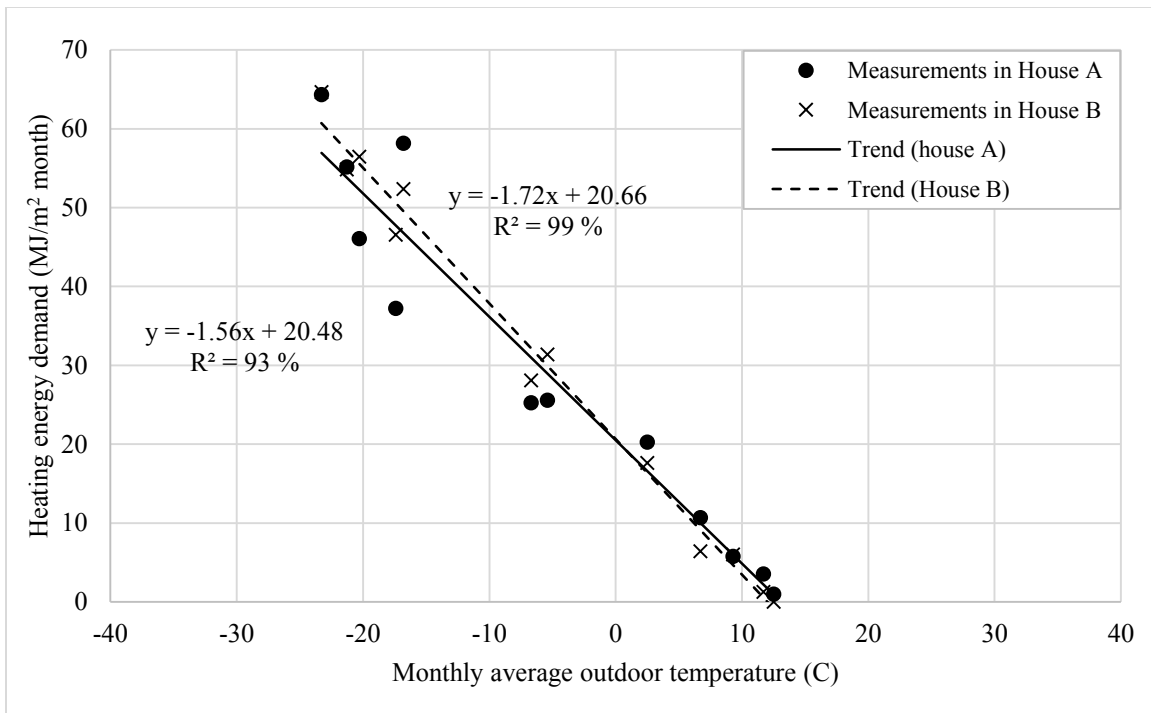
Figure 4.2: Monthly signature of space heating energy demand from October 2014 to September 2015

The monthly signature of energy demand for domestic hot water (Figure 4.3) revealed that the energy demand of house A is about three times less sensitive to the changes in outdoor air temperature than of the house B (a = 0.023 for house A versus 0.085 for house B). This could be due to the changes in the occupancy pattern (e.g., number of people, energy-related habits).
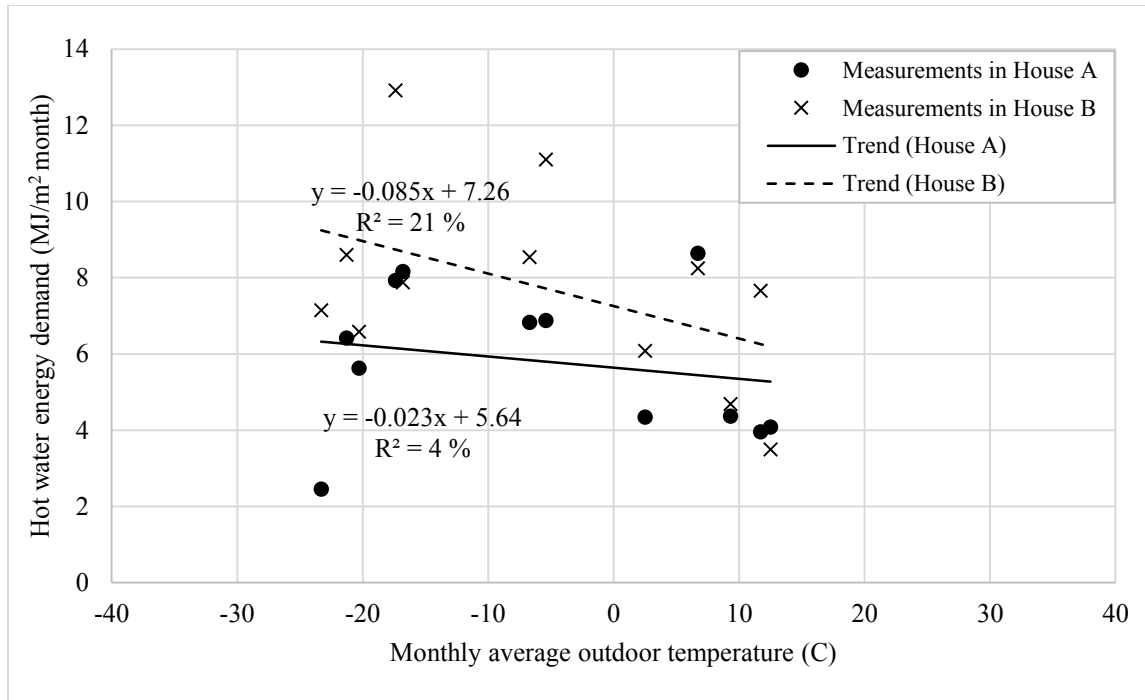
Figure 4.3: Monthly signature of domestic hot water energy demand from October 2014 to September 2015

The slopes a of the monthly electricity use signatures are almost equal, which indicates an almost equal variation with the decrease of outdoor air temperature (Figure 4.4). There is however a significant difference between the intersects b = 6.3 MJ/(m^2 month) for house A and 1.95 MJ/(m^2 month) for house B, which indicates a large difference in monthly electricity use, due to the people's energy-related habits. These results coincide with the difference in the annual electricity use (Table 4.1).
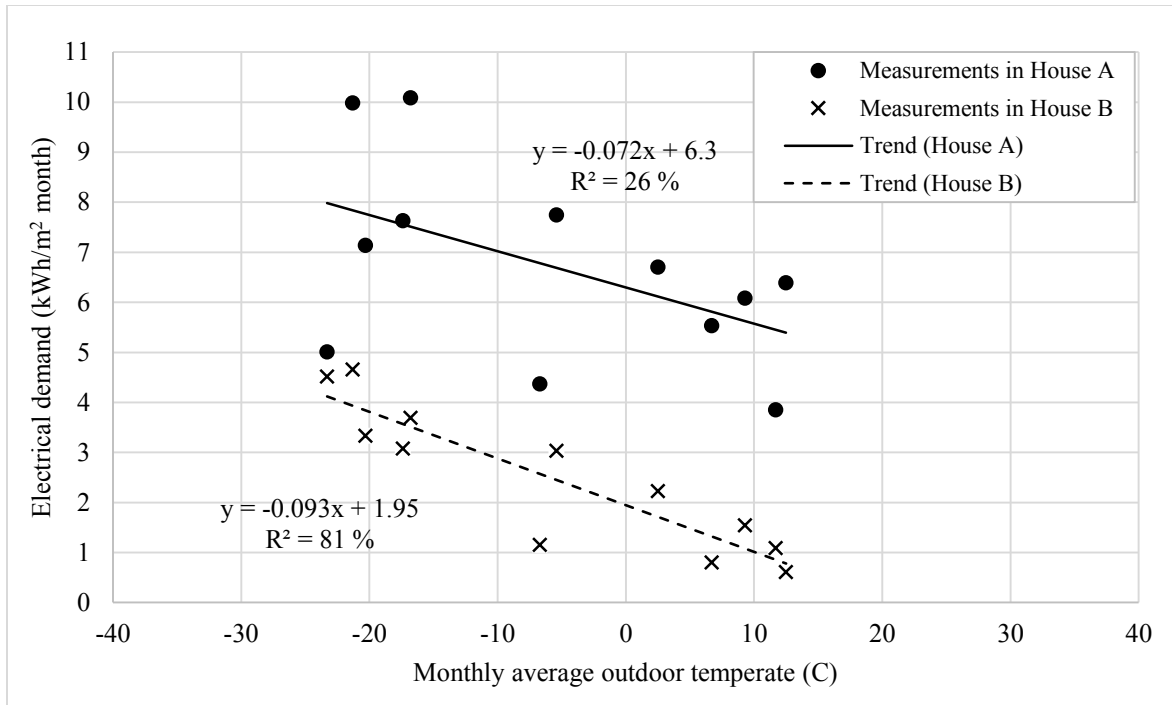
Figure 4.4: Monthly signature of electricity use for appliances, fans, pumps and others end-uses from October 2014 to September 2015

The monthly signature of natural gas use is presented in Table 4.5 versus the monthly average outdoor air temperature. The slope a = 2.38 MJ/(m^2 ^{o}C month) reflects the sensitivity of the natural use to the outdoor temperature. For each 1 ^{o}C of reduction in the average monthly outdoor air temperature, the heating gas use is increased by 2.38 MJ/(m^2 ^{o}C month).

When the monthly average outdoor air temperature is 0 ^{o}C, the monthly natural gas use is 39.85 MJ/(m^2 month).
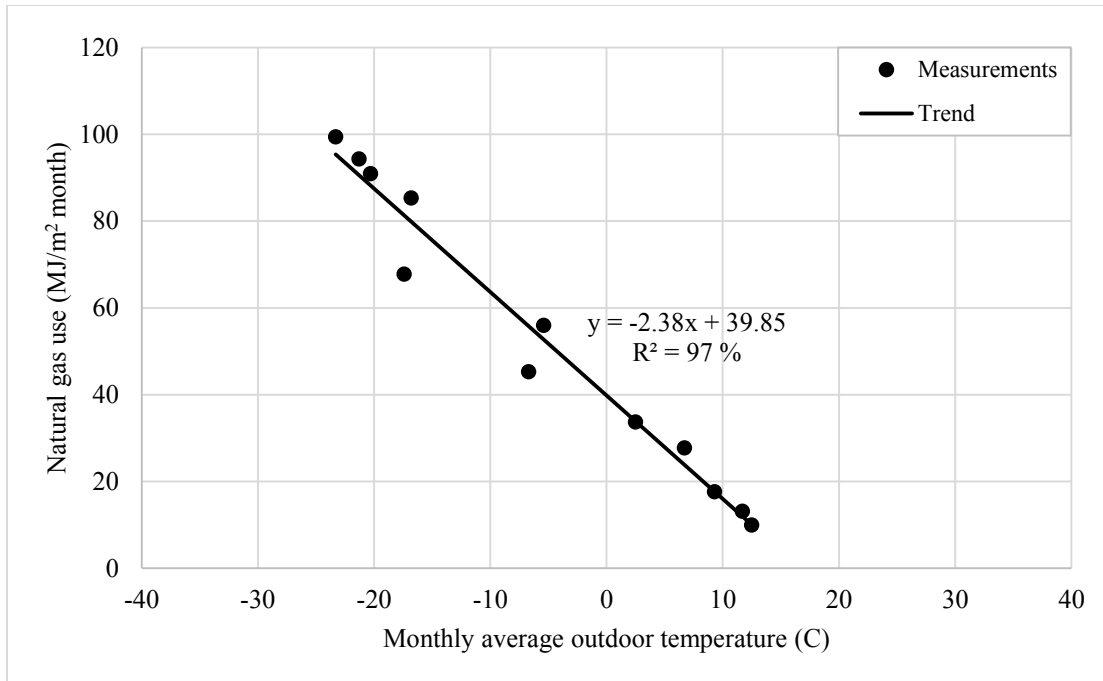
Figure 4.5: Monthly signature of natural gas use by the boiler that serves both houses A and B, from October 2014 to September 2015

The monthly signature of photovoltaic production versus monthly average outdoor temperature is presented in Figure 4.6. The sensitivity of the photovoltaic production for both houses A and B to the outdoor air temperature is detected by slope a = 0.075 kWh/(m^2 ^{o}C month) which by every 1 ^{o}C increase in outdoor temperature, the photovoltaic production is increased. the photovoltaic production is 2.21 kWh/(m^2 ^{o}C month) when outdoor temperature is 0°C.
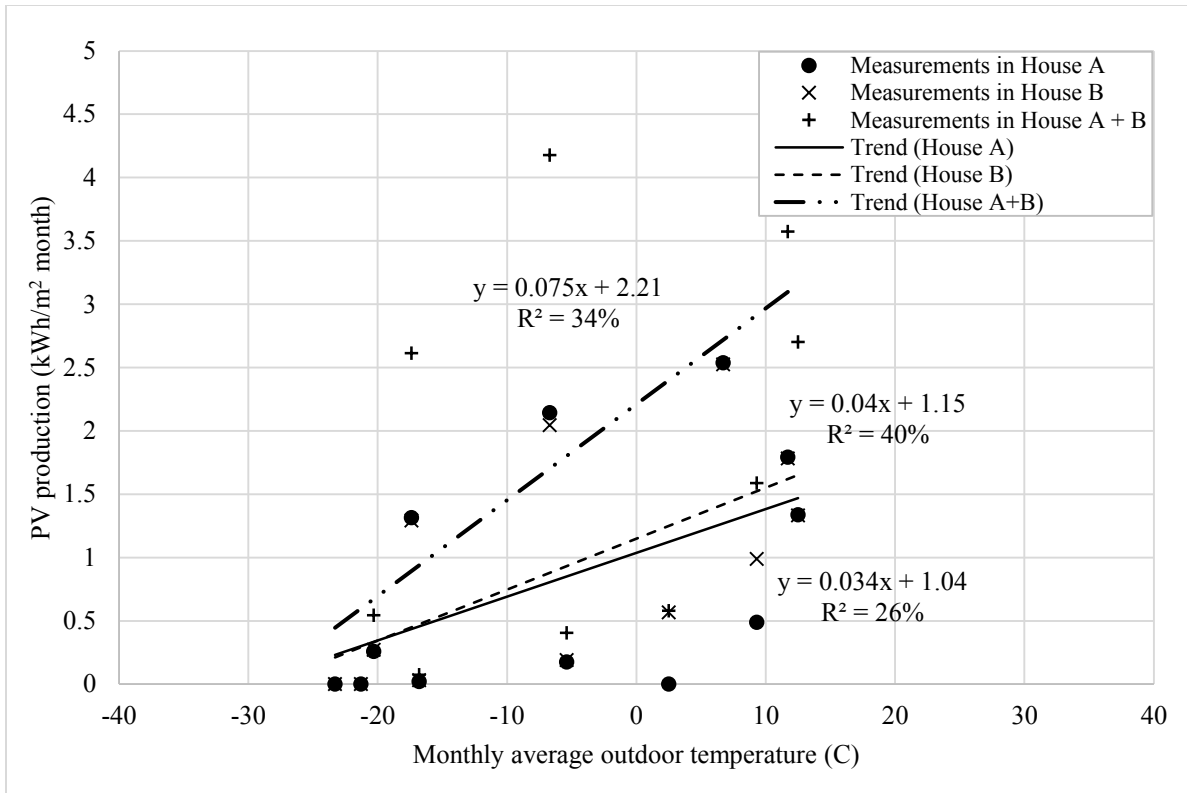
Figure 4.6: Photovoltaic production in houses A and B from October 2014 to September 2015

4.6. Daily energy demand, use and production

The heating energy demand of house A has larger daily variation around the mean value, compared with the house B (Figure 4.7 and Figure 4.8). The heating system turns on when the outdoor air temperature is 13.6 ℃ for house A, and 13.0 ℃ for house B.
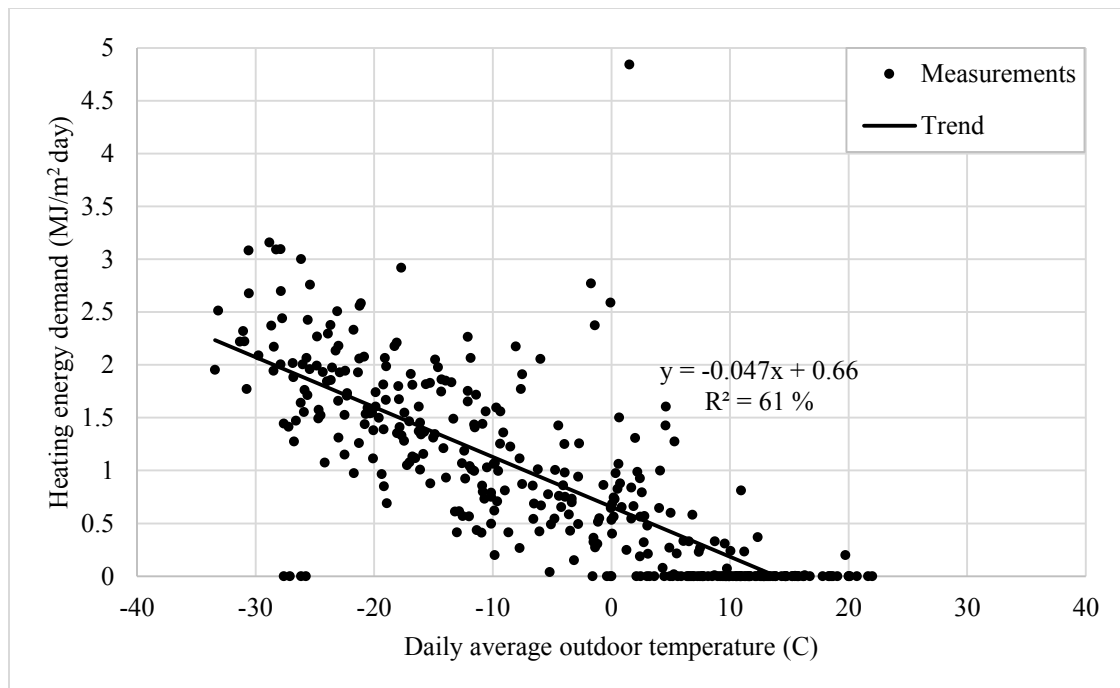
Figure 4.7: Daily signature of space heating energy demand of house A from October 2014 to September 2015
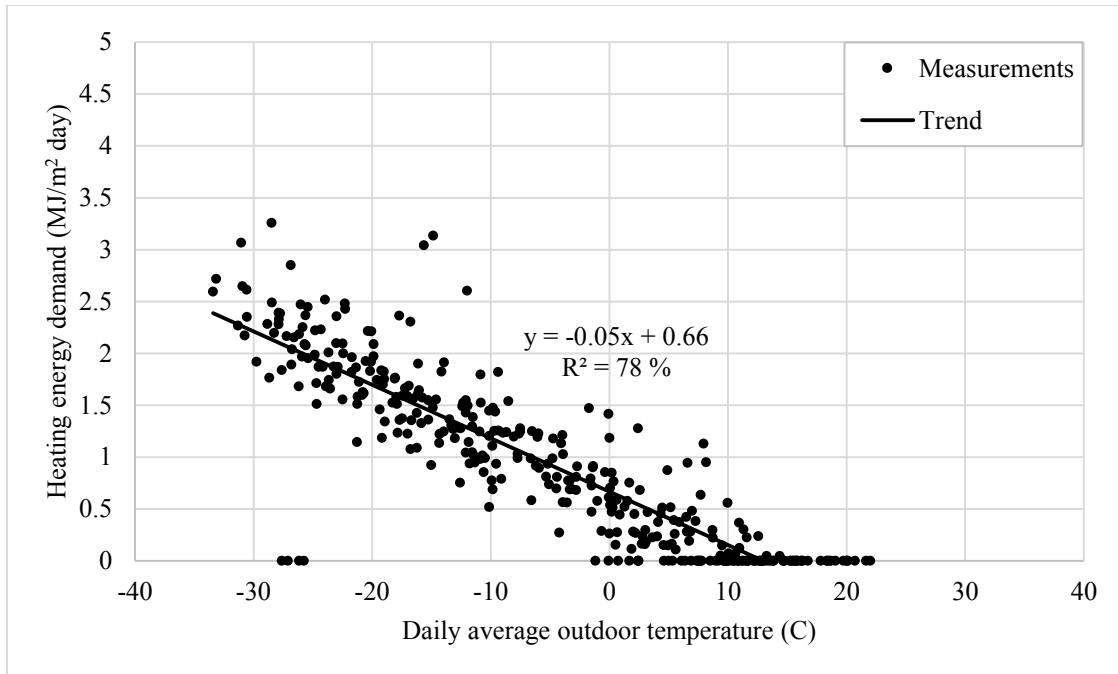
Figure 4.8: Daily signature of space heating energy demand of house B from October 2014 to September 2015

The daily signature of the domestic hot water demand shows a different pattern: the daily values of house B have larger daily variation around the mean value, compared with the house A (Figure 4.9 and Figure 4.10).
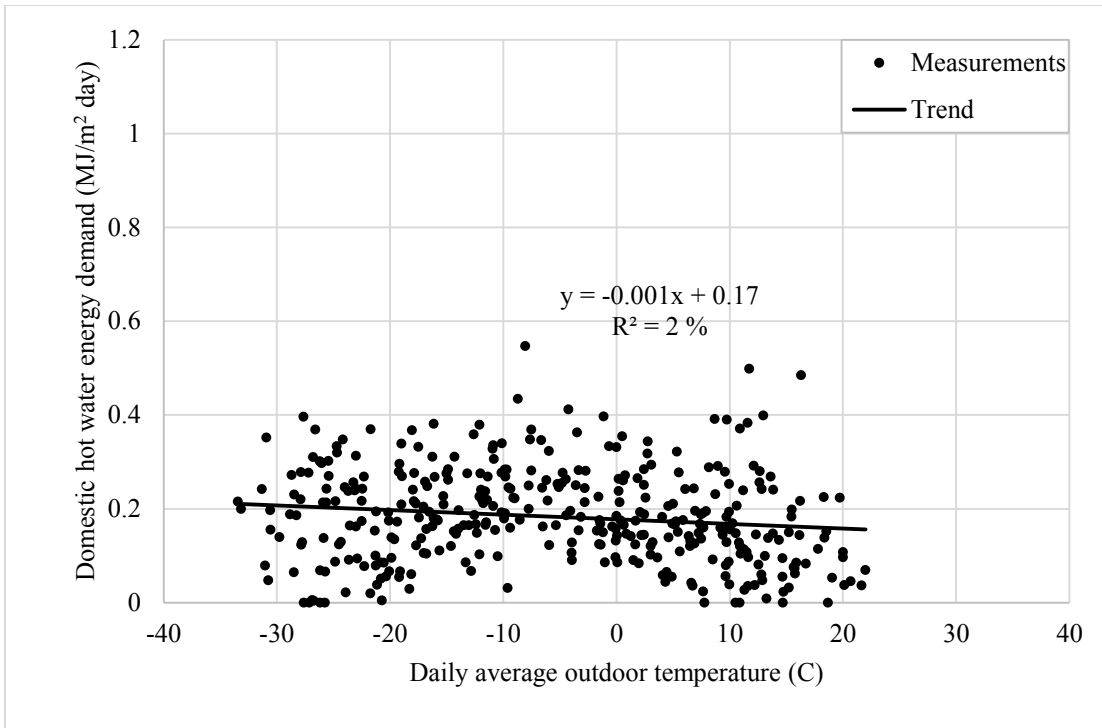
Figure 4.9: Daily signature of domestic hot water energy demand of house A from October 2014 to September 2015
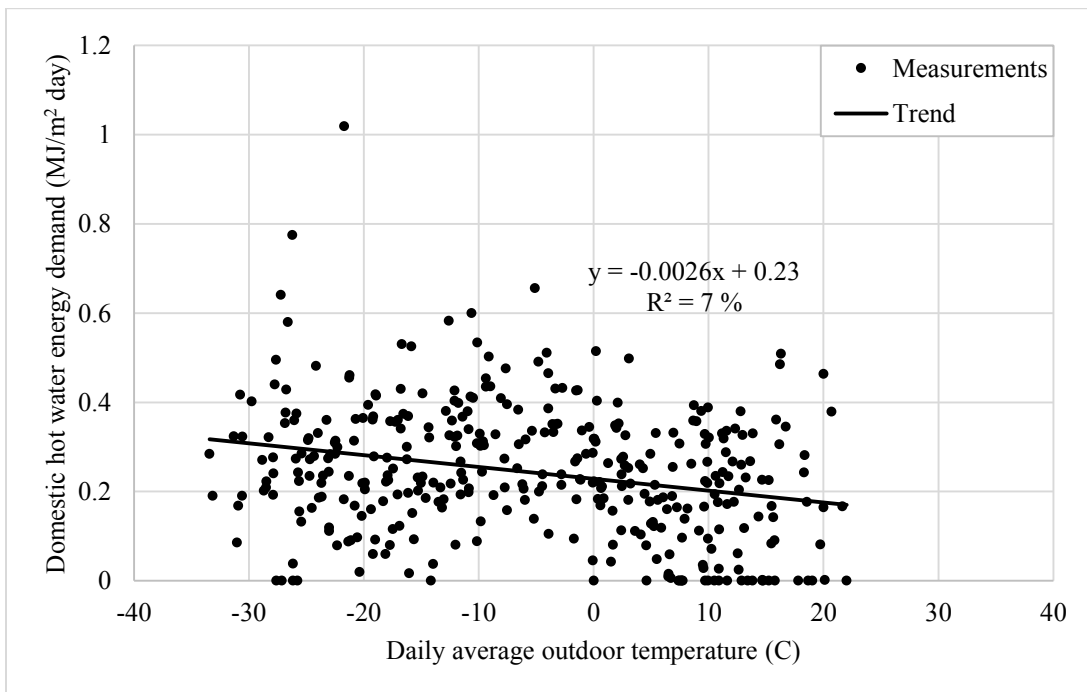
Figure 4.10: Daily signature of domestic hot water energy demand of house B from October 2014 to September 2015

Figure 4.11 to Figure 4.16 show the daily total heating and hot water energy demand, electrical use, photovoltaic production and solar hot water energy production in houses A and B.

Total daily heating and domestic hot water energy demand in house A in Figure 4.11 shows more dispersion of values around the average compare to house B (Figure 4.12). Total energy demand for space heating and domestic hot water in house B is more dependent on daily outdoor temperature according to 78% coefficient of determination.
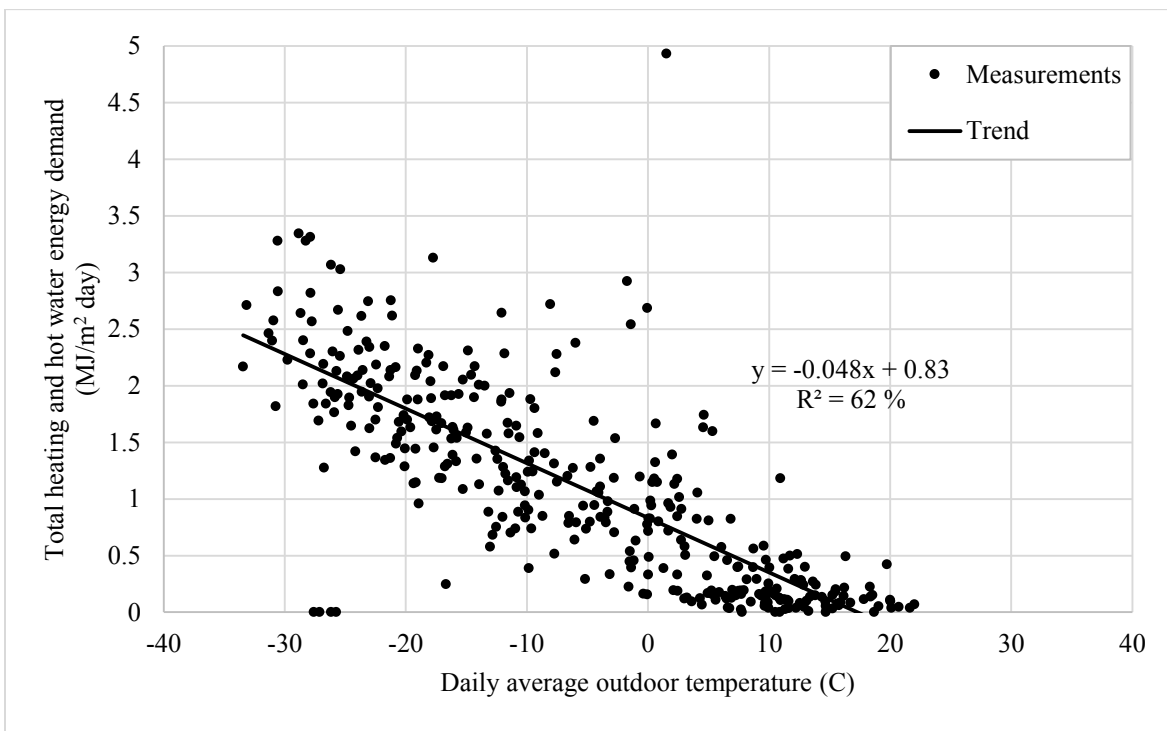
Figure 4.11: Total daily heating & domestic hot water energy demand in house A from October 2014 to September 2015
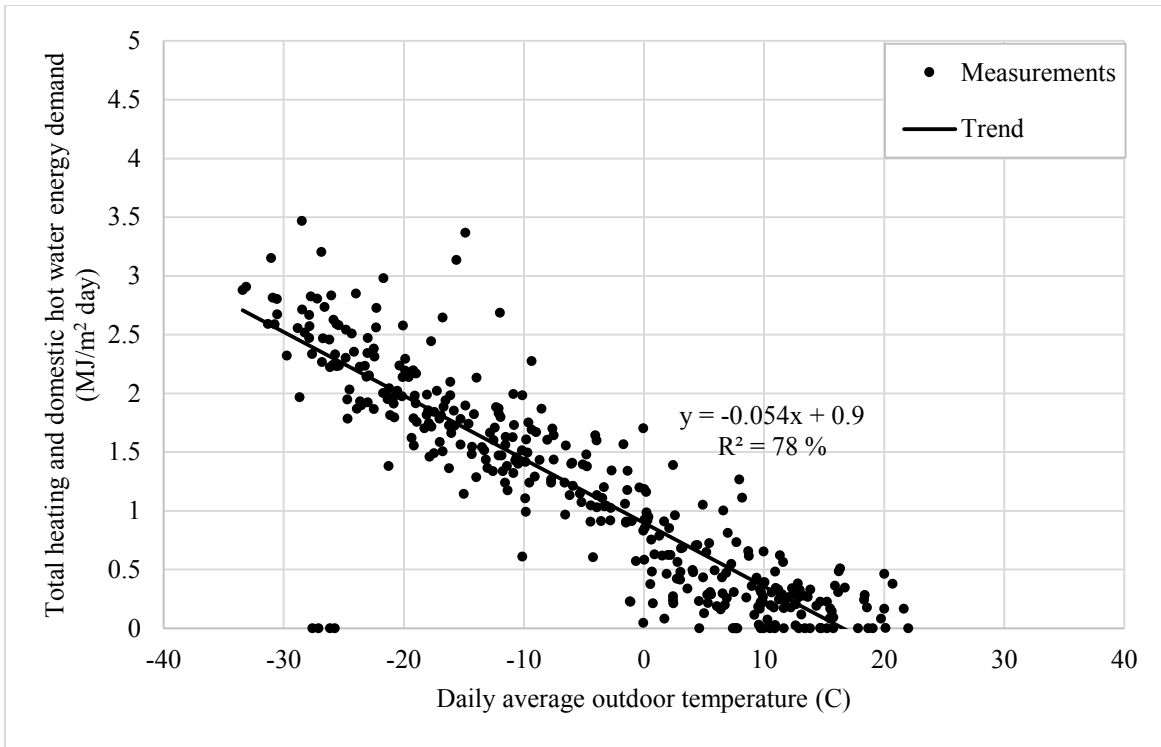
Figure 4.12: Total daily heating & domestic hot water energy demand in house B from October 2014 to September 2015

Regarding the electrical use, daily signatures in Figure 4.13 and Figure 4.14 show house B is more temperature-dependent in electrical use compare to house A and more dispersions exist in house A (Figure 4.13).
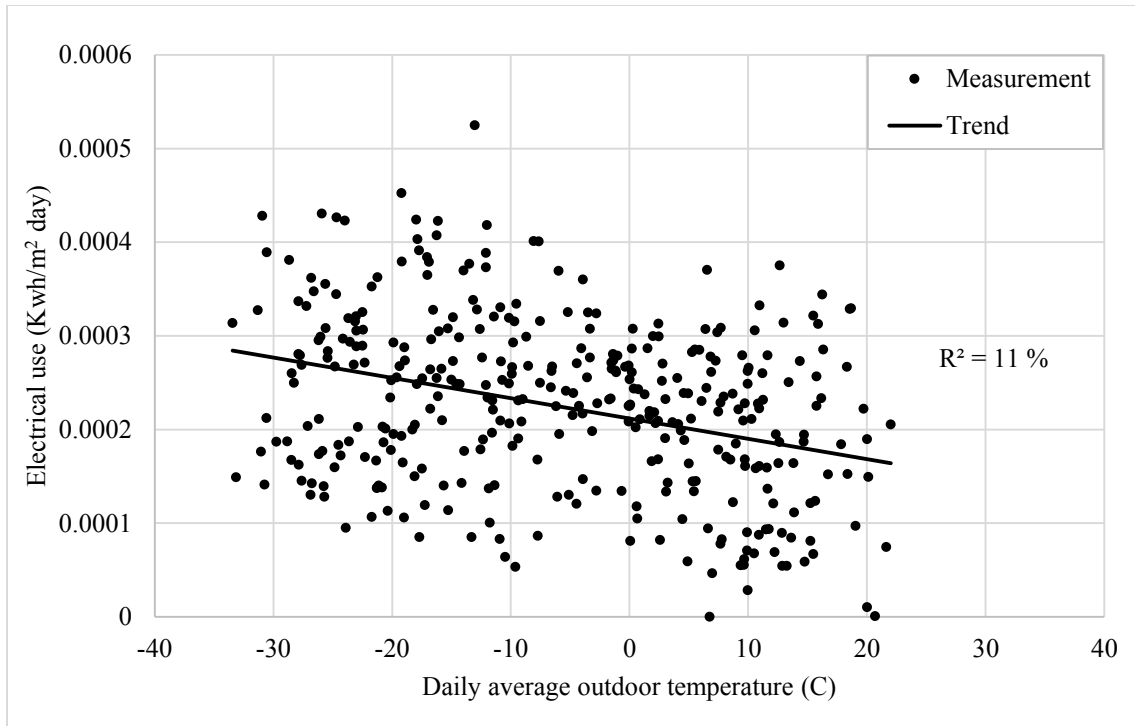
Figure 4.13: Daily electrical use in house A from October 2014 to September 2015
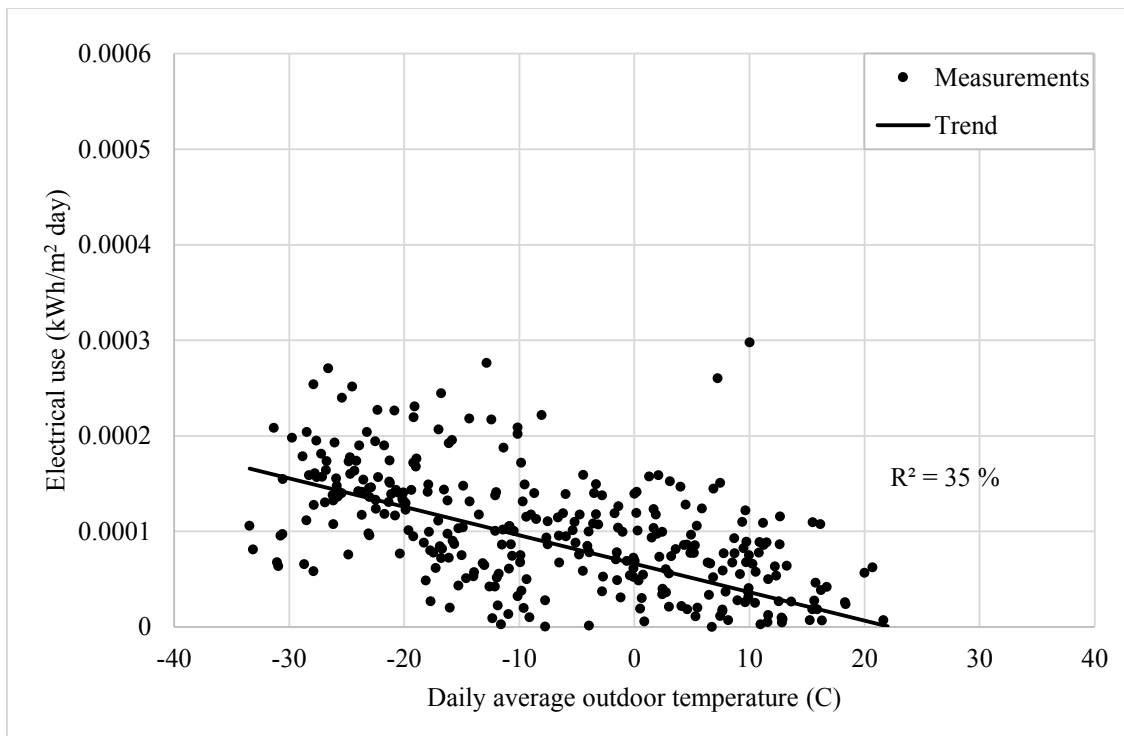
Figure 4.14: Daily electrical use in house B from October 2014 to September 2015
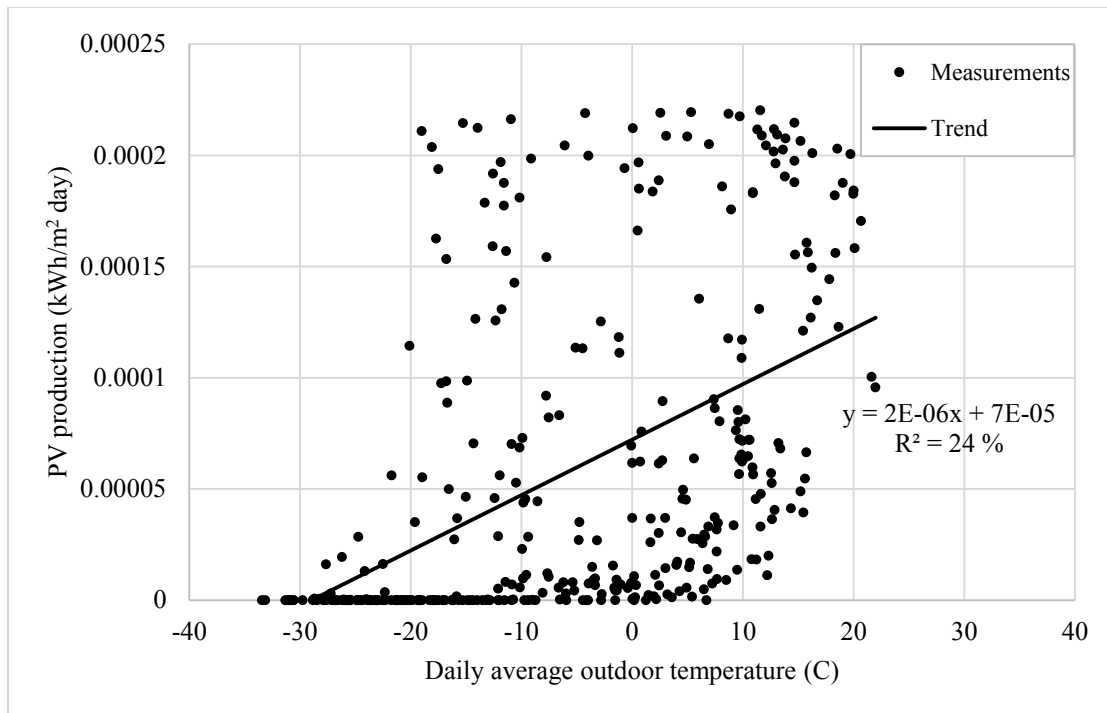
Figure 4.15: Daily PV production in houses A and B from October 2014 to September 2015

The solar hot water production is around 0.06 MJ/(m² °C day) when outdoor temperature is 0 °C as shown in Figure 4.16.
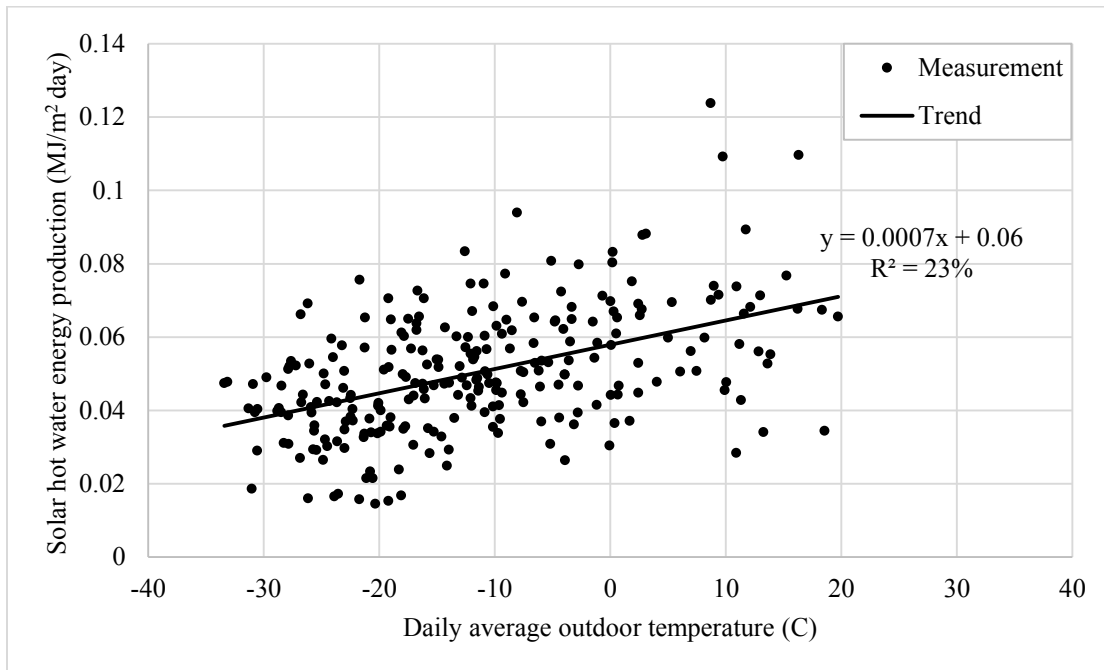
Figure 4.16: Daily solar hot water energy production in houses A and B from October 2014 to September 2015

The hourly signatures of space heating energy demand are presented in Appendix A for comparison with the monthly and daily signatures for both houses A and B. As noticed with the daily energy signatures, there is a larger variation of the hourly values for house A compared with house B, perhaps due to changes in occupancy, thermostat settings, assuming that the heating system works properly.

For comparison purposes, Table 4.5 presents the slope (a) and intersect (b) of the monthly, daily and hourly energy demand of houses A and B. Among the two options (i.e., monthly versus daily values), the rest of this report will use the daily values that have less dispersion than the hourly data, and give more information than the monthly data.

Table 4.5: Comparison of the coefficients of the monthly, daily and hourly energy signatures of houses A and B

Energy signature	Monthly				Daily				Hourly			
	a (MJ/m^2 °C)		b (MJ/m^2)		a (MJ/m^2 °C)		b (MJ/m^2)		a (MJ/m^2 °C)		b (MJ/m^2)	
House	A	B	A	B	A	B	A	B	A	B	A	B
Space heating energy demand	-1.56	-1.71	20.48	20.65	-0.04	-0.05	0.65	0.66	0	0.02	0	0.02
Domestic hot water energy demand	-0.03	-0.08	5.64	7.25	0	0	0.17	0.22	0	0	0	0
Energy demand for space heating and domestic hot water	-1.6	-1.8	26.12	27.92	-0.04	-0.05	0.83	0.9	0	0.3	0	0.3
Total electricity use	-0.08	-0.1	6.51	1.96	0	0	0	0	0	0	0	0
Total photovoltaic (PV) production A+B	0.07		2.21		2.21		0		0		0	
Solar hot water production A + B	-0.16		-1.37		-1.37		0.06		-0.03		0	

4.7. Analysis of Heat Recovery Ventilator (HRV)

In heat recovery ventilator, outdoor air is pre-heated by passing through heat recovery ventilator and it is heated up by means of exiting indoor air from inside of the house and passing through heat recovery ventilator. The schematic view of the heat recovery ventilator is illustrated in Figure 4.17. The sensible thermal effectiveness of the heat recovery ventilator (HRV) (ε) (-) is calculated with Equation 4.4.

$$\text{Outside} \quad T_1 \longrightarrow \qquad \longleftarrow T_3 \quad \text{Inside}$$

$$\text{Exhaust Air} \qquad \qquad T_2$$
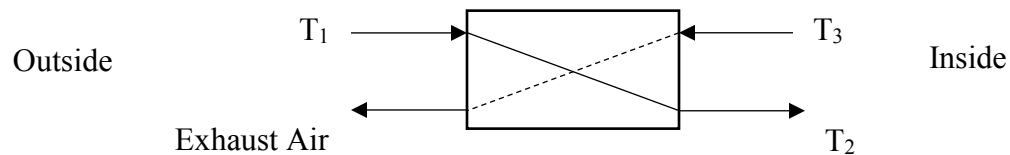
Figure 4.17: Schematic view of the heat recovery ventilator

$$\varepsilon = \frac{T_2 - T_1}{T_3 - T_1}$$

4.4

where: T_1 = the air temperature that enters the heat recovery ventilator; in the absence of pre-heating process $T_1 = T_O$ (outdoor air temperature) (ºC)

T_2 = the supply air temperature leaving heat recovery ventilator and entering the space (ºC)

T_3 = the inside air temperature leaving the space and entering the heat recovery ventilator (ºC)

4.7.1. Sensible thermal effectiveness of Heat Recovery Ventilator of house B

Since there are only a few measurements of HRV in house A, some of them with errors, this section presents only the sensible thermal effectiveness of the HRV of house B. Equation 4.4 shows the calculation of the sensible effectiveness from the measurements.

Monthly (Figure 4.18), daily (Figure 4.19) and hourly (Figure 4.20) thermal effectiveness signatures revealed that the sensible thermal effectiveness of the HRV does not vary with the outdoor air temperature. The average derived value is 0.71 (Figure 4.18) from monthly data, 0.72 from daily data, and 0.73 (Figure 4.20) from hourly data. The hourly effectiveness shows a larger dispersion when the outdoor air temperature is above 6-8ºC, probably due to the uncertainty of measurements at smaller air temperature differences. The derived effectiveness of 0.72 is lower than the manufacturer's specifications of 0.83 at 0ºC and 0.89 at -25ºC.
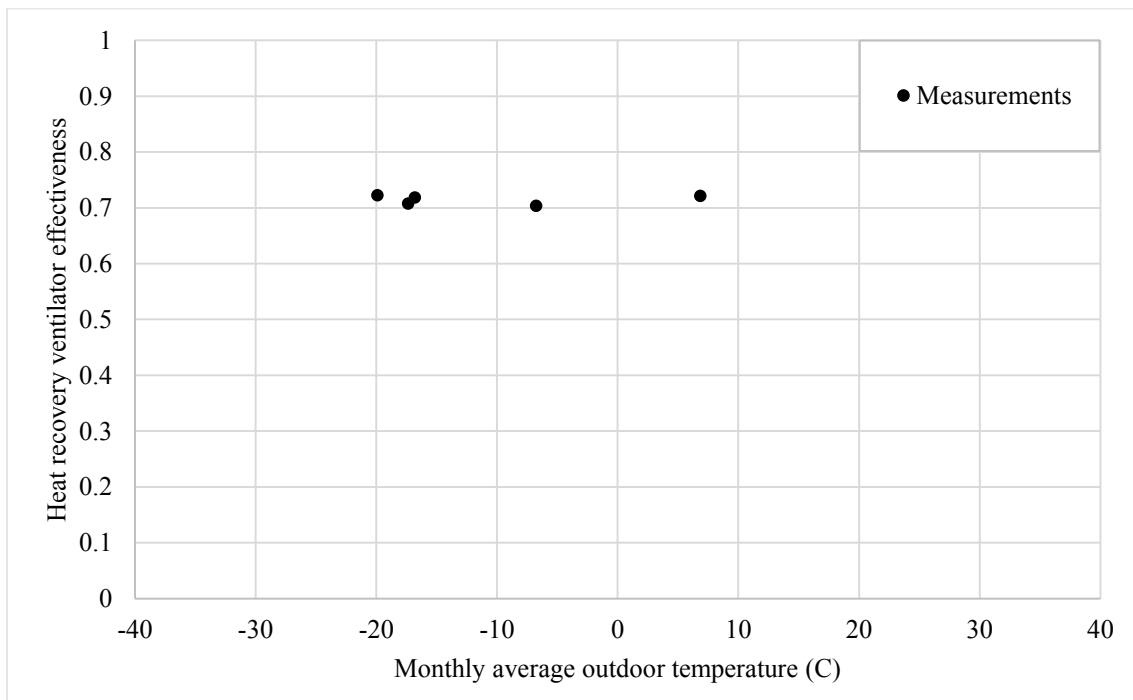
Figure 4.18: Heat recovery unit effectiveness of house B versus monthly average outdoor temperature from October 2014 to September 2015
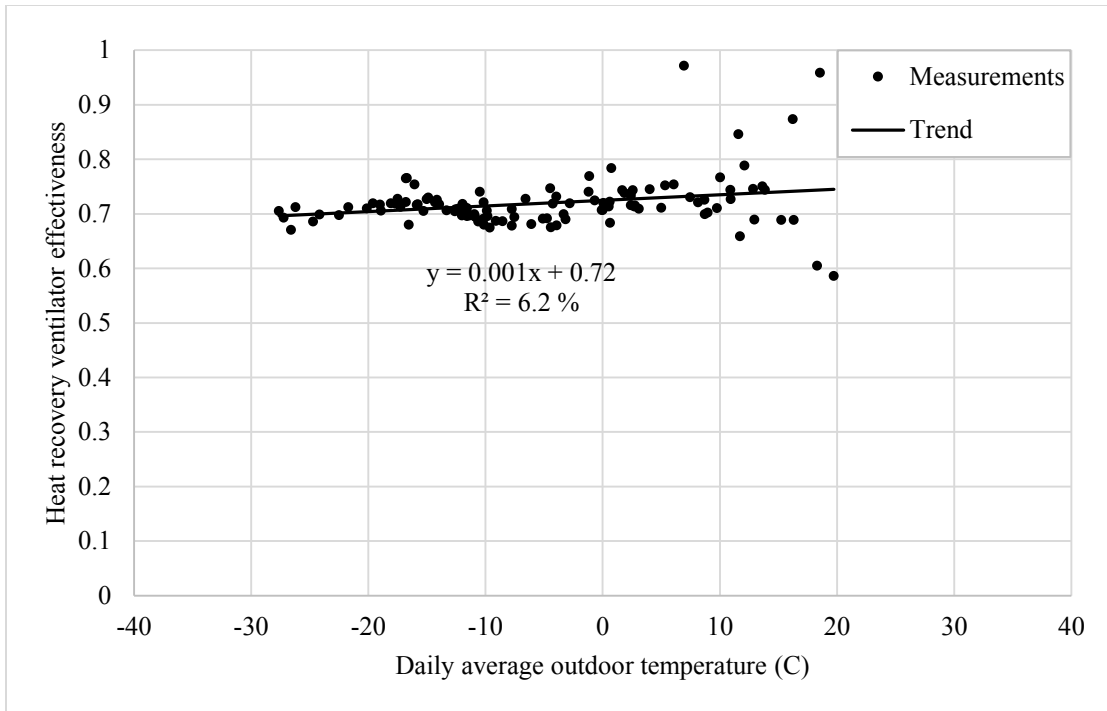
Figure 4.19: Daily signature of the sensible effectiveness versus daily average outdoor temperature in house B from October 2014 to September 2015
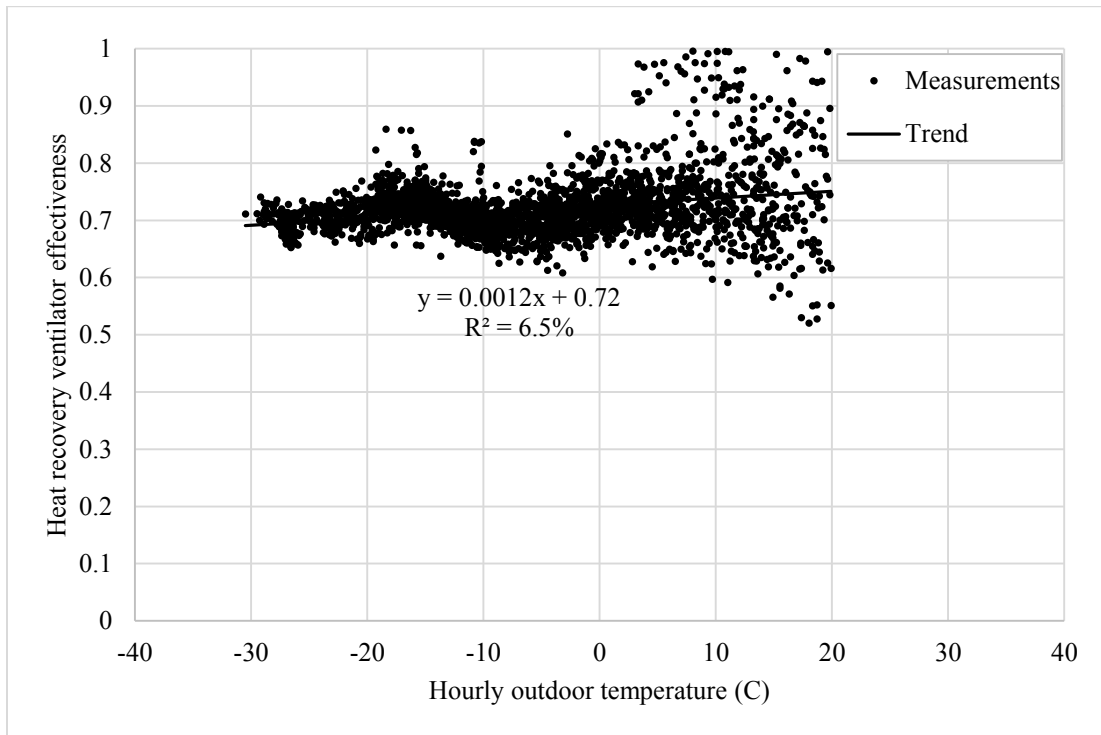
Figure 4.20: Hourly signature of the sensible effectiveness versus Hourly average outdoor temperature in house B from October 2014 to September 2015

Considering Figure 4.20, by the time that outdoor temperature is negative from -30 $^{\circ}$C to 0 $^{\circ}$C, hourly thermal effectiveness is more converged and the coefficient of determination (R^2) is higher.

When the outdoor temperature is positive, effectiveness points commence to disperse, since it can be seen for the values with outdoor temperatures of above 4 $^{\circ}$C. So, the sensible thermal effectiveness of the heat recovery ventilator is less temperature-dependent when outdoor temperatures is above 0 $^{\circ}$C.

4.8. Supply and return temperature of water from boiler

In this section, monthly, daily and hourly supply and return temperature of water from boiler for space heating purpose is analyzed. Toward this approach, monthly (Figure 4.21), daily (Figure 4.22) and hourly (Figure 4.23) supply and return signatures disclosed that, supply and return temperature of the water is highly sensitive to the outdoor temperature. Approximately, at 12 °C the boiler starts to heat the supply water in order to raise water temperature to about 29 °C. Boiler heats the water temperature around 0.7 °C by every 1 °C decrease in outdoor air temperature. The pick point of supply water temperature is 57 °C (Figure 4.22).
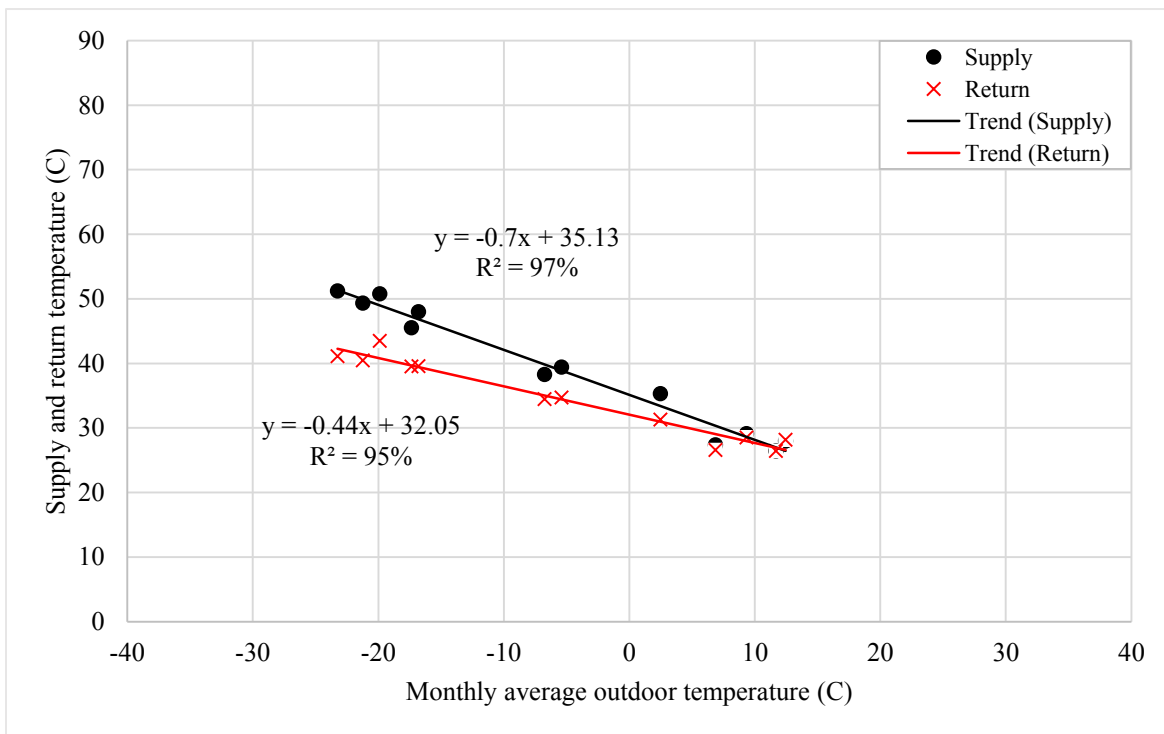
Figure 4.21: Supply and return water temperature versus monthly average outdoor temperature in house B from October 2014 to September 2015
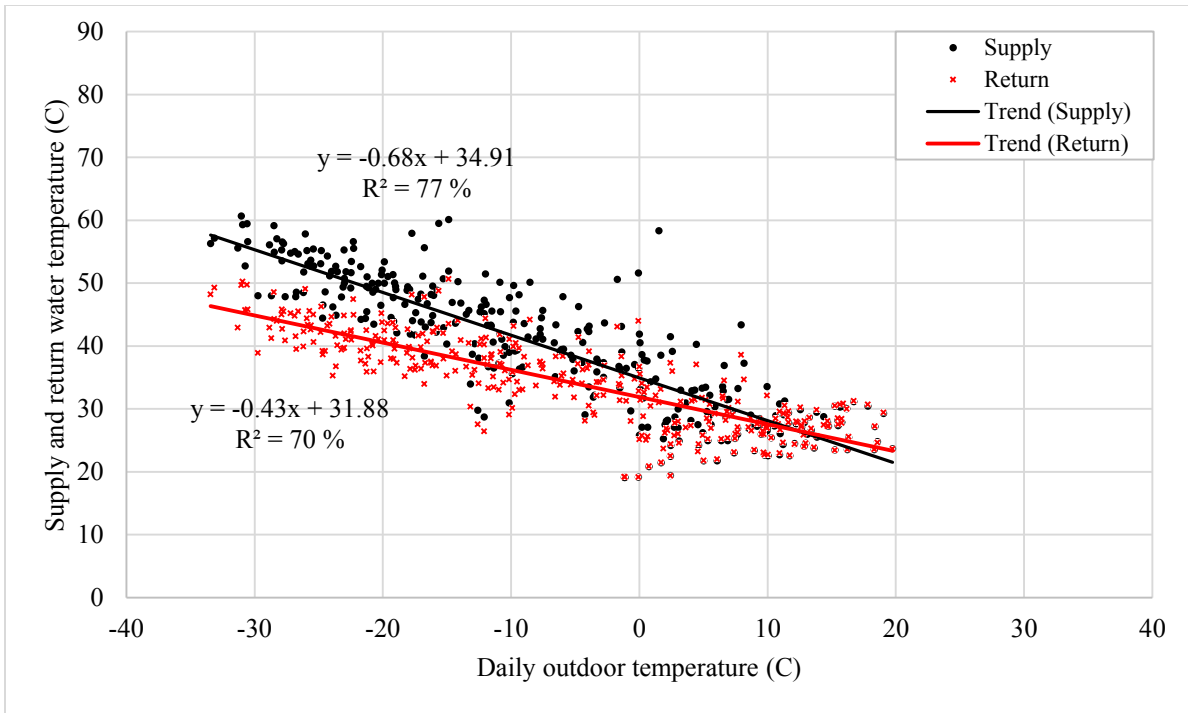
Figure 4.22: Daily supply and return water temperature versus daily outdoor temperature in house B from October 2014 to September 2015
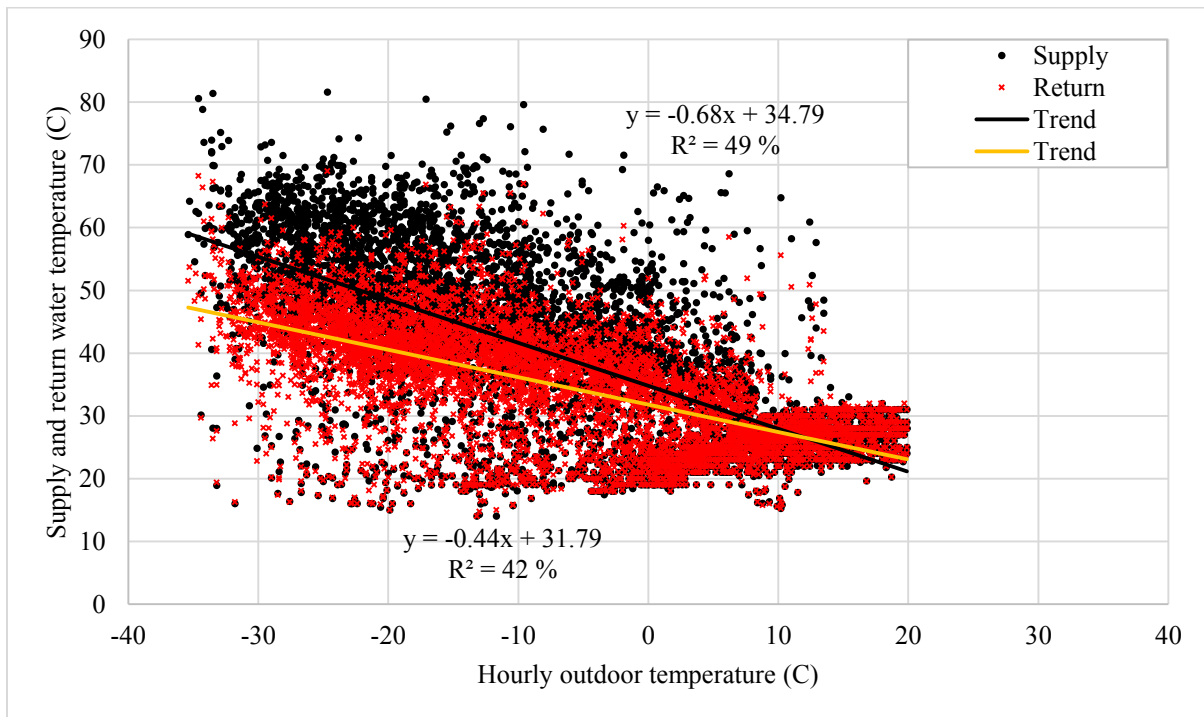
Figure 4.23: Hourly supply and return water temperature versus daily outdoor temperature in house B from October 2014 to September 2015

Supply and return temperatures of water in every month of a year from October 2014 to September 2015 are presented in Table 4.6, which reveals that the heating season starts in August with supply temperature of 29.14 ºC but low heating is required and lasts by the end of May. The highest heating capacity of boiler is used in January when the monthly outdoor temperature is -23 ºC, and the boiler heats up the supply water temperature to around 51 ºC.

Table 4.6: Monthly supply and return water temperature for the space heating system in house B

Month	Supply temperature to space (ºC)	Return temperature to boiler (ºC)	Temperature difference (ºC)	Outdoor air temperature (ºC)
October 2014	39.46	34.73	4.73	-5.4
November 2014	48	39.6	8.4	-16.81
December 2014	49.33	40.47	8.86	-21.24
January 2015	51.25	41.13	10.12	-23.25
February 2015	50.78	43.52	7.26	-19.9
March 2015	45.55	39.52	6.03	-17.36
April 2015	38.3	34.47	3.83	-6.75
May 2015	27.38	26.6	0.78	6.86
June 2015	26.45	26.43	≈ 0	11.68
July 2015	28	28.2	≈ 0	12.45
August 2015	29.14	28.55	0.59	9.34
September 2015	35.34	31.33	4.01	2.47

4.9. Carpet plot

Hourly energy performance distribution through days of a month is illustrated in a graph called Carpet plot. Carpet plots for hourly space heating and domestic hot water energy demands and electrical use in 31 days of January for house A are plotted in Figure 4.24 to Figure 4.26, respectively.

Hourly distribution of solar hot water and photovoltaic productions in July 2015 are plotted in Carpet plots as shown in Figure 4.27.

Same Carpet plots regarding energy performance distribution in April 2015 are presented in appendix B.
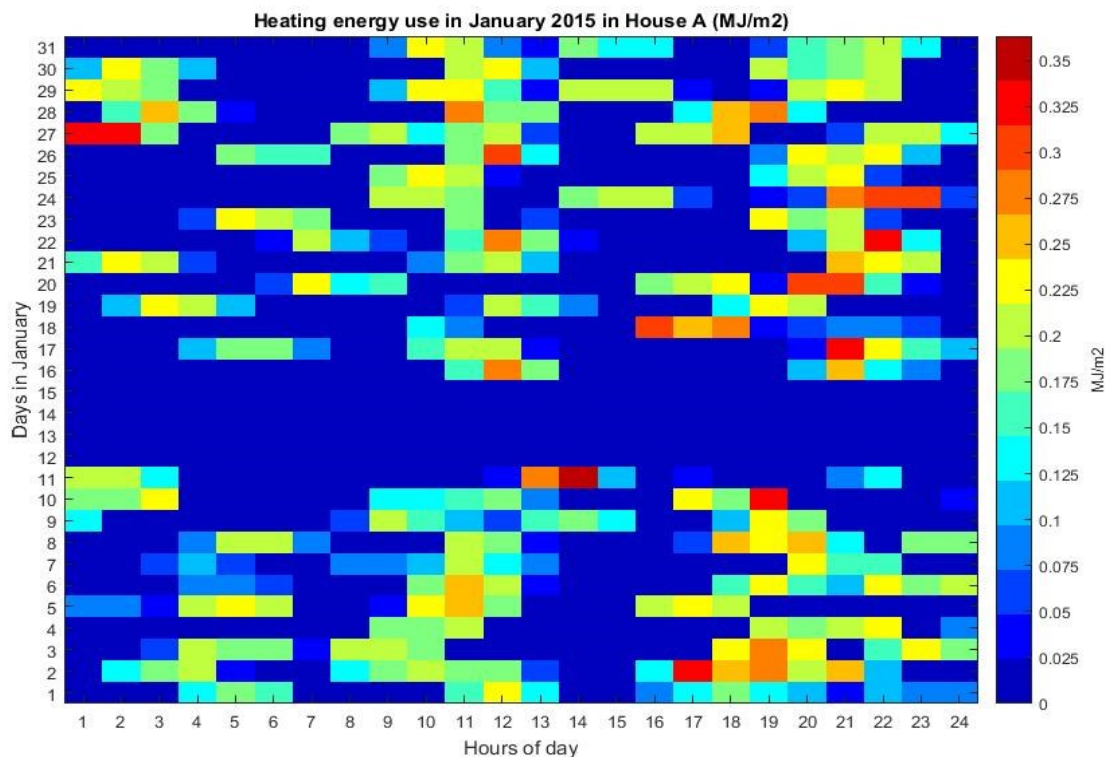
Figure 4.24: Hourly heating energy demand in House A in January 2015

The most heating energy demand during a day is between 4 P.M to 10 P.M as Figure 4.24 presents.
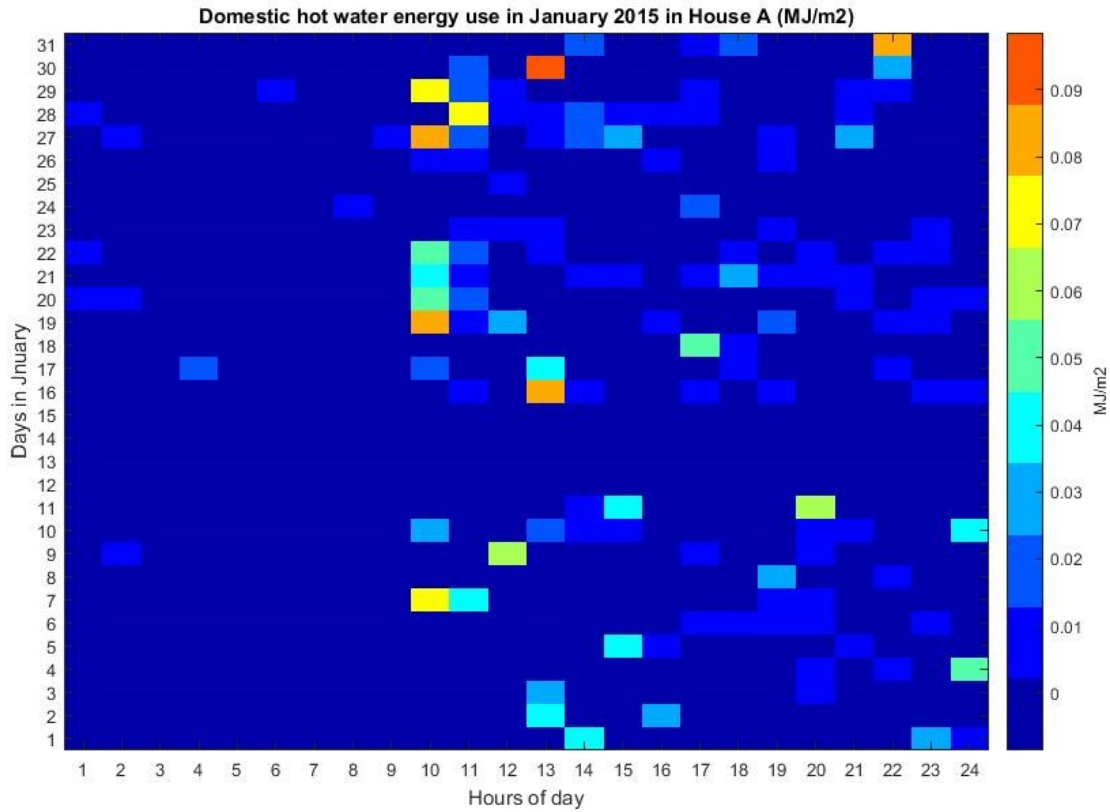
Figure 4.25: Hourly domestic hot water energy demand in House A in January 2015

Domestic hot water energy demand is mostly between 10 A.M to 11 P.M, which the highest demand is at 10 A.M.
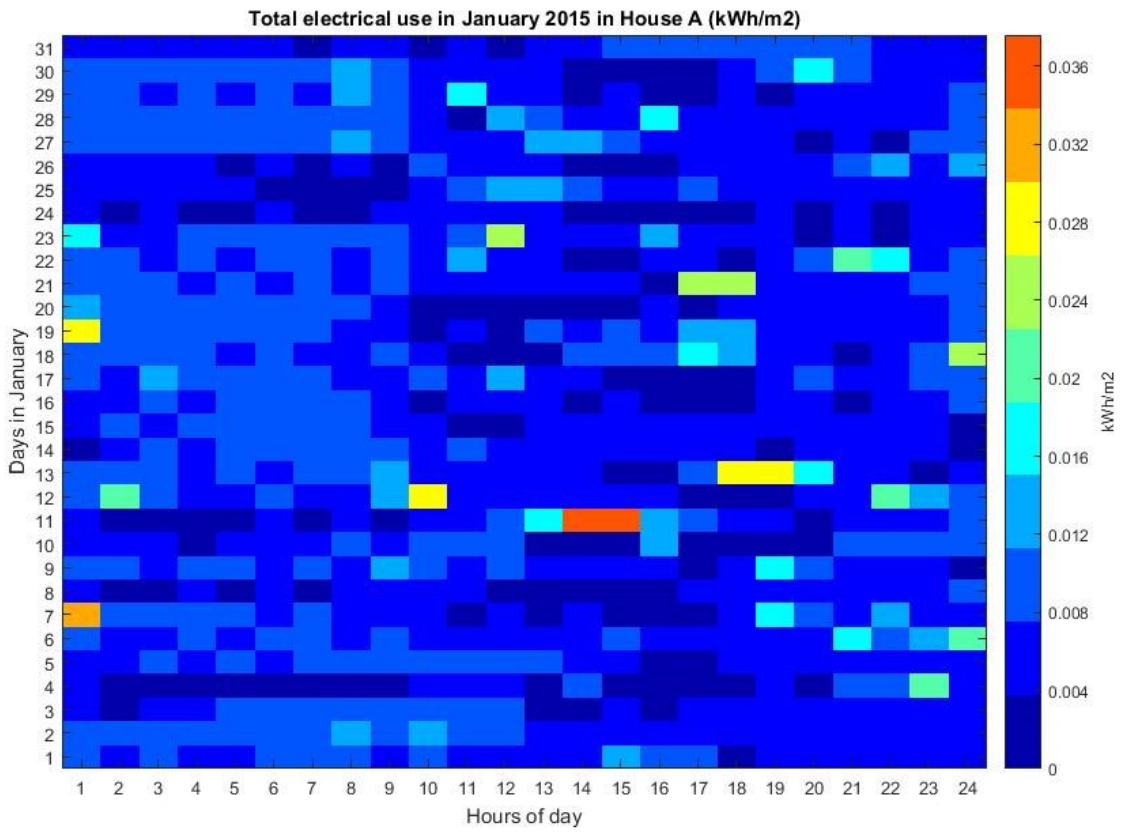
Figure 4.26: Hourly total electrical use in house A in January 2015
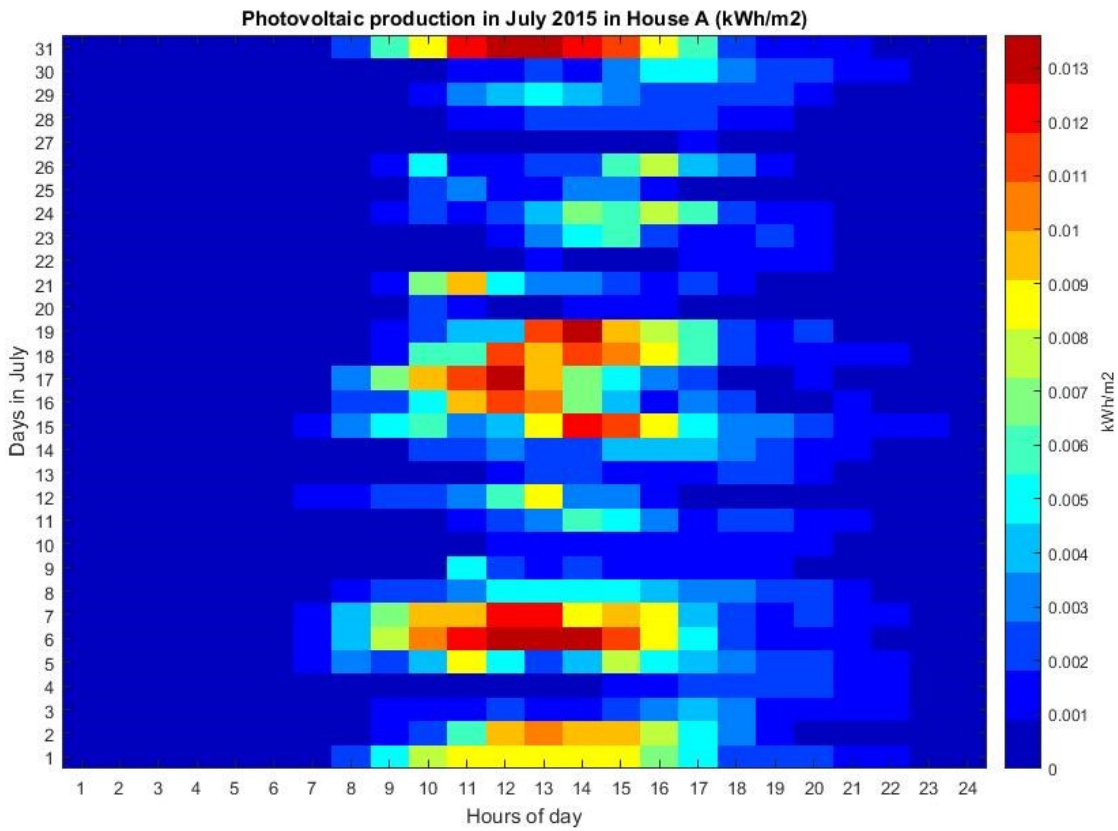
Figure 4.27: Hourly photovoltaic production in House A in July 2015

Photovoltaic production in house A in July 2015 happens between 7 A.M to 10 P.M (Figure 4.27). Between 9 A.M to 5 P.M the production range is high, and the maximum PV production happens between 11 A.M to 3 P.M.

The scope of the Carpet plot is hourly analysis of energy demand and production through days of a month which can be helpful for the mechanical room operators in order to manage performance of the heating equipment system. For instance, in July or even in the months when sunlight is high, a great deal proportion of domestic hot water demand can be provided by pre-heating via solar hot water system which in consequence the natural gas use will be diminished.

4.10. Discussion

House B uses more natural gas for space heating and domestic hot water demands and has less electrical use compare to house A.

Daily energy performance values are more suitable for further analysis, due to less fluctuations and dispersions compare to hourly values, and more values in a specific period compare to monthly values so it will give more information.

Heat recovery unit effectiveness is about 70 to 72 % during heating season.

Supply and return water temperature from boiler for space heating is highly temperature-dependent.

5. ONGOING COMMISSIONING OF HEATING SYSTEMS

This section proposes an approach for using the measurements recorded in these two semi-detached houses, for the ongoing commissioning that consists in the comparison of measured data with predictions from benchmarking models. In this study, the comparison of the heating energy demand of the two semi-detached houses A and B can detect abnormally higher or lower heating energy demand, which might be due to faults or failures of equipment or sensors, change in controls or people's energy-related behavior. Those findings should be communicated as warnings with appropriate comments to the house' owner or maintenance team.

For this purpose, a data set is selected from the measurements recorded at the beginning of the ongoing commissioning period, from which, the benchmarking model is developed. The model is then used to predict the heating energy demand for the following days, eventually until the end of heating season.

Measurements of the heating water flow rate, and the supply and return hot water temperatures for each house have been recorded at 1-minute time step, from which the hourly and daily values of the heating energy demand are calculated. The values of daily heating energy demand are almost normally distributed. The outliers, which have values outside the range $\bar{y} \pm 2 \cdot \sigma$, are removed, where, $\bar{y}$ is the average value, and σ is the standard deviation. Thus, 95.5% of the available data remained in the analysis data set [59].

In this study, the benchmarking model has the form of daily signature of space heating energy demand (Equation 2.4). The daily signature was preferred instead of monthly signature, because it permits the prediction of daily heating energy demand, rather than the total monthly

value. It was also preferred instead of hourly signature to avoid the use of high dispersion of data that makes the model less reliable.

5.1. Benchmarking models

5.1.1.   Training, testing and application data sets

The data set of measurements of December 2014 is selected as the reference, and used for the initial development of benchmarking models. The data set is composed of (1) the training data set, which is used to identify the models` coefficients, and (2) the testing data set, which deploys the balance of data set to verify the models` accuracy. The models are initially trained with a data set of the first three weeks of December 2014 (i.e., December 1-21, and tested with a data set of the last week of December (i.e., December 22 to 31). The tested models are then used along with the application (prediction) data set to estimate the daily heating energy demand.

Once the benchmarking models are tested, they can be used unchanged over the application time interval by using the static window technique, or the models can be retrained with new data from recent measurements by using the augmented window technique. In the first case, for instance the daily heating energy demand is predicted for the remaining part of the heating season from January 1 to March 31, 2015. In the second case, the trained data set is augmented every time with two weeks of data. After the model is re-trained, the second week of new data is used as a testing data set. For instance, the models are re-trained with a data set of five weeks (December 1, 2014 to January 4, 2015), and are tested with a data set from the following week of January 5 to 11, 2015. The new retrained models are then used for prediction of the daily heating energy demand from January 12 to March 31, 2015.

5.1.2. Quality of predictions of benchmarking models

Three statistical indices are used: (1) the Coefficient of determination R^2 (Equation 5.1) [28] for the models training, and (2) the Root Mean Squared Error RMSE (Equation 5.2) and the Coefficient of Variance of Root Mean Squared Error (CV(RMSE)) (Equation 5.3) for the models testing and predictions.

$$R^2 = \left[1 - \frac{\sum_{i=1}^{n}(y_i - \hat{y}_i)^2}{\sum_{i=1}^{n}(y_i - \bar{y}_i)^2}\right] \cdot 100 \qquad\qquad 5.1$$

$$RMSE = \sqrt{\frac{\sum_{i=1}^{n}(\hat{y}_i - y_i)^2}{n-1}} \qquad\qquad 5.2$$

$$CV\,(RMSE) = \frac{\sqrt{\frac{\sum_{i=1}^{n}(\hat{y}_i - y_i)^2}{n-1}}}{\bar{y}} \cdot 100 \qquad\qquad 5.3$$

where y_i is the measured value, $\hat{y}_i$ is the predicted value, $\bar{y}_i$ is the average measured value and n is the number of values.

According to [28] the model predictions of the whole building energy consumption, when using hourly data, is acceptable if CV(RMSE) is less than 30%; and the model using monthly data is acceptable if CV (RMSE) is between 5 to 15%. Since the ASHRAE guideline 14 does not specify the acceptance criterion for the models using daily data, the maximum value of CV(RMSE) of 30% is used in this study.

5.1.3. Training and testing the benchmarking models

The daily signatures of space heating energy demand of houses A and B, identified from the training data set of December 2014, are almost identical (Equations 5.4 and 5.5, and Figure 5.1 and Figure 5.2). In the case of the static window technique, these models are not retrained when

new data become available. When the augmented window technique is applied, the models are retrained every time with a new training data set, in which the previous training data set is augmented with new data of two weeks.

$$E = -0.069 \cdot To + 0.24 \; [MJ/m^2 \; day] \qquad\qquad \text{for house A} \qquad\qquad 5.4$$

$$E = -0.07 \cdot To + 0.25 \; [MJ/m^2 \; day] \qquad\qquad \text{for house B} \qquad\qquad 5.5$$
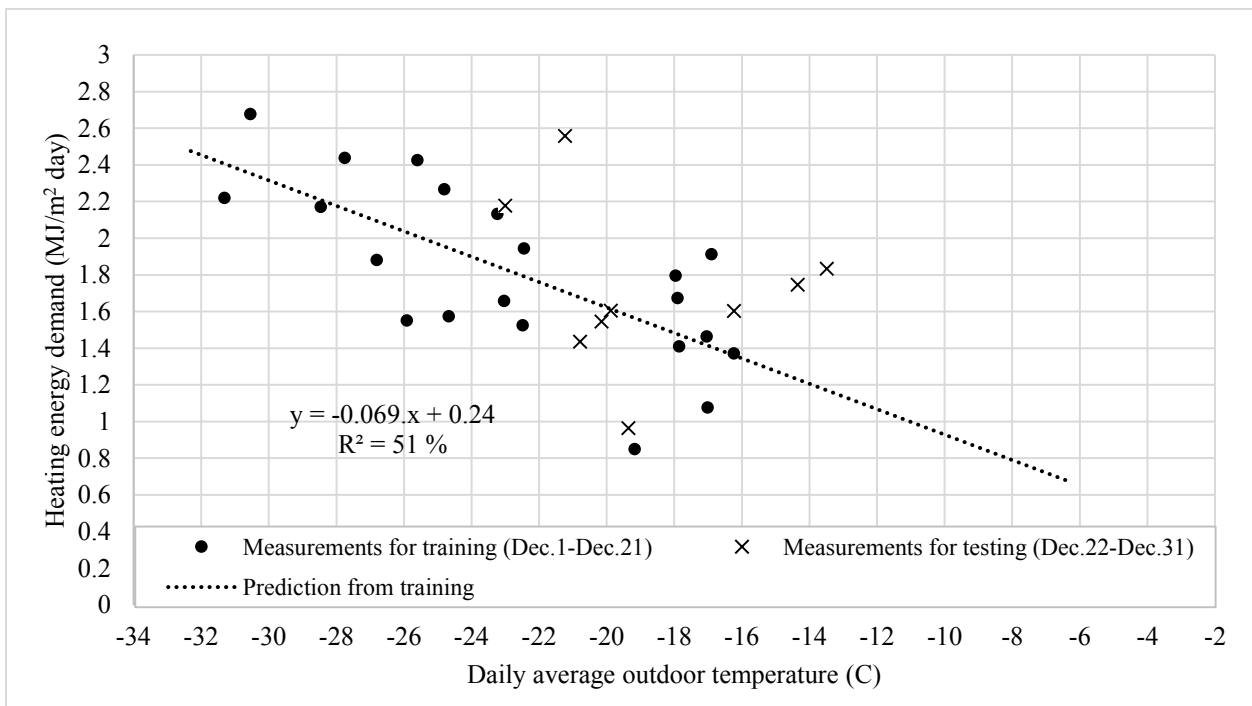
Figure 5.1: Daily signature of space heating energy demand as a benchmarking model of house A with static window technique from data set of December 1-21, 2014

Figure 5.2: Daily signature of space heating energy demand as a benchmarking model of house B with static window technique from data set of December 1-21, 2014

The daily signatures for both static window and augmented window techniques are presented in Table 5.1, reveal important information that can be extracted from the daily signatures about the thermal performance of these two houses:

a. The daily heating energy demand of house B is more sensitive to the changes in the outdoor air temperature, as indicated by the coefficient a. By assuming the same level of thermal insulation of both houses, this result can indicate differences in terms of air infiltration, and operation of heat recovery ventilators.

b. The temperature T_{ref} is estimated from the daily signature, and indicates the approximate daily average outdoor air temperature when the heating is required in the house. The low value of $T_{ref} = 3.5\text{-}3.6°C$ indicates important heat gains in both houses in December due to the number and activities of occupants. The results with larger training data sets (e.g., Dec 1-Jan 18) reveal

that the internal heat gains were smaller in the house A (T_{ref} = 20.2ºC) than in the house B (T_{ref} = 4.7ºC).

c. The house A has a higher daily heating energy demand when the daily average outdoor air temperature is 0ºC, as indicated by the coefficient b, calculated at the daily average outdoor air temperature is 0ºC. This result also indicates that the internal heat gains were smaller in the house A.

d. Most CV(RMSE) values listed in Table 5.1 are below the value of 30%, which indicate that the trained benchmarking models have an acceptable accuracy, and thus can be used for the prediction purposes. The last training period of house A and the training periods of Dec.1-Feb.15 for house B that uses the augmented window technique are the exceptions, with CV(RMSE) of 45-46%.

Table 5.1: Coefficients of the trained benchmarking models, and statistical indices of the difference between measurements and predictions over the testing period

House	Training period	Benchmarking model E = a·To + b			Statistical indices over the testing period	
		a (MJ/m² ºC day)	b (MJ/m²day)	T_{ref} (ºC)	RMSE (MJ/m² day)	CV(RMSE) (%)
Static window technique						
A	Dec 1-21, 2014	-0.069	0.24	3.5	0.51	29
B		-0.07	0.25	3.6	0.20	13
Augmented window technique						
A	Dec 1-21	-0.069	0.24	3.5	0.51	29
	Dec 1-Jan 4	-0.054	0.64	11.9	0.46	23
	Dec 1-Jan 18	-0.044	0.89	20.2	0.38	21
	Dec 1-Feb 1	-0.042	0.92	21.9	0.16	8
	Dec 1-Feb 15	-0.042	0.91	21.7	0.44	33
	Dec 1-March 1	-0.053	0.62	11.7	0.56	45
B	Dec 1-21	-0.07	0.25	3.6	0.2	13
	Dec 1-Jan 4	-0.07	0.25	3.6	0.29	16
	Dec 1-Jan 18	-0.068	0.32	4.7	0.25	14
	Dec 1-Feb 1	-0.063	0.42	6.7	0.16	8
	Dec 1-Feb 15	-0.067	0.36	5.4	0.82	46
	Dec 1-March 1	-0.05	0.78	15.6	0.25	17

5.1.4. Comparison of the measurements and predictions over the application period

The scope of using these benchmarking models is to detect differences between the measurements of daily space heating energy demand and the expected values that are predicted by the benchmarking models. Large difference might indicate changes in the operation of heating system, changes in the number of occupants and activities, and faults in sensors. This is the first step in the ongoing commissioning, which is normally followed up by the identification of causes of such a change.

Figure 5.3 shows an example of such a comparison over the time interval from January 1 to March 31, 2015, when trained model developed in December 2014 was used for the predictions, without retraining (i.e., static window technique). For instance, when the daily average outdoor air temperature is -20ºC, the daily space heating energy demand of house A is predicted to be 1.6 MJ/m^2 (red line in Figure 5.3). At the same daily average outdoor air temperature, the measurements show the daily space heating energy demand is between 1.1 and 1.8 MJ/m^2. In most days, the measured space heating energy demand is lower in house A than the benchmarks.
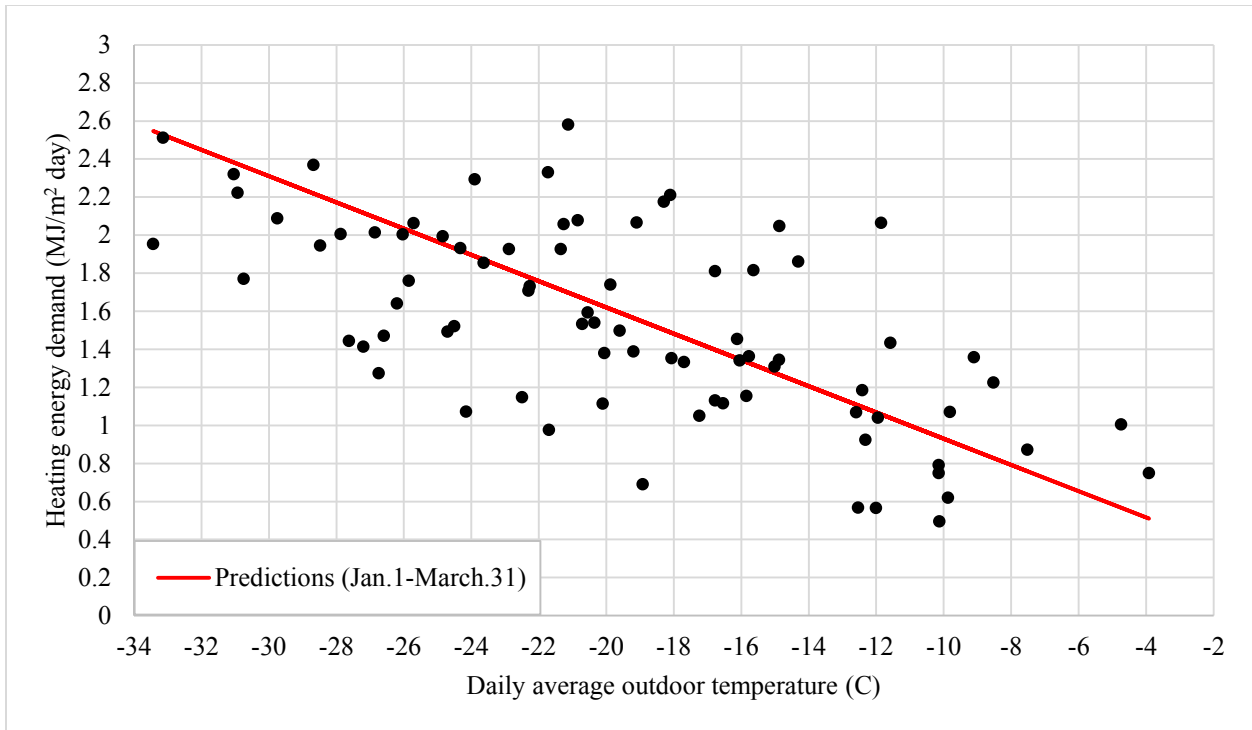
Figure 5.3: Predictions of the daily heating energy demand of house A using static window, and measurements from January 1 to March 31, 2015
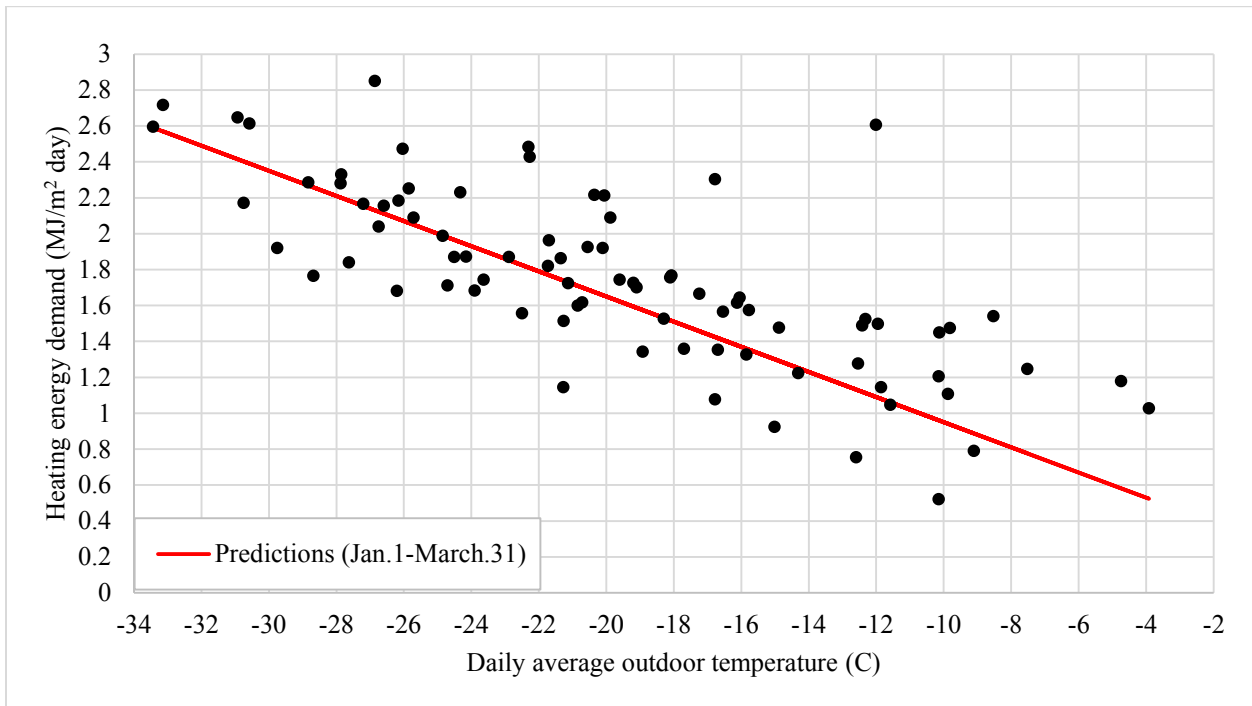
Figure 5.4: Predictions of the daily heating energy demand of house B using static window, and measurements from January 1 to March 31, 2015

Two statistical indices, RMSE and CV(RMSE), are used to quantify the difference between the measurements of the daily space heating energy demand and the benchmarks of house A and house B (Table 5.2 and Table 5.3). In the case of House A, the CV(RMSE) values are higher than the corresponding values over the testing period, and also higher than the criterion of 30% that shows a significant variation, especially starting with January 26 (augmented window technique) and February 9 (static window technique).

In the case of House B, the CV(RMSE) values over the application period are lower than 30% (i.e., between 21 and 23%), however higher than the values over the testing period. The results indicate more significant changes in the operation of heating system of house A compared with house B.

Table 5.2: Statistical indices of the difference between measurements and predictions over the application period, when using the static window technique

| House | Application period | Statistical indices over the application period | |
		RMSE (MJ/m² day)	CV(RMSE) (%)
A	Jan 1-March 31	0.42	27
	Jan 12-March 31	0.4	27
	Jan 26-March 31	0.4	28
	Feb 9-March 31	0.44	34
	Feb 23-March 31	0.44	36
	March 9-March 31	0.46	37
B	Jan 1-March 31	0.36	21
	Jan 12-March 31	0.37	21
	Jan 26-March 31	0.39	22
	Feb 9-March 31	0.4	24
	Feb 23-March 31	0.31	21
	March 9-March 31	0.25	17

Table 5.3: Statistical indices of the difference between measurements and predictions over the application period, when using the augmented window technique

House	Application period	Statistical indices over the application period	
		RMSE (MJ/m² day)	CV(RMSE) (%)
A	Jan 1-March 31	0.42	27
	Jan 12-March 31	0.41	28
	Jan 26-March 31	0.46	32
	Feb 9-March 31	0.50	38
	Feb 23-March 31	0.50	41
	March 9-March 31	0.47	37
B	Jan 1-March 31	0.36	21
	Jan 12-March 31	0.37	21
	Jan 26-March 31	0.37	21
	Feb 9-March 31	0.37	23
	Feb 23-March 31	0.29	20
	March 9-March 31	0.31	21

5.1.5. Estimation of total heating energy demand of application period

The benchmarking model can be used along with the outdoor air temperature bins to estimate the total heating energy demand [60] over a given application period (Equation 5.6).

$$E_P = \sum_{i=1}^{n}(a \cdot T_O + b) \cdot BIN(T_O) \ [MJ/m^2] \qquad\qquad 5.6$$

where, E_P is the predicted total energy demand based on the benchmarking model; a is the slope and b is the intersect of the non-weather dependent energy demand, both identified during the training phase (Table 5.1); T_O is the daily average outdoor temperature (°C); and $BIN(T_o)$ is the number of days of occurrence of the outdoor air temperature bin having T_O as centre. Table 5.4 shows an example of the temperature bins over three months of heating season. For each application period, a similar table was used.

Table 5.4: Outdoor air temperature bins at Inuvik from January 1st to March 31st, 2015

Temperature BIN (C)	T_o (ºC)	Number of days
-33.5 , -32.5	-33	2
-32.5 , -31.5	-32	-
-31.5 , -30.5	-31	3
-30.5 , -29.5	-30	1
-29.5 , -28.5	-29	1
-28.5 , -27.5	-28	4
-27.5 , -26.5	-27	4
-26.5 , -25.5	-26	4
-25.5 , -24.5	-25	3
-24.5 , -23.5	-24	4
-23.5 , -22.5	-23	1
-22.5 , -21.5	-22	5
-21.5 , -20.5	-21	7
-20.5 , -19.5	-20	5
-19.5 , -18.5	-19	3
-18.5 , -17.5	-18	4
-17.5 , -16.5	-17	4
-16.5 , -15.5	-16	5
-15.5 , -14.5	-15	3
-14.5 , -13.5	-14	1
-13.5 , -12.5	-13	2
-12.5 , -11.5	-12	6
-11.5 , -10.5	-11	-
-10.5 , -9.5	-10	5
-9.5 , -8.5	-9	2
-8.5 , -7.5	-8	1
-7.5 , -6.5	-7	-
-6.5 , -5.5	-6	-
-5.5 , -4.5	-5	1
-4.5 , -3.5	4	1
-3.5 , -2.5	-3	-
Total	-	82

Tables 5.5 and 5.6 summarize the comparison of the predicted heating energy demand for houses A and B over different time intervals, by using the static and augmented techniques for training the benchmarking models, with the measurements. When the models are trained in December 2014 and used for the prediction of rest of heating season from January to March (for static and augmented window techniques), the difference is 7.8% (house A) and 3.6% (house B). However,

this result indicates that, on the average over a longer prediction time interval, the measurements of total heating energy demand are close with the predictions.

For both model training techniques and all application time intervals, the measurements of total heating energy demand of House A are lower than the predictions, while in the case of House B the measurements are higher than the predictions. There is a clear difference between the two houses when the augmented window technique is used: the benchmarking model of House A overestimates the measurements by 13.2% to 23.6%, while the benchmarking model of House B underestimates by 3.5% to 11.3%, except the last application period when it overestimates by 12.5%.

In this case study, the predictions by the benchmarking models, which are retrained with the augmented window technique, are useful for the comparison with measurements over shorter time intervals.

The comparison between measurements and predictions reveal more significant changes in the operation of heating system of House A compared with house B, and thus converges to the same conclusion as presented in section 5.1.4. For instance, the measurements over the prediction time interval of March 2 to March 31 are lower than the predictions by 23.6% (House A) and 12.5% (House B).

Table 5.5: Predicted versus measured heating energy demand for houses A and B with the static window technique

Data sets		Measured space heating demand (MJ/m^2)		Predicted space heating demand (MJ/m^2)		(Predicted – Measured)/Measured (%)	
Training	Prediction	House A	House B	House A	House B	House A	House B
Dec 1-Dec 21, 2014	Jan 1- March 31, 2015	136.26	156.08	147.84	150.56	7.8	-3.6
	Jan 12-March 31, 2015	113.56	133.78	126.88	129.22	10.5	-3.5
	Jan 26-March 31, 2015	96.17	116.66	101.02	102.9	4.8	-13.4
	Feb 9-March 31, 2015	67.06	84.21	73.38	74.76	8.6	-12.6
	Feb 23-March 31, 2015	43.87	55.09	49.45	50.4	11.2	-9.3
	March 2-March 31, 2015	27.7	33.87	31.15	34.8	11	2.7

Table 5.6: Predicted versus measured heating energy demand for houses A and B with the

augmented window technique

Data sets		Measured space heating demand (MJ/m²)		Predicted space heating demand (MJ/m²)		(Predicted – Measured)/Measured (%)	
Training	Prediction	House A	House B	House A	House B	House A	House B
Dec 1, 2014- Dec 21, 2014	Jan 1- March 31, 2015	136.26	156.08	147.84	150.56	7.8	-3.6
Dec 1, 2014- Jan 4, 2015	Jan 12- March 31, 2015	113.56	133.78	134.11	129.22	15.3	-3.5
Dec 1, 2014- Jan 18, 2015	Jan 26- March 31, 2015	96.17	116.66	110.85	104.82	13.2	-11.3
Dec 1, 2014- Feb 1, 2015	Feb 9- March 31, 2015	67.06	84.21	82.58	76.84	18.8	-9.6
Dec 1, 2014- Feb 15, 2015	Feb 23- March 31, 2015	43.87	55.09	56.84	52.46	22.8	-5
Dec 1, 2014- March 1, 2015	March 2- March 31, 2015	27.7	33.87	36.25	38.69	23.6	12.5

5.2. Conclusions

This section presented the development and use of the benchmarking models using static and augmented window techniques, from the measurements of space heating energy demand of two Inuvik houses from December 1, 2014 to March 31, 2015. The statistical indices over the testing period indicate that the trained benchmarking models have an acceptable accuracy, and thus can be used for the prediction purposes.

The benchmarking models are used to detect differences between the measurements of daily space heating energy demand and the expected values that are predicted by the benchmarking models. Large difference might indicate changes in the operation of heating system, changes in the number of occupants and activities, and faults in sensors. This is the first step in the ongoing commissioning, which is normally followed up by the identification of causes of such a change.

This section revealed that three weeks training data set of December 2014, using static window technique, provides an accurate benchmarking model of the daily space heating demand over the rest of heating season (January to March 2015). However, this result indicates that, on the average over a longer prediction time interval, the measurements of total heating energy demand are close with the predictions.

On the other hand, the predictions by the benchmarking models, which are retrained with the augmented window technique, are useful for the comparison with measurements over shorter time intervals.

6. PRINCIPAL COMPONENT ANALYSIS (PCA) METHOD FOR OUTLIER DETECTION AND VARIABLE IDENTIFICATION

6.1. PCA methodology

The method consists in the transformation of observations (measurements) of j-variables from the Building Automation System (BAS) into a reduced set of k-variables (k < j), which are known as Principal Components (PC) [61]. In other words, the observations of j-variables are projected into a k-dimensional PC-based space. The transformed observations in the PC-based space are named scores.

The matrix of training data set X_{tr} (i;j) is composed of i observations for each j variable. The data normalization is performed by using (Equation 6.1):

$$zX_{j,tr} = \frac{X_{j,tr} - \mu_{j,tr}}{\sigma_{j,tr}} \qquad\qquad 6.1$$

where: $zX_{j,tr}$ = the j-column of the normalized training data set

$X_{j,tr}$ = the j-column of the original training data set

$\mu_{j,tr}$ = the average value of the j-column of the original training data set

$\sigma_{j,tr}$ = the standard deviation of the j-column of the original training data

The matrix (i, j) of normalized values is then transformed into the matrix (j × j) of coefficients (Q), by using the PCA transformation available in Matlab [62]. The first column of matrix Q, corresponds to the first principal component (PC), the second column corresponds to the

second PC, and so on. The first row corresponds to the first variable listed in the original training data set, the second row corresponds to the second variable, and so on.

The matrix (F) of the projection of original measurements in the PC-based space, called scores, is created (Equation 6.2).

$$F_{tr} = zX_{j,tr} \cdot Q \qquad\qquad 6.2$$

The scores corresponding to the normal operation conditions form a cloud of points, which can be surrounded by a threshold or frontier. Different 2D, 3D or n-dimensional models can be used to analytically define the threshold. This study uses an ellipsoid threshold model (Equation 6.3). Those scores outside the threshold correspond to abnormal performance (Equation 6.4).

$$\sum_{j=1}^{k} \frac{f_{ij}^{\;2}}{(sx_j)^2} = 1 \qquad\qquad 6.3$$

$$\sum_{j=1}^{k} \frac{f_{ij}^{\;2}}{(sx_j)^2} > 1 \qquad\qquad 6.4$$

where: f_{ij} = the score of the i-observation along the j-principal direction

sx_j = the ellipsoid semi-axis along the j-principal direction

$sx_j = 2.\sigma_j$

σ_j = the standard deviation of the scores along the j-principal direction

6.2. Case study

This case study uses the measurements from October 1, 2014 to September 30, 2015 in two houses A and B of Inuvik, NWT, Canada. The measurements are recorded at 1-minute time step, from which the hourly and daily values are calculated to eliminate the noise in data.

Measurements of December 2014 (Table 6.1) related to the space heating and domestic hot water (DHW) are used as reference values for the training of the ellipsoid threshold model. The scope of this study is to identify those variables that might affect the heating and domestic hot water energy demands of February 2015 compared with the reference month of December 2014.

Table 6.1: Measured variables of space heating and DHW for houses A and B

System	Variables	Unit	Symbol
Space heating	Water flow rate (House A)	L/min	F_{hA}
	Water flow rate (House B)	L/min	F_{hB}
	Supply water temperature (House A)	ºC	$T_{supplyA}$
	Return water temperature (House A)	ºC	$T_{returnA}$
	Supply water temperature (House B)	ºC	$T_{supplyB}$
	Return water temperature (House B)	ºC	$T_{returnB}$
Domestic hot water	Water flow rate (House A)	L/min	F_{wA}
	Water flow rate (House B)	L/min	F_{wB}
	Supply water temperature (House A)	ºC	$T_{w\_supplyA}$
	Return water temperature (House A)	ºC	$T_{w\_returnA}$
	Supply water temperature (House B)	ºC	$T_{w\_supplyB}$
	Return water temperature (House B)	ºC	$T_{w\_returnB}$

6.2.1. Transformation of observations

After the data normalization of the hourly values, Q_h matrix for space heating and Q_w for domestic hot water are generated (Equations 6.5 and 6.6).

$$Q_h = \begin{pmatrix} 0.4540 & -0.1762 & -0.3506 & 0.6398 & -0.4686 & -0.1053 \\ -0.4144 & 0.3625 & 0.3404 & 0.7311 & 0.2131 & -0.0332 \\ 0.4655 & 0.0184 & 0.5559 & -0.0627 & 0.0952 & -0.6789 \\ 0.4716 & -0.0202 & 0.4949 & 0.0714 & 0.0287 & 0.7255 \\ 0.4178 & 0.3690 & -0.4548 & 0.0648 & 0.6914 & 0.0152 \\ 0.0920 & 0.8371 & -0.0211 & -0.2074 & -0.4971 & 0.0180 \end{pmatrix} \qquad 6.5$$

$$Q_w = \begin{pmatrix} -0.4150 & 0.0034 & 0.7218 & 0.0212 & 0.4969 & 0.2439 \\ -0.4299 & -0.1750 & -0.6184 & 0.1394 & 0.6028 & -0.1393 \\ 0.1135 & 0.6607 & -0.1587 & 0.5698 & 0.0801 & 0.4409 \\ 0.5530 & -0.2760 & -0.1345 & -0.3326 & 0.3877 & 0.5822 \\ 0.1681 & 0.6476 & 0.0025 & -0.5333 & 0.3446 & -0.3862 \\ 0.5440 & -0.1930 & 0.2311 & 0.5103 & 0.3381 & -0.4885 \end{pmatrix} \qquad 6.6$$

where the rows correspond to the variables listed in Table 6.1, and the columns correspond to each principal component. For instance, $Q_{h11} = 0.4540$ is the coefficient of water flow rate for space heating of house A that is used by the first principal component.

Previous studies [61, 63-65] suggested that the number of PCs should be selected in such a way to explain at least 75% to 90% of minimum cumulative variance in the initial data set. This study uses the first two PCs ($k = 2$) that contain about 89% of cumulative variance for the space heating (Figure 6.1) and around 70% of cumulative variance for domestic hot water, and also facilitates the 2D graphical representation of the PC-based space.
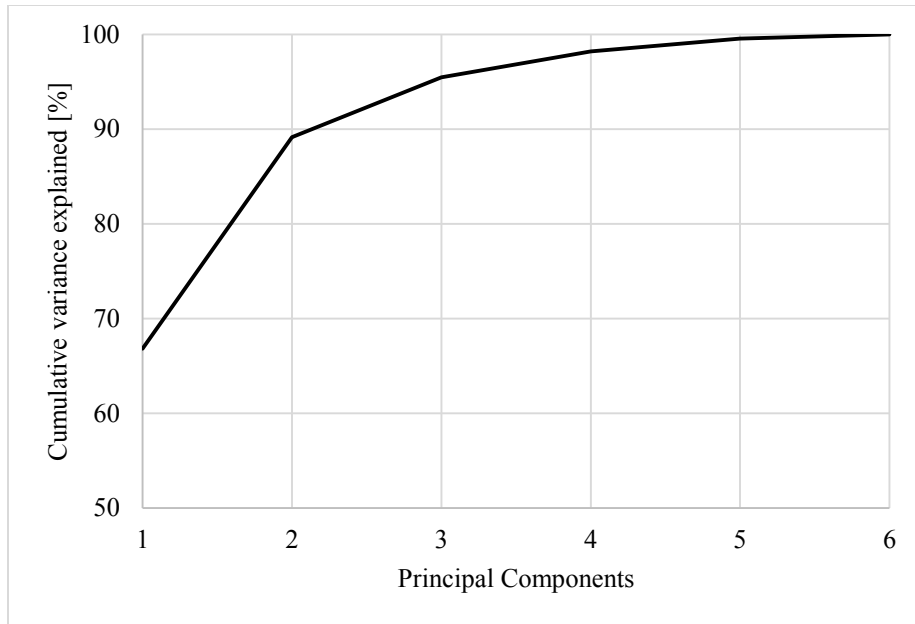
Figure 6.1: Cumulative variance in the initial data set of December 2014 versus the number of

PCs for space heating
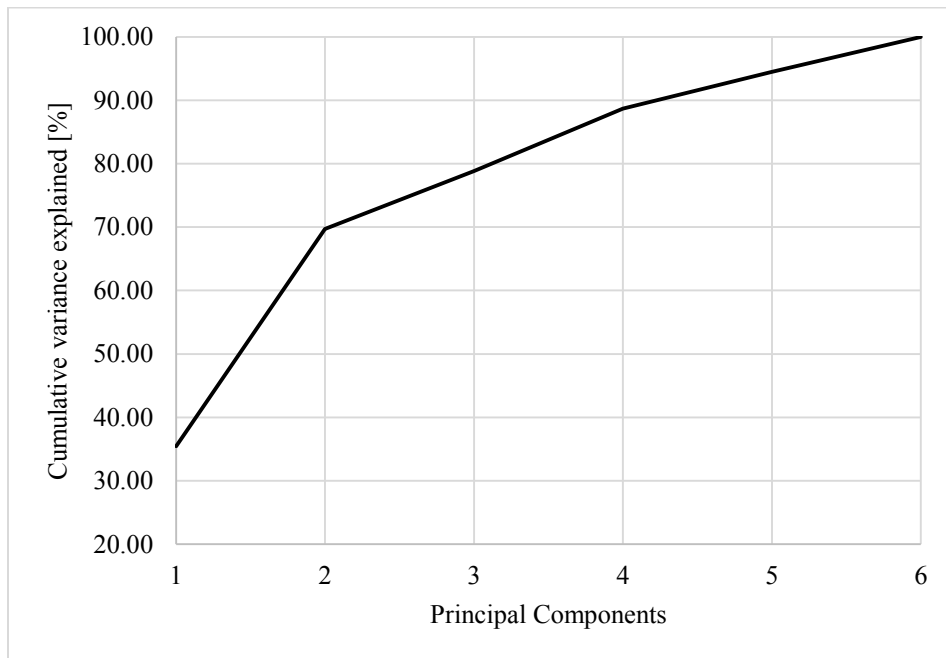
Figure 6.2: Cumulative variance in the initial data set of December 2014 versus the number of

PCs for DHW

6.2.2. Ellipsoid threshold model

Figure 6.3 and Figure 6.4 show the scores distribution and the threshold model in the PC-based space, for the space heating and domestic hot water of houses A and B, respectively, by using the first two PCs (PC#1 and PC#2).

The scores inside the ellipsoid indicate the normal operation, while those outside the ellipsoid are identified as outliers that correspond to abnormal performance. Out of total number of 406 scores for space heating, there are 56 outliers or about 14% in the PC#1-PC#2 space, and out of 194 scores for DHW, there are 29 outliers (15%) in the PC#1-PC#2 space.
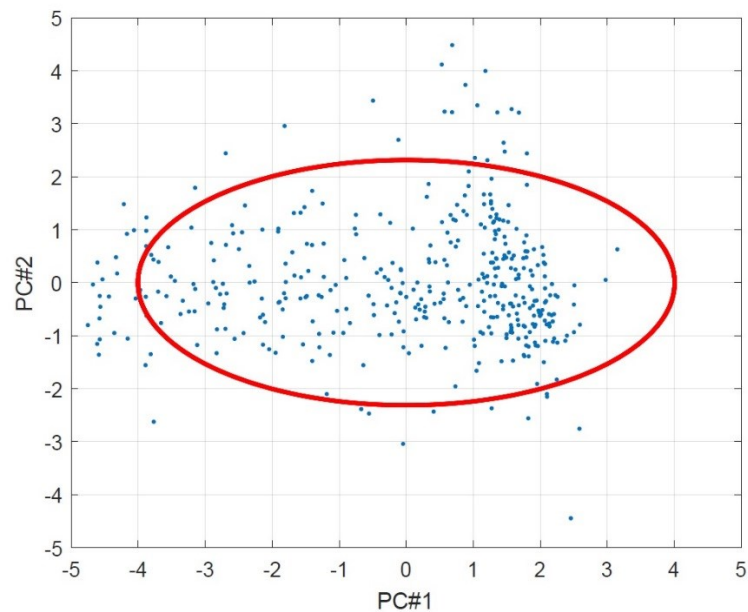
Figure 6.3: Scores distribution in the PCs-based space (PC#1 and PC#2) for space heating of houses A and B in December 2014
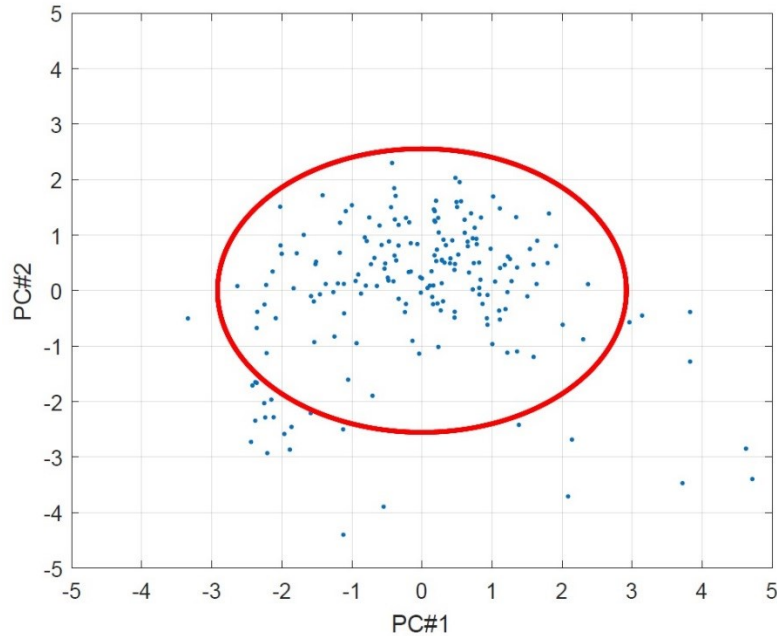
Figure 6.4: Scores distribution in the PCs-based space (PC#1 and PC#2) for DHW of houses A and B in December 2014

6.2.3. Variables identification

Once the outliers are identified in the PC-based space, the next phase is the identification of those variables from Table 1 that might generate the outliers.

For each variable in Table 1 the following steps are undertaken, using as an example, $T_{supplyB}$, which is the fifth variable in Table 1 and Q_h matrix (Equation *6.5*):

(1) In the PC-based space (PC#1 – PC#2) (Figure 43), a line is drawn through the origin and the point P of coordinates; $Q_{h51} = 0.4178$ (i.e., for PC#1) and $Q_{h52} = 0.369$ (for PC#2);

(2) The Euclidean distance between each outlier (e.g., point S) and the zero-value of $T_{supplyB}$ axis is calculated (Equation 6.8).

(3) The Euclidian distance is then calculated for each outlier with respect to all other variables (Table 17) for space heating of houses A and B.

(4) The variable with the highest Euclidean distance for each outlier indicate the variable that might have the highest impact on the abnormal performance.
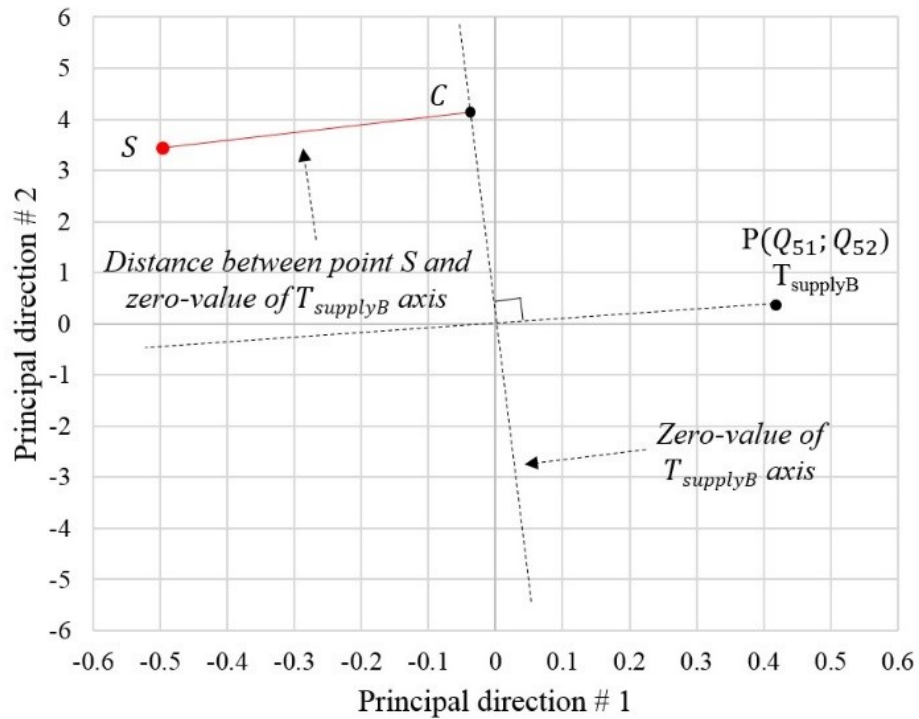
Figure 6.5: Euclidean distance of the outlier (S) from the zero-value of $T_{supplyB}$ axis in the PC#1-PC#2 space for space heating

The Euclidean distance $\overline{SC}$ of the outlier S is calculated as follows;

$$\overline{SC} = \sqrt{(x_s - x_c)^2 + (y_s - y_c)^2} \qquad\qquad 6.7$$

where:

$$x_C = \left(\frac{y_p}{x_p} \cdot x_s - y_s\right) \cdot \frac{x_p \cdot y_p}{x_p^2 + y_p^2} \qquad\qquad 6.8$$

$$y_C = -\frac{x_p}{y_p} \cdot x_c \qquad\qquad 6.9$$

where: $\overline{SC}$ = the Euclidean distance

x_C and y_C = the coordinates of the projection of outlier S on the zero-value axis

of variable

x_S and y_S = the coordinates of the outlier S in the PC#1 - PC#2 space

x_P = ($Q_{5,1}$) the coordinates of point P from the Q matrix

y_P = ($Q_{5,2}$) the coordinates of point P from the Q matrix

The number of occurrences of the first highest Euclidean distance for each variable for space heating and domestic hot water (Tables 18 and 19) reveal that the measurements of the temperature of supply water for space heating of house A ($T_{supplyA}$), and of the return temperature of water for space heating for house B ($T_{returnB}$) are responsible for about 27% and 29% of outliers. Moreover, measurements of the flow rate of water for domestic hot water for house B is responsible for 31% of outliers, and each of return temperature of water for house A and supply temperature of water for house B are responsible for 24% of outliers.

Table 6.2: Variables with the highest impact on the outliers for space heating for houses A and B in December 2014

Case	Variables	December 2014	
		1st highest Euclidean distance	
Space heating	F_{hA}	6	10.7%
	F_{hB}	8	14.3%
	$T_{supplyA}$	15	26.8%
	$T_{returnA}$	5	8.9%
	$T_{supplyB}$	6	10.7%
	$T_{returnB}$	16	28.6%
Total outliers		56 (100%)	

Table 6.3: Variables with the highest impact on the outliers for DHW for houses A and B in December 2014

Case	Variables	December 2014	
		1st highest Euclidean distance	
Domestic hot water	F_{wA}	3	10.3%
	F_{wB}	9	31%
	$T_{w\_supplyA}$	1	3.4%
	$T_{w\_returnA}$	7	24.1%
	$T_{w\_supplyB}$	7	24.1%
	$T_{w\_returnB}$	2	6.9%
Total outliers		29 (100%)	

6.2.4. Application of the trained ellipsoid threshold model on new data set

The trained ellipsoid threshold model developed with data of December 2014, considered to be the reference month, is now applied to measurements of February 2015, called the application data set. The normalized values of the new data set are calculated with Equation $6.10$6.10.

$$zX_{j.ap} = \frac{X_{j.ap} - \mu_{j,tr}}{\sigma_{j,tr}}$$

6.10

where: $zX_{j.ap}$ = the j-column of the normalized application data set

$X_{j.ap}$ = the j-column of the new data set

$\mu_{j,tr}$ = the average value of the j-column of the training data set of December 2014

$\sigma_{j,tr}$ = the standard deviation of the j-column of the training data set of December 2014

The F matrix of scores is calculated with Equation 6.11 and displayed in

Figure 6.6.

$$F_{ap} = zX_{ap}.Q$$

6.11

where: Q = the matrix which is given in Equations 6.5 and 6.6 for the training data set of December 2014, for space heating and domestic hot water

77

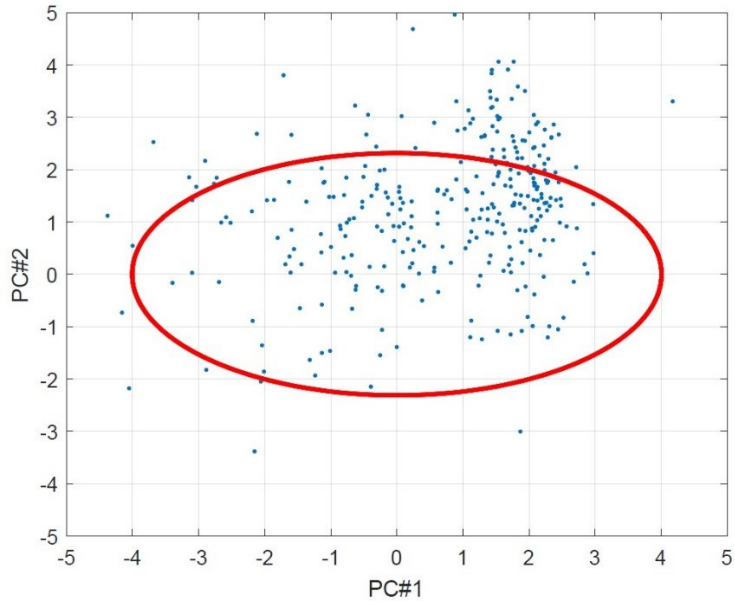*Figure 6.6: Scores distribution in the PCs-based space (PC#1 and PC#2) for space heating of houses A and B in February 2015, compared with the trained ellipsoid threshold model from data of December 2014*
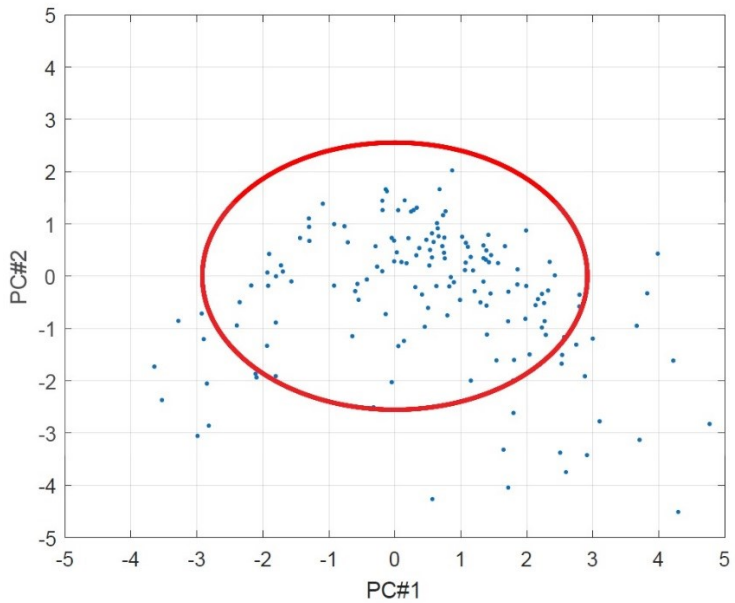
Figure 6.7: Scores distribution in the PCs-based space (PC#1 and PC#2) for DHW of houses A and B in February 2015, compared with the trained ellipsoid threshold model from data of December 2014

Overall the measurements of February 2015 led to 94 outliers compared with only 56 in December 2014 for space heating, and 35 outliers in February respect to 29 in December 2014 for DHW. When the first Euclidean distance is considered (Table 6.4), the supply and return water temperature for space heating of house B ($T_{supplyB}$) and ($T_{returnB}$) are responsible for about 46% and 37% of outliers, respectively. For DHW, water flow rate of house B (F_{wB}) and return temperature of water for house A ($T_{w\_returnA}$). The outliers could be generated by faults or by changes of the operation conditions due to changes of thermostat set point, or changes due to number and activities of people inside the house activities.

Table 6.4: Variables with the highest impact of the outliers for space heating for houses A and B in February 2015

Case	Variables	February 2015 1st highest Euclidean distance	
Space heating	F_{hA}	3	3%
	F_{hB}	11	12%
	$T_{supplyA}$	1	1%
	$T_{returnA}$	1	1%
	$T_{supplyB}$	43	46%
	$T_{returnB}$	35	37%
Total outliers		94 (100%)	

Table 6.5: Variables with the highest impact of the outliers for DHW for houses A and B in February 2015

Case	Variables	February 2015	
		1st highest Euclidean distance	
Domestic hot water	F_{wA}	2	5.7%
	F_{wB}	11	31.4%
	$T_{w\_supplyA}$	3	8.6%
	$T_{w\_returnA}$	15	42.9%
	$T_{w\_supplyB}$	1	2.9%
	$T_{w\_returnB}$	3	8.6%
Total outliers		35 (100%)	

6.3. Discussion

The water temperatures $T_{supplyB}$ and $T_{returnB}$ for space heating and F_{wB} and $T_{w\_returnA}$ for domestic hot water are identified by the PCA method as the variables that generated the outliers in the PC-based space in February 2015. The outliers identified by the PCA method are displayed on the graphs of hourly supply water temperature of house B (Figure 6.8) and return water temperature of house B (Figure 6.9) for space heating, and water flow rate of house B (Figure 6.10) and return temperature of water (Figure 6.11) for domestic hot water. Those outliers are displayed at the border of the data clouds. The use of 2nd highest Euclidean distance in the PCA method might reveal other abnormal values.

Figure 6.8: Hourly supply water temperature for house B for space heating versus hourly outdoor temperature in February 2015
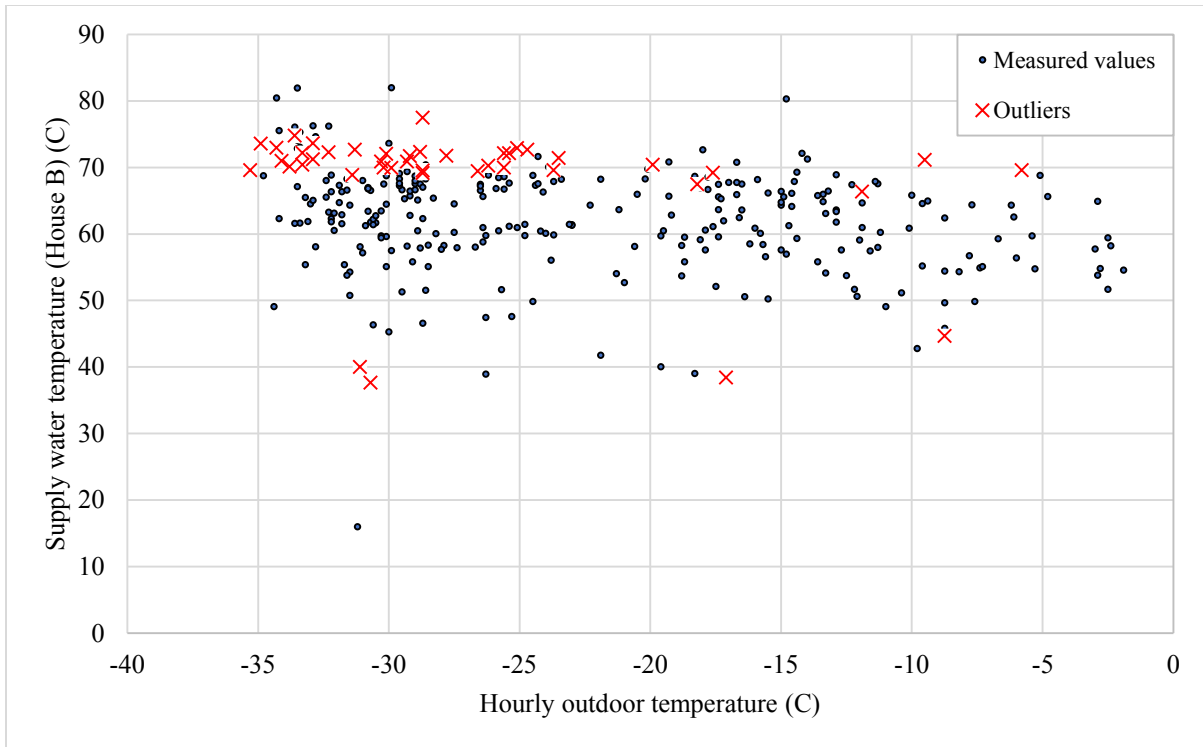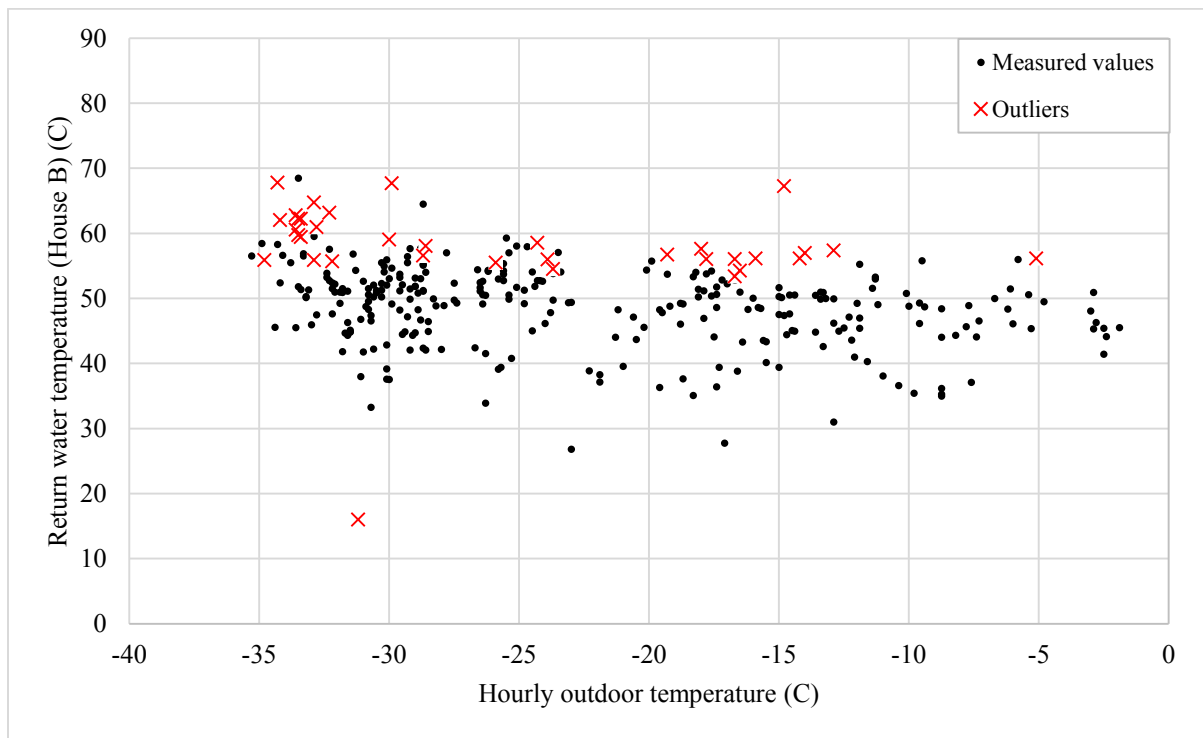

Figure 6.9: Hourly return water temperature for house B for space heating versus hourly outdoor temperature in February 2015
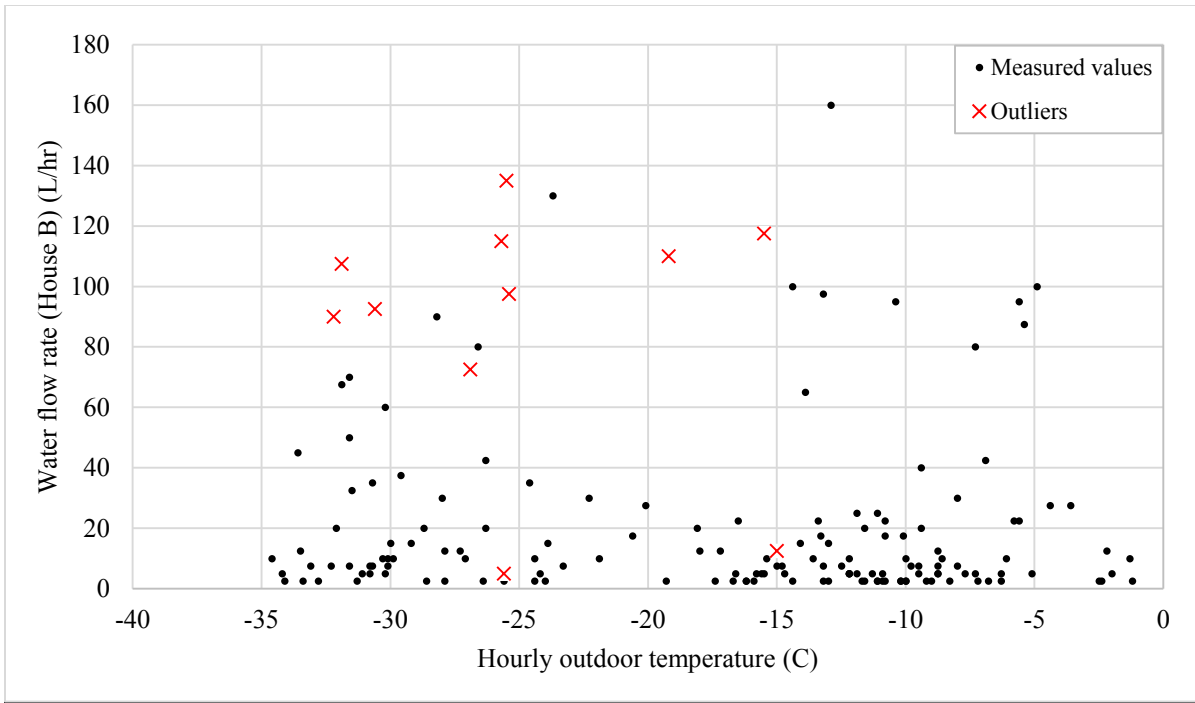
Figure 6.10: Hourly water flow rate for house B for DHW versus hourly outdoor temperature in February 2015
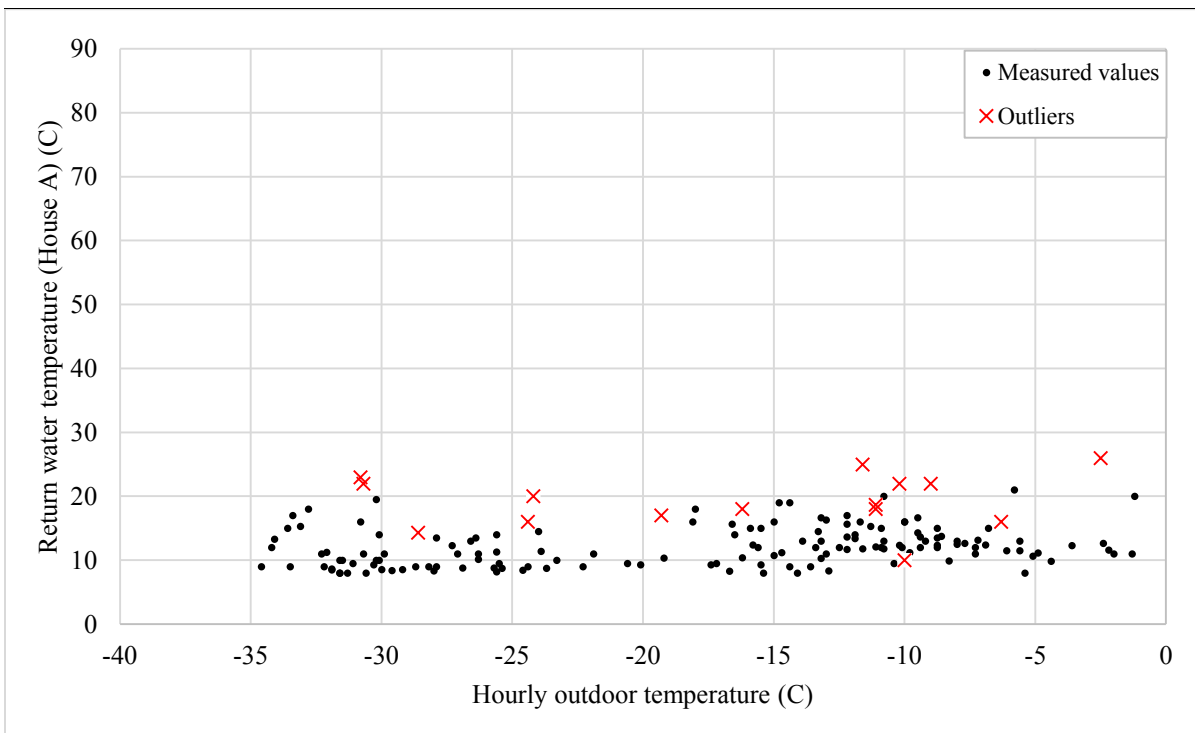

Figure 6.11: Hourly return water temperature for house B for DHW versus hourly outdoor temperature in February 2015

To validate the PCA results, a modified data set is derived in which the abnormal values of those two water temperatures, $T_{supplyB}$ and $T_{returnB}$ of February 2015, which are outside the range given by (Equation 6.12) are removed from the data file. Then, the modified application data set of February 2015 is used by the PCA method.

$$\mu_{j,tr} - 2 \cdot \sigma_{j,tr} < X_{j,app} < \mu_{j,tr} + 2 \cdot \sigma_{j,tr} \qquad\qquad 6.12$$

As a result of removing the abnormal values of $T_{supplyB}$ and $T_{returnB}$ for space heating, and F_{wB} and $T_{w\_returnA}$ for domestic hot water, the number of outliers is reduced in the PC#1-PC#2 based space (Table 6.6 and Table 6.7). This result proves that the two temperatures $T_{supplyB}$ and $T_{returnB}$ for space heating and F_{wB} and $T_{w\_returnA}$ for DHW are the cause of the outliers identified by the PCA method.

Table 6.6: Number of outliers for each variable of space heating in February 2015 with original and modified data sets

Case	Variables	Original data set	Modified data set
		1st highest Euclidean distance	1st highest Euclidean distance
Space heating	F_{hA}	3	3
	F_{hB}	11	9
	$T_{supplyA}$	1	0
	$T_{returnA}$	1	1
	$T_{supplyB}$	43	5
	$T_{returnB}$	35	9
Total outliers		94	27

Table 6.7: Number of outliers for each variable of DHW in February 2015 with original and modified data sets

Case	Variables	Original data set	Modified data set
		1st highest Euclidean distance	1st highest Euclidean distance
Domestic hot water	F_{wA}	2	0
	F_{wB}	11	2
	$T_{w\_supplyA}$	3	6
	$T_{w\_returnA}$	15	5
	$T_{w\_supplyB}$	1	3
	$T_{w\_returnB}$	3	2
Total outliers		35	18

6.4. Conclusions

The PCA-based method for the detection of outliers, and the identification of variables was applied in this study to the measurements from two houses, recently built in Inuvik, NWT, Canada. Measurements of December 2014 related to the space heating and domestic hot water are used as reference values for the training of the ellipsoid threshold model. The supply and return water temperatures for house B for heating energy demand, and for domestic hot water, water flow rate for house B, and return temperature of water for house A, were identified as the main sources of outliers in February 2015. The identification of variables with abnormal values were compared with two different approaches: the graphical representation of hourly values, and the use of a modified data set. The two approaches identified the water temperatures, $T_{supplyB}$ and $T_{returnB}$ for space heating, and F_{wB} and $T_{w\_returnA}$ for domestic hot water as the main sources of outliers in February 2015 by the PCA method.

The PCA-based method for fault detection and identification should be implemented in the BAS for the ongoing commissioning of heating systems, to help the building operator to take timing actions.

7. CONCLUSIONS

In this research, energy performance analysis of two semi-detached houses located in Inuvik, Northwest Territories of Canada was conducted with every one-minute measured values.

The two houses A and B in Inuvik with 9,769 HDD (ºC-day) that use 145.5 kWh/(m² year) of natural gas perform better in terms of space heating energy demand than the two low-energy houses in Greenland with 8,276 HDD (ºC-day), which use 90 and 140 kWh/(m² year), respectively, because those two houses in Greenland are in a "warmer" weather, with about 1,000 HDD (ºC-day) lower than in Inuvik.

Total energy demand for space heating and domestic hot water of both houses, which must be supplied by the natural gas boiler, is 122.4 kWh/(m² year), and the annual natural-gas energy use is 178.2 kWh/(m² year).

The annual average thermal efficiency of the boiler is 0.69, compared with manufacturer rated AFUE (Annual Fuel Use Efficiency) efficiency of 0.96.

Total annual solar hot water production of 1.7 kWh/(m² year) is negligible (7.5%) compared with the annual domestic hot water energy demand of 22.6 kWh/(m² year). The reduction of total natural gas use can be achieved by increasing the contribution of solar system to the preparation of domestic hot water.

Total annual electricity produced by the PV panels of 21 kWh/(m² year) is 20.8% of the annual electricity use of 101 kWh/(m² year).

The sensible thermal effectiveness of the HRV has an average value of 0.72 from daily data, which is lower than the manufacturer's specifications of 0.83 at 0ºC and 0.89 at -25ºC.

Daily energy performance values are more suitable for further analysis, due to less fluctuations and dispersions compare to hourly values, and more observations in a specific period compared with monthly values, therefore, it will give more information.

In this thesis, the energy demand signatures were developed as benchmarking models of daily space heating energy demand in houses A and B, using daily values with static and augmented window techniques for retraining. The benchmarking model trained as a static window with three weeks of data in December 2014, was an acceptable model for the prediction of heating energy demand of the rest of heating season (Jan.1 to March.31, 2015). However, this result indicates that, on the average over a longer prediction time interval, the measurements of total heating energy demand are close with the predictions. The predictions by the benchmarking models, which are retrained with the augmented window technique, are useful for the comparison with measurements over shorter time intervals.

This research expanded an approach proposed by Cotrufo and Zmeureanu [43] for the use of PCA-based method for the outliers` detection and identification of variables which are the main sources of outliers for space heating and domestic hot water systems. It was concluded that, supply and return water temperatures for house B for space heating system, and water flow rate of house B and return water temperature for house A in domestic hot water system, are the main sources of abnormal performance in February 2015.

7.1. Contributions

After completion of this thesis, it is noteworthy to mention the following contributions:

1. Development of benchmarking models with static and augmented window techniques using daily values of space heating energy demand in the ongoing commissioning of heating systems in houses within heating season for prediction of heating energy demand and detection of differences between measurements and expected predicted values.

2. Estimation the accuracy of the static and augmented window techniques in training the benchmarking models.

3. Verification of the use of PCA-based method for the identification of variables which are the major sources of abnormal performance in space heating and domestic hot water systems.

7.2. Future works

The presented method in this study for development of benchmarking models revealed a good potential for prediction of heating energy demand through the ongoing commissioning houses in northern Canada. Therefore, for expanding and verification of the proposed approach in this study, it is recommended to apply this methodology to other buildings with complex HVAC systems in order to detect the differences between measured and expected predicted values.

Another part of this study was expanding an approach for the application of PCA-based method for the identification of variables which are the main sources of outliers. Therefore, in future work it is recommended to focus on the verification of the proposed method for complex HVAC systems with many correlated physical variables, and the comparison of the identified faults with physical faults.

REFERENCES

[1] IEA. Key world statistics. 2017.

     https://www.iea.org/publications/freepublications/publication/KeyWorld2017.pdf

[2] eQUEST. Electric Power Research Institute. http://www.doe2.com/equest/.

[3] EnergyPlus. The United States Department of Energy. https://energyplus.net/.

[4] TRNSYS. Thermal energy system specialists. http://www.trnsys.com/.

[5] Li, Z., Y. Han, P. Xu. 2014. Methods for benchmarking building energy consumption

     against its past or intended performance: An overview. Applied Energy 124: 325-334.

[6] Chung, W. 2011. Review of building energy-use performance benchmarking

     methodologies. Applied Energy 88: 1470-1479.

[7] Karaguzel, O. T. 2011. Development of whole-building energy performance models as

     benchmarks for retrofit projects. IEEE. Phoenix, AZ, USA 2011.

     DOI: 10.1109/WSC.2011.6147810.

[8] Chung, W. 2012. Construction of benchmarking models using fuzzy linear regression

     techniques. 9th International conference of fuzzy systems and knowledge discovery.

     Sichuan, China. DOI: 10.1109/FSKD.2012.6233784.

[9] Monfet, D., R. Zmeureanu. 2012. Ongoing commissioning of water-cooled electric chillers

     using benchmarking models. Applied Energy 92: 99-108.

[10] Teyssedou, G., R. Zmeureanu, D. Giguere. 2013. Benchmarking model for the ongoing commissioning of the refrigeration systemof an indoor ice rink. Automation in Construction 35: 229-237

[11] Wang, E., Z. Shen, K. Grosskopf. 2014. Benchmarking energy performance of building envelopes through a selective residual-clustering approach using high dimensional dataset. Energy and Buildings 75: 10-22.

[12] Tremblay, V., R. Zmeureanu. 2014. Benchmarking models for the ongoing commissioning of heat recovery process in a central heating and cooling plant. Energy 70: 194-203.

[13] Fumo, N., M.A. Rafe Biswas. 2015. Regression analysis for prediction of residential energy consumption. Renewable and Sustainable Energy Reviews 47: 332-343.

[14] Capozzoli, A., M. S. Piscitelli, F. Neri, D. Grassi, G. Serale. 2016. A novel methodology for energy performance benchmarking of buildings by means of Linear Mixed Effect Model: The case of space and DHW heating of out-patient Healthcare Centres. Applied Energy 171: 592-607.

[15] Jeong, J., T. Hong, C. Ji, J. Kim, M. Lee, K. Jeong. 2016. Development of an integrated energy benchmark for a multi-family housing complex using district heating. Applied Energy 179: 1048-1061.

[16] Park, H. S., M. Lee, H. Kang, T. Hong, J. Jeong. 2016. Development of a new energy benchmark for improving the operational rating system of office buildings using various data-mining techniques. Applied Energy 173: 225-237.

[17] Pino- Mejias, R., A. Perez-Fagallo, C. Rubio-Bellido, J. A. Pulido-Arcas. 2017. Comparison of linear regression and artificial neural networks models to predict heating and cooling energy demand, energy consumption and CO2 emissions. Energy 118: 24-36.

[18] Arregi, B., R. Garay. 2017. Regression analysis of the energy consumption of tertiary buildings. Energy Procedia 122: 9-14.

[19] Shams Amiri, S., M. Mottahedi, S. Asadi. 2015. Using multiple regression analysis to develop energy consumption indicators for commercial buildings in the U.S. Energy and Buildings 109: 209-216.

[20] Korolija, I., Y. Zhang, L. Marjanovic-Halburd, V. I. Hanby. 2013. Regression models for predicting UK office building energy consumption from heating and cooling demands. Energy and Buildings 59: 214-227.

[21] Aghdaei, N., G. Kokogiannakis, D. Daly, T. McCarthy. 2017. Linear regression models for prediction of annual heating and cooling demand in representative Australian residential dwellings. Energy Procedia 121: 79-86.

[22] Liu, J., H Chen H, Liu J, Li Z, Huang R, Xing L, Wang J, Li G. An energy performance evaluation methodology for individual office building with dynamic energy benchmarks using limited information. Applied Energy 2017; 206: 193-205.

[23] Zhang, Y., Z. O`Neill, B. Dong, G. Augenbroe. 2015. Comparisons of inverse modeling approaches for predicting building energy performance. Building and Environment 86: 177-190.

[24] Abushakra, B., M. T. Paulus. 2016. An hourly hybrid multi-variate change-point inverse model using short-term monitored data for annual prediction of building energy performance, part I: Background (1404-RP). Science and Technology for the Built Environment 22: 976-983

[25] Abushakra, B., M.T. Paulus. 2016. An hourly hybrid multi-variate change-point inverse model using short-term monitored data for annual prediction of building energy performance, part II: Methodology (1404-RP). Science and Technology for the Built Environment 22: 984-995.

[26] Abushakra, B., M. T. Paulus.2016. An hourly hybrid multi-variate change-point inverse model using short-term monitored data for annual prediction of building energy performance, part III: Results and analysis (1404-RP). Science and Technology for the Built Environment 22: 996-1009.

[27] International Performance Measurement and Verification Protocol (IPMVP). Concepts and options for determining energy and water savings 1. Efficiency Valuation Organization, vol. 1, 2012.

[28] American Society of Heating Refrigerating and Air-Conditioning Engineers (ASHRAE), Measurement of energy and demand savings. ASHRAE Guideline 14-2002.

[29] Hammarsten, S. A critical appraisal of energy-signature models. 1987. Applied Energy 26 (2): 97-110.

[30] Rabl., A., A. Rialhe.1992. Energy signature models for commercial buildings: test with measured data and interpretation. Energy and Buildings 19: 143-154.

[31] Belussi, L., L. Danza. 2012. Method for the prediction of malfunctions of buildings through real energy consumption analysis: Holistic and multidisciplinary approach of energy signature. Energy and Buildings 55: 715-720.

[32] Yu, F. W., K.T. Chan. Energy signatures for assessing the energy performance of chillers. 2005. Energy and Buildings 37: 739-746.

[33] Westergren, K. E., H. Hogberg, U. Norlen. Monitoring energy consumption in single-family houses. 1999. Energy and Buildings 29: 247-257.

[34] Sjogren, J. U., S. Andersson, T. Olofsson. Sensitivity of the total heat loss coefficient determined by the energy signature approach to different time periods and gained energy. 2009. Energy and Buildings 41: 801-808.

[35] Zhang, Y., Z. O'Neill, T. Wagner, G. Augenbroe. 2013. An inverse model with uncertainty quantification to estimate the energy performance of an office building. 13th conference of International Building Performance Simulation Association. Chambery, France.

[36] Roth, K., D. Westphalen, J. Brodrick. 2008. Ongoing Commissioning. ASHRAE Journal. 50 (3): 66-71.

[37] Katipamula, S., M.R. Brambley. 2005. Methods for Fault Detection, Diagnostics, and Prognostics for Building Systems—A Review, Part 2 . HVAC & R Research 11 (1) :3-26.

[38] Jia, Y., T.A. Reddy. Characteristic Physical Parameter Approach to Modeling Chillers Suitable for Fault Detection, Diagnosis, and Evaluation. 2003. Solar Energy Engineering 125 (3): 258-265.

[39] Draper, N. R., H. Smith. Applied Regression Analysis, 2nd ed. 1981. New York, USA. John Wiley & Sons, Inc.

[40] Hadley, D. L., S.D. Tomich. 1986. Multivariate statistical assessment of meteorological influence on residential space heating. ACEEE (9).

[41] Xu, X., F. Xiao, S. Wang. 2008. Enhanced chiller sensor fault detection, diagnosis and estimation using wavelet analysis and principal component analysis methods. Applied Thermal Engineering 28: 226-237.

[42] Hu, Y., H. Chen, J. Xie, X. Yang, C. Zhou. 2012. Chiller sensor fault detection using a self-Adaptive Principal Component Analysis method. Energy and Buildings. 54: 252-258.

[43] Cotrufo, N. and R. Zmeureanu. 2016. PCA-based method of soft fault detection and identification for theongoing commissioning of chillers. *Energy and Buildings.* 130: 443-452.

[44] Gajjar, S., M. Kulahci, A. Palazoglu. 2016. Use of Sparse Principal Component Analysis (SPCA) for Fault Detection. IFAC-PapersOnLine.49 (7): 693-698.

[45] Beghi, A., R. Brignoli, L. Cecchinato, G. Menegazzo, M. Rampazzo, F. Simmini. 2016. Data-driven Fault Detection and Diagnosis for HVAC water chillers. Control Engineering Practice. 53: 79-91.

[46] Hu, Y., G. Li, H. Chen, H. Li, J. Liu. 2016. Sensitivity analysis for PCA-based chiller sensor fault detection. International journal of refrigeration. 63: 133-143.

[47] Hu, Y., H. Chen, G. Li, H. Li, R. Xu, J. Li. 2016. A statistical training data cleaning strategy for the PCA-based chillersensor fault detection, diagnosis and data reconstruction method. Energy and Buildings.112: 270-278.

[48] Guo, Y., G. Li, H. Chen, Y. Hu, H. Li, L. Xing, W. Hu. 2017. An enhanced PCA method with Savitzky-Golay method for VRF system sensor fault detection and diagnosis. *Energy and Buildings*. 142: 167-178.

[49] Guo, Y., G. Li, H. Chen, Y. Hu, H. Li, J. Liu, M. Hu, W. Hu. 2017. Modularized PCA method combined with expert-based multivariate decoupling for FDD in VRF systems including indoor unit faults. *Applied Thermal Engineering*. 115: 744-755.

[50] Canada Mortgage and Housing Corporation. ftp://ftp.cmhc-schl.gc.ca/chic-ccdh/Research_Reports-Rapports_de_recherche/eng_unilingual/Ca1%20MH%2014D21_w.pdf

[51] National Research Council of Canada. 1997. Model National Energy Code of Canada for Buildings. Ottawa, Canada.

[52] Intelligent Energy Europe, NorthPass. Very Low-Energy House Concepts in North European Countries. 2012.

[53] Naugler, T. Passivehouse. 2012. http://www.passivehousecanada.com/projects/naugler-house/

[54] Vladykova, P., C. Rode, J. Kragh, M. Kotol. Low-Energy House in Arctic Climate: Five Years of Experience. Journal of Cold Regions Engineering 26(3): 79-100.

[55] Rode, C., J. Kragh, E. Borchersen, P. Vladykova, S. Furbo, J. Dragsted. 2009. Performance of the Low-energy House in Sisimiut. Cold Climate HVAC.

[56] Simonson, C. 2005. Energy consumption and ventilation performance of a naturally ventilated ecological house in a cold climate. Energy and Buildings 37 (1): 23-35.

[57] Giovanni, R., S. A. Tiziano. 2006. Concerted Action Multigeneration Energy Systems with Locally Integrated Applications (CAMELIA) - Energy consumption of buildings in European Union. European Commission. Italy.

[58] Natural Resources of Canada. Survey of Household Energy Use 2011.

[59] American Society of Heating Refrigerating and Air-Conditioning Engineers (ASHRAE), Engineering analysis of experimental data. ASHRAE Guideline 2-2005.

[60] Zmeureanu, R. Assessment of the energy savings due to the building retrofit. 1990. Building and Environment 25 (2): 95-103.

[61] Cotrufo, N. and R. Zmeureanu. 2016. PCA-based method of soft fault detection and identification for theongoing commissioning of chillers. Energy and Buildings 130: 443-452.

[62] Mathworks/Statistics and Machine Learning Toolbox, Matlab. 2017: http://www.mathworks.com/help/stats/pca.html?searchHighlight=PCA&s_tid=doc_srchtitle.

[63] Morrison, P., F. Donald. 1976. Multivariate statistical method, 2nd ed. New York, USA.

[64] Ladd, J.W. and D.M. Driscoll. 1980. A comparison of objective and subjective means of weather typing: an example from west Texas. American Meteorological Society.19: 691-704.

[65] Jolliffe, I.T. 1986. Principal Component Analysis, *Springer*. New York, USA.

APPENDICES

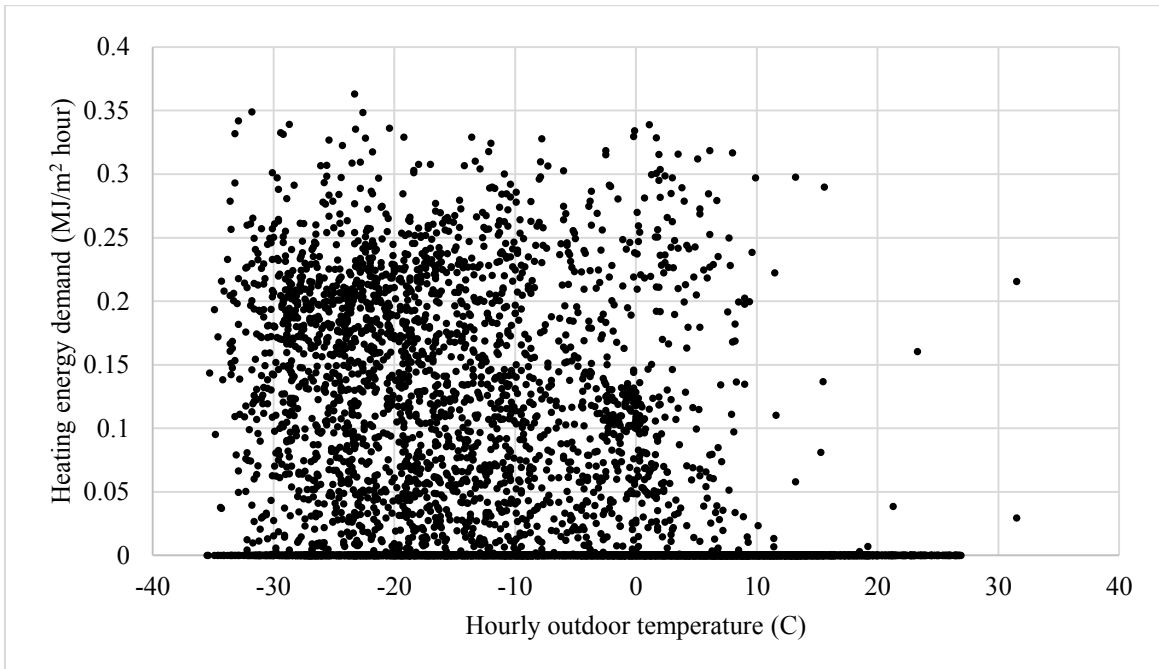APPENDIX A: Hourly variation of heating energy demand versus outdoor air temperature

Figure A. 1: Hourly heating energy demand in house A from October 2014 to September 2015
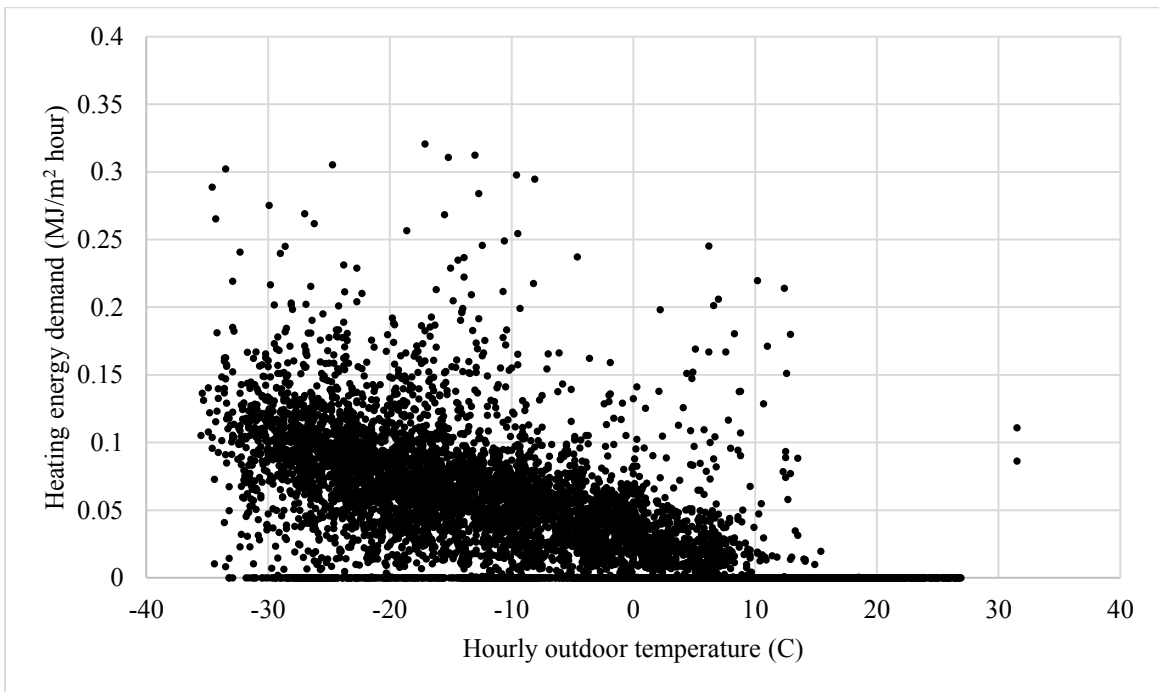
Figure A. 2: Hourly heating energy demand in house B from October 2014 to September 2015

APPENDIX B: Carpet plots of heating energy demand, domestic hot water energy demand, electrical use, solar hot water energy production and PV production in April 2018
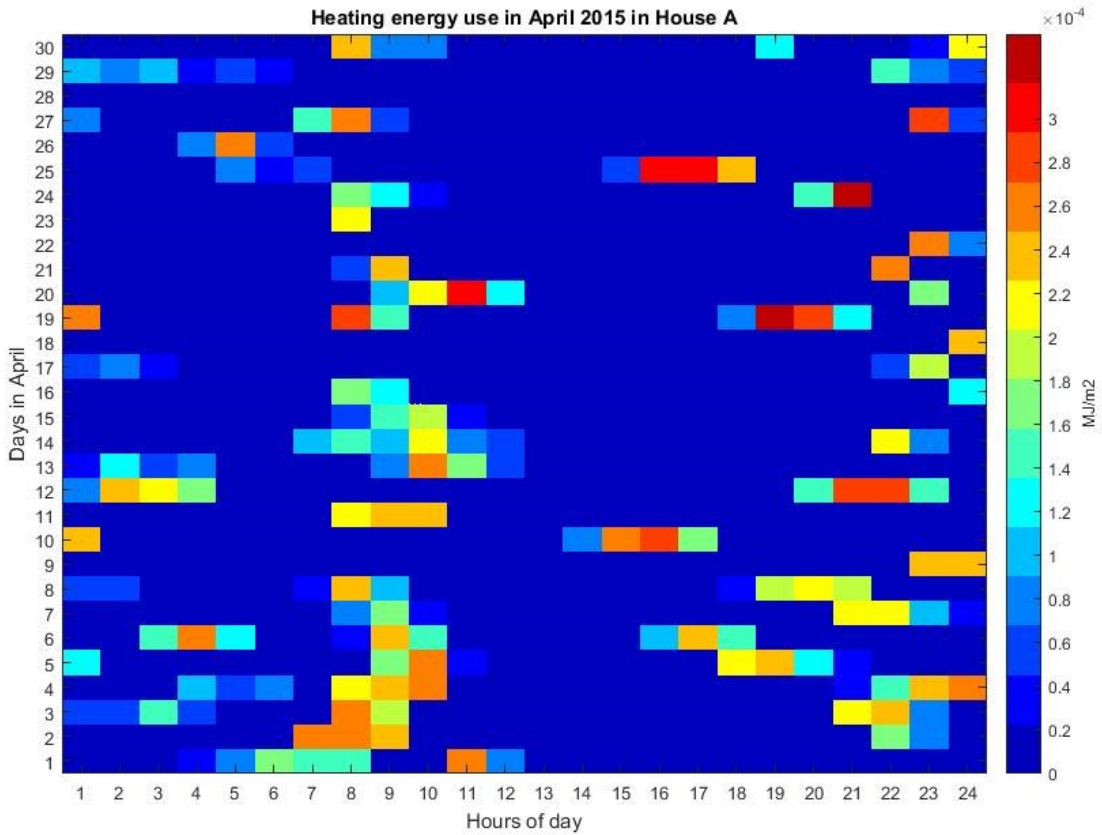
Figure B. 1: Hourly heating energy demand in House A in April 2015

The most heating energy demand period in April 2015 is between 7 to 11 A.M and 6 to 11 P.M.
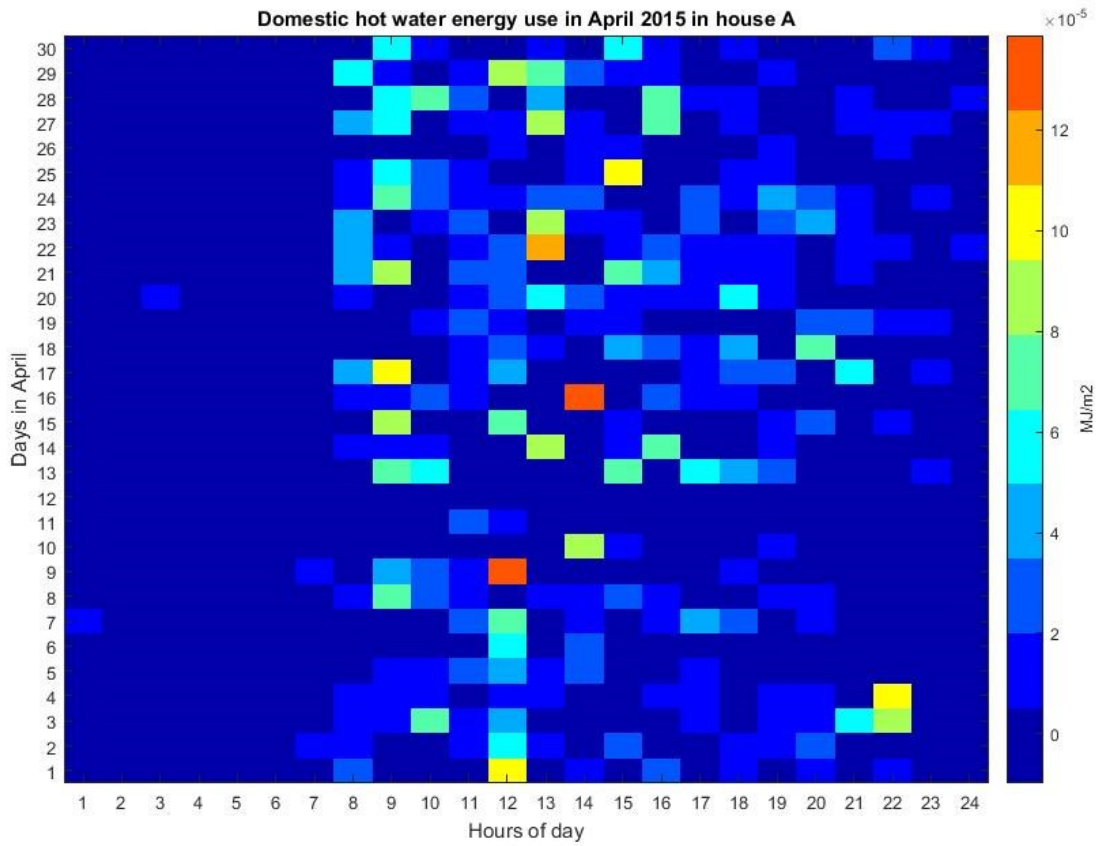
Figure B. 2: Hourly domestic hot water energy demand in House A in April 2015

Demand for domestic hot water is between 8 A.M to 10 P.M.
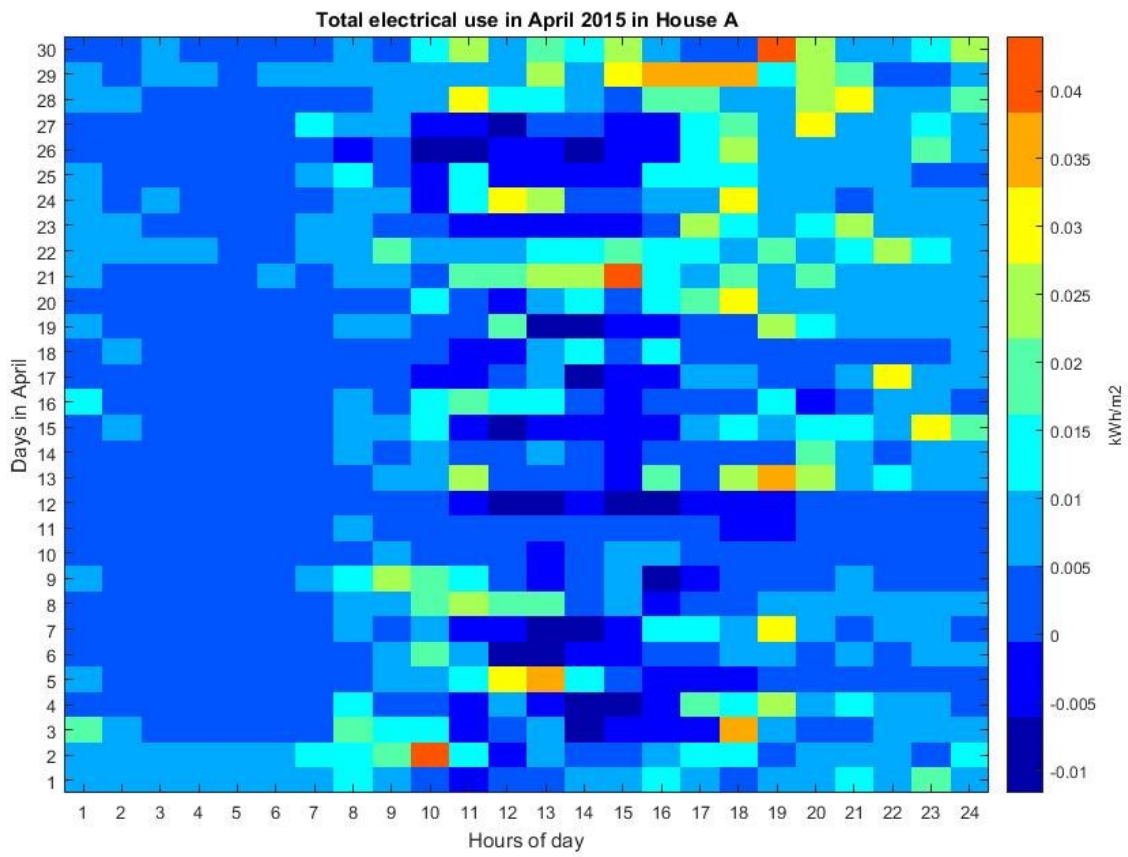
Figure B. 3: Hourly total electrical use in House A in April 2015

Electrical use in April is mostly between 4 to 11 P.M.
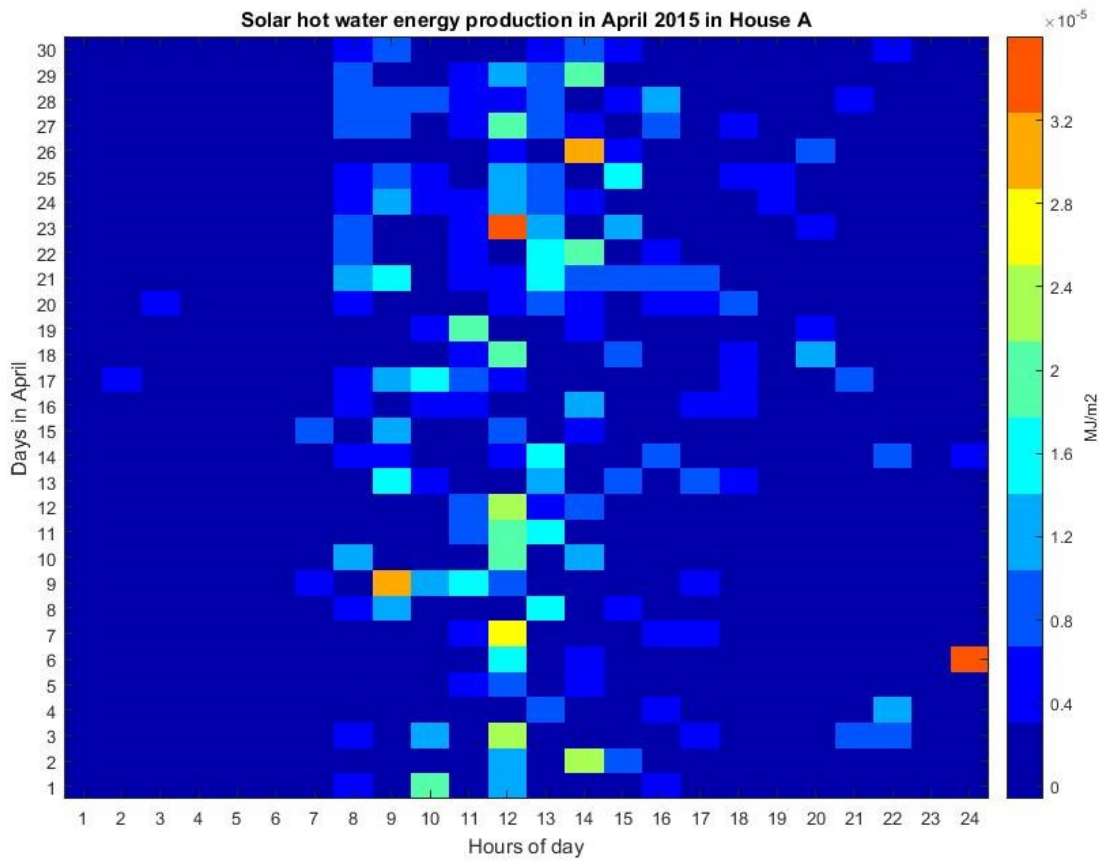
Figure B. 4: Hourly solar hot water energy production in House A in April 2015

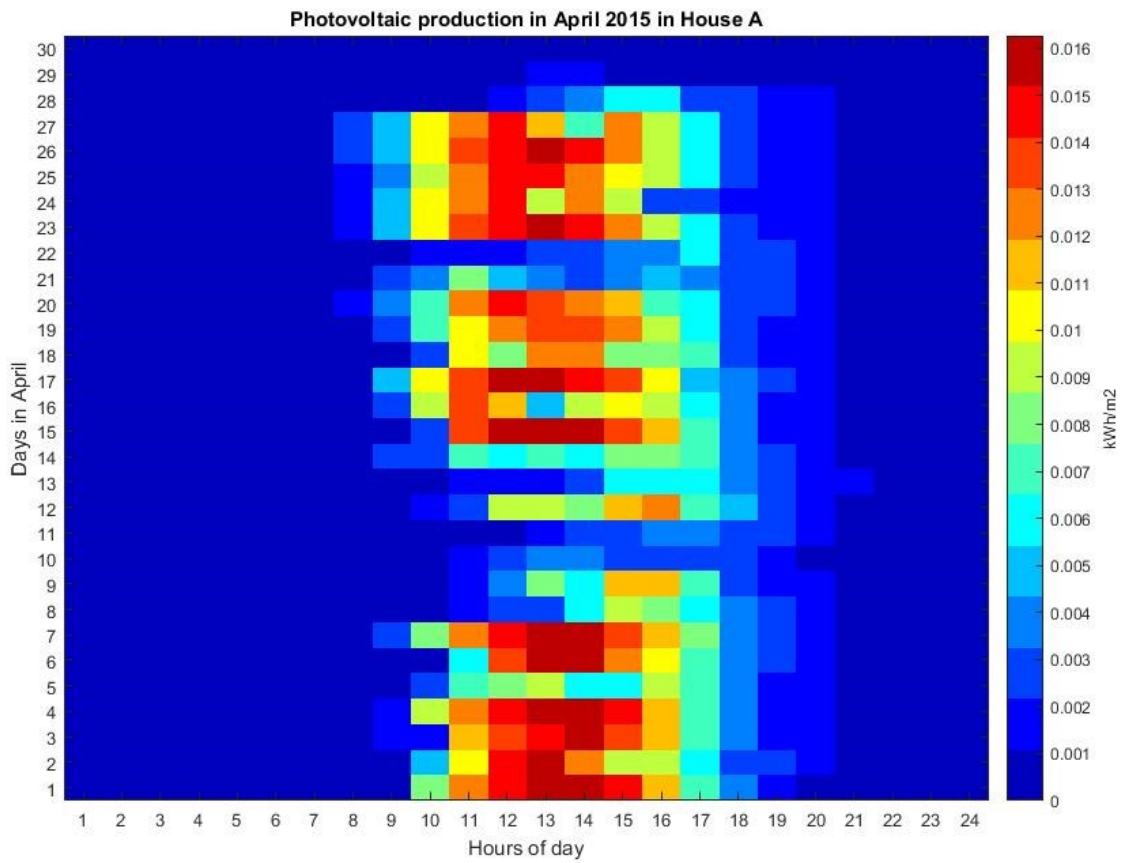In April, solar hot water energy production starts roughly at 8 P.M till 5 P.M which the maximum production is between 12 and 1 P.M.

Figure B. 5: Hourly photovoltaic production in House A in April 2015

Photovoltaic production in April 2015 is mostly between 10 A.M to 5 P.M, which between 1 and 2 P.M is the pick point.
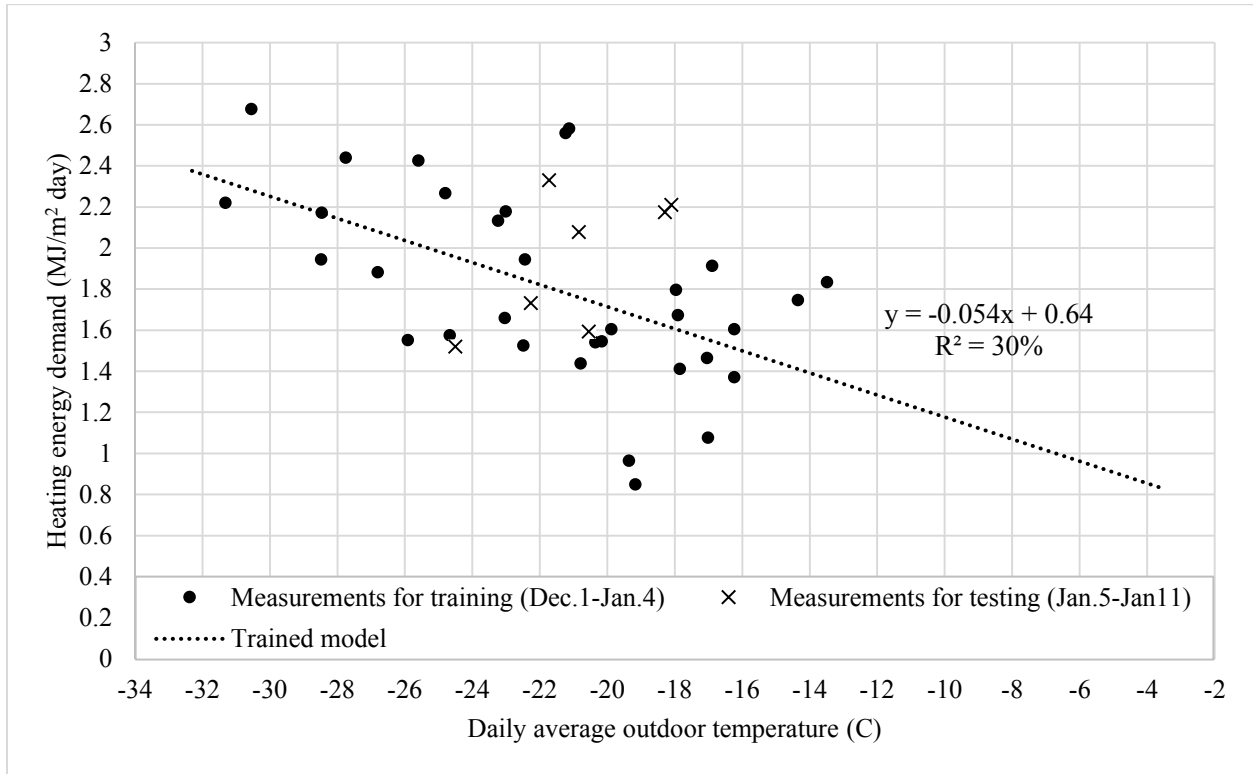
Figure C. 1: Daily signature of space heating energy demand as a benchmarking model of house A with augmented window technique from five weeks data set of Dec.1, 2014 to Jan.4, 2015
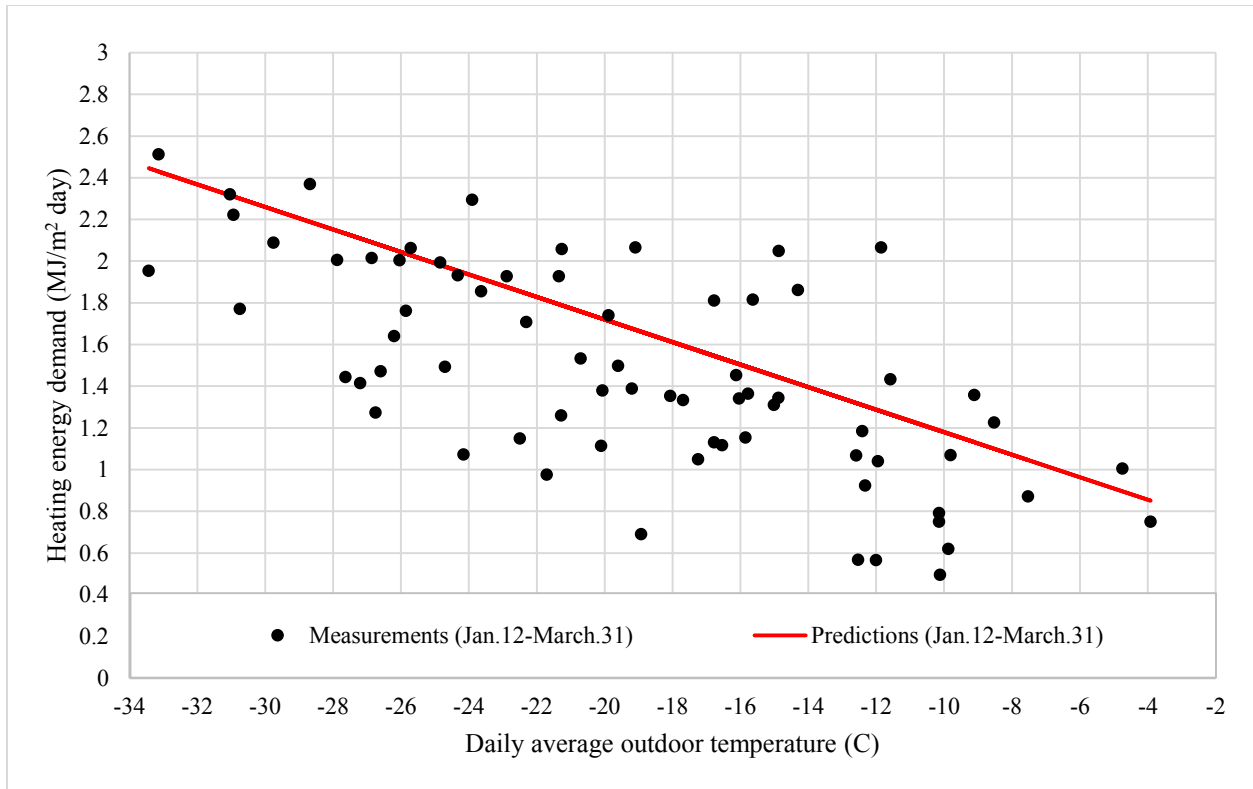
Figure C. 2: Predictions of the daily heating energy demand of house A using five weeks training data set with augmented window technique, and measurements from Jan.12 to March 31, 2015

Table C. 1: Coefficients of the benchmarking model using augmented window technique with five weeks training data set, and statistical indices of differences between the measurements and models forecasts of daily heating energy demand in house A

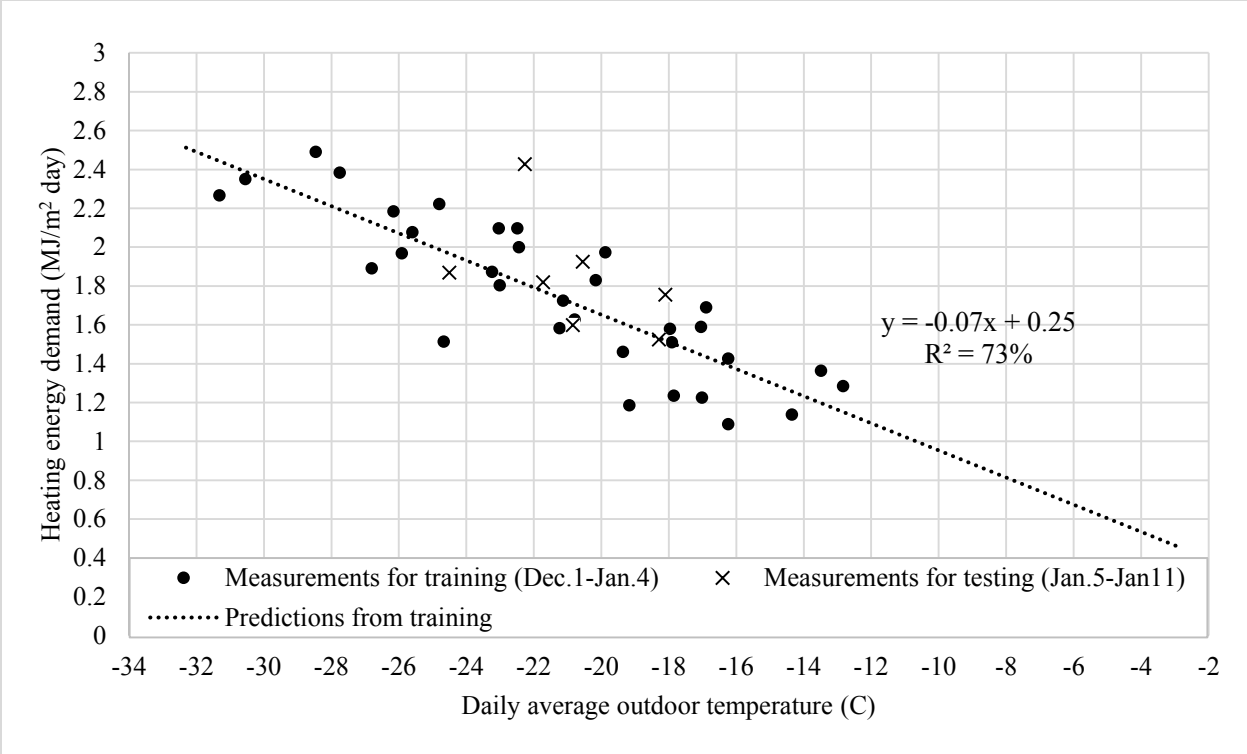| Period	Training period			Testing and prediction periods	
	a (MJ/m^2 °C day)	b (MJ/m^{2}day)	R^2 (%)	RMSE (MJ/m^2 day)	CV(RMSE) (%)
Dec.1-Jan.4 (Training)				-	-
Jan.5-Jan.11 (Testing)	-0.054	0.64	30	0.46	23
Jan.12-March.31 (Prediction)				0.4	27

Figure C. 3: Daily signature of space heating energy demand as a benchmarking model of house

B with augmented window technique from five weeks data set of Dec.1, 2014 to Jan.4, 2015
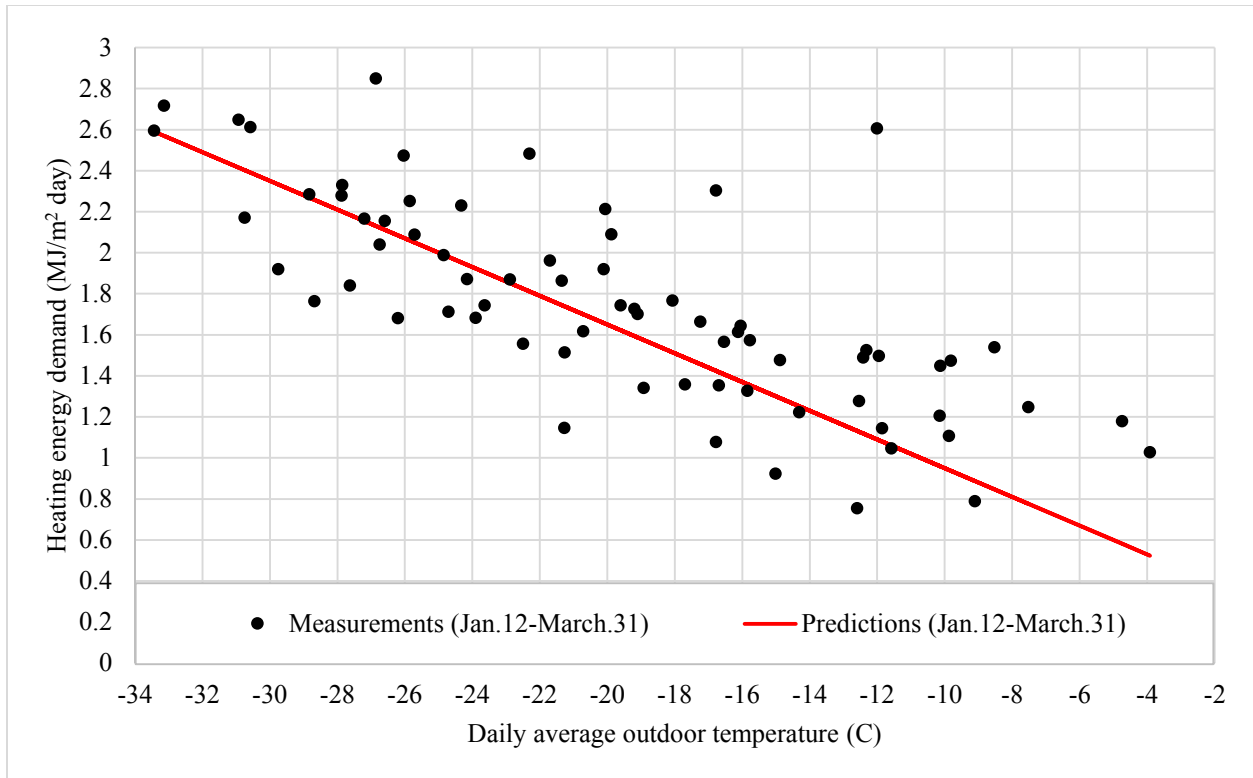
Figure C. 4: Predictions of the daily heating energy demand of house B using five weeks training data set with augmented window technique, and measurements from Jan.12 to March.31, 2015

Table C. 2: Coefficients of the benchmarking model using augmented window technique with five weeks training data set, and statistical indices of differences between the measurements and models forecasts of daily heating energy demand in house B

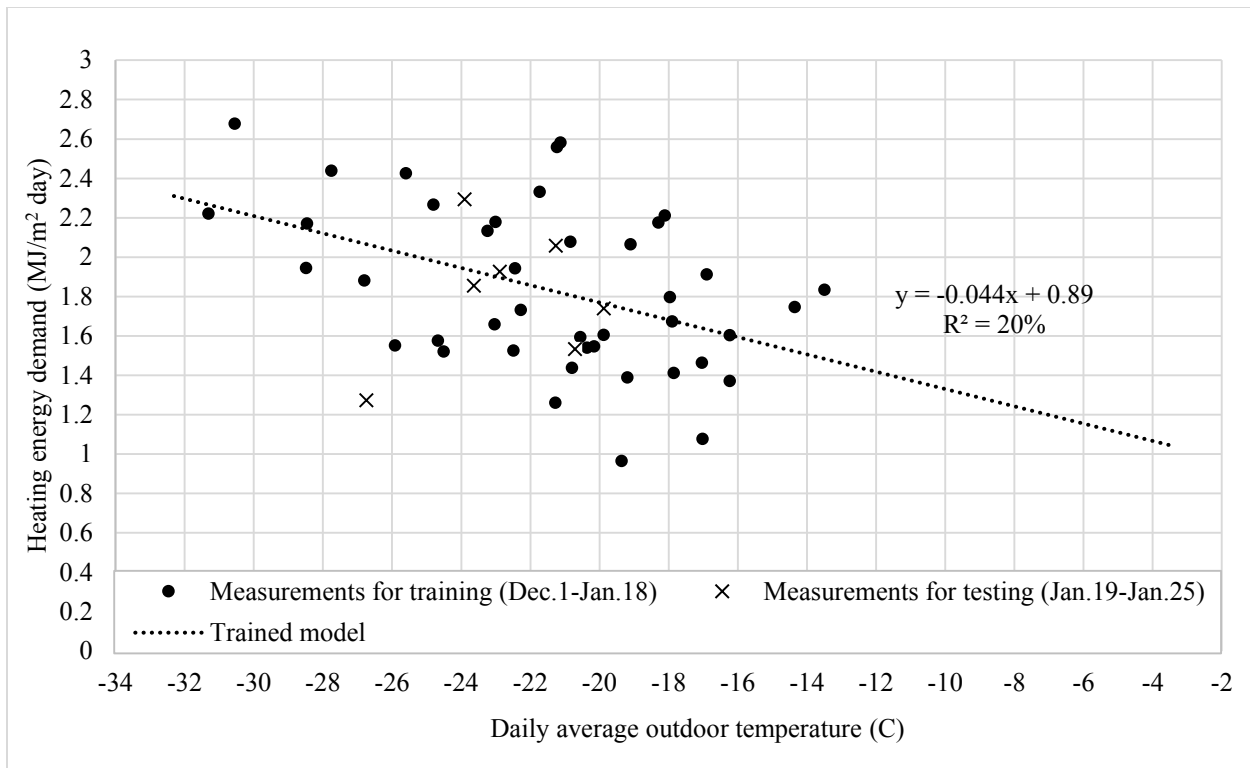| Period	Training period			Testing and prediction periods	
	a (MJ/m^2 °C day)	b (MJ/m^2 day)	R^2 (%)	RMSE (MJ/m^{2}day)	CV(RMSE) (%)
Dec.1-Jan.4 (Training)				-	-
Jan.5-Jan.11 (Testing)	-0.07	0.25	73	0.29	16
Jan.12-March.31 (Prediction)				0.37	21

Figure C. 5: Daily signature of space heating energy demand as a benchmarking model of house A with augmented window technique from seven weeks data set of Dec.1, 2014 to Jan.18, 2015
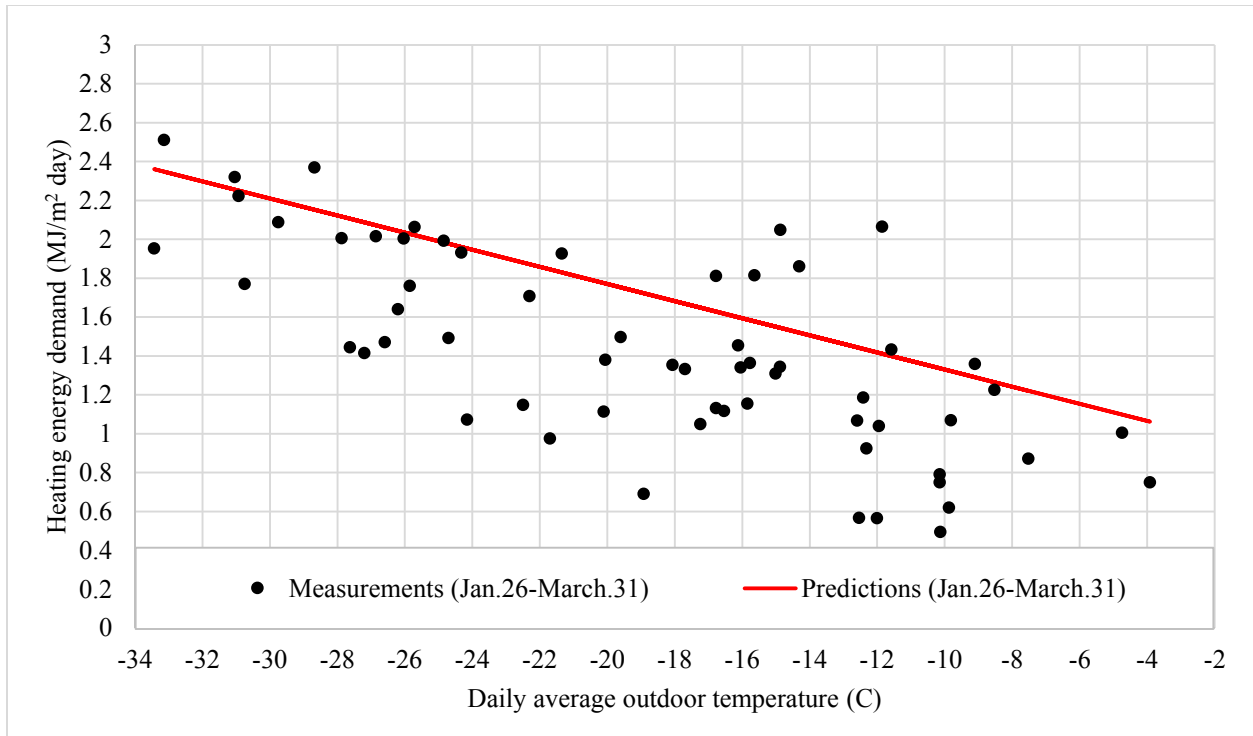
Figure C. 6: Predictions of the daily heating energy demand of house A using seven weeks training data set with augmented window technique, and measurements from Jan.26 to March.31, 2015

Table C. 3: Coefficients of the benchmarking model using augmented window technique with seven weeks training data set, and statistical indices of differences between the measurements and models forecasts of daily heating energy demand in house A

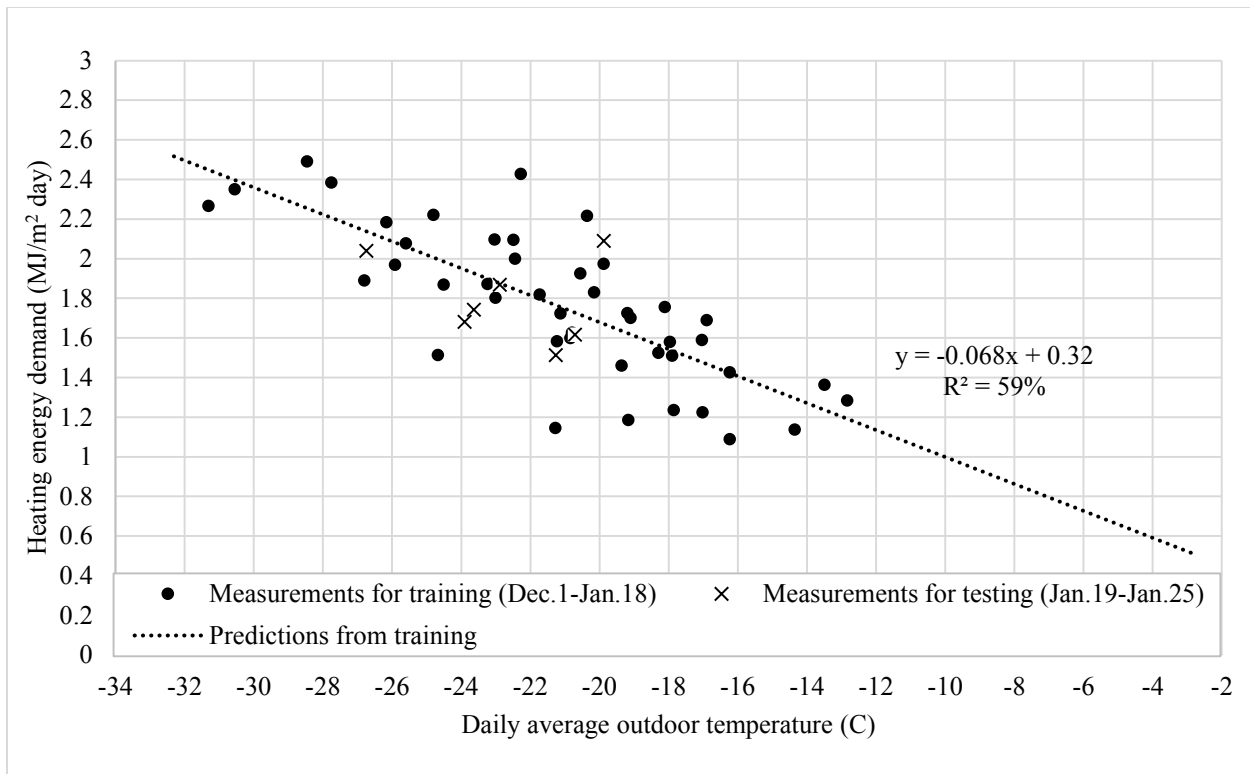| Period	Training period			Testing and prediction periods	
	a (MJ/m² °C day)	b (MJ/m²day)	R² (%)	RMSE (MJ/m² day)	CV(RMSE) (%)
Dec.1-Jan.18 (Training)				-	-
Jan.19-Jan.25 (Testing)	-0.044	0.89	20	0.38	21
Jan.26-March.31 (Prediction)				0.46	32

Figure C. 7: Daily signature of space heating energy demand as a benchmarking model of house B with augmented window technique from seven weeks data set of Dec.1, 2014 to Jan.18, 2015
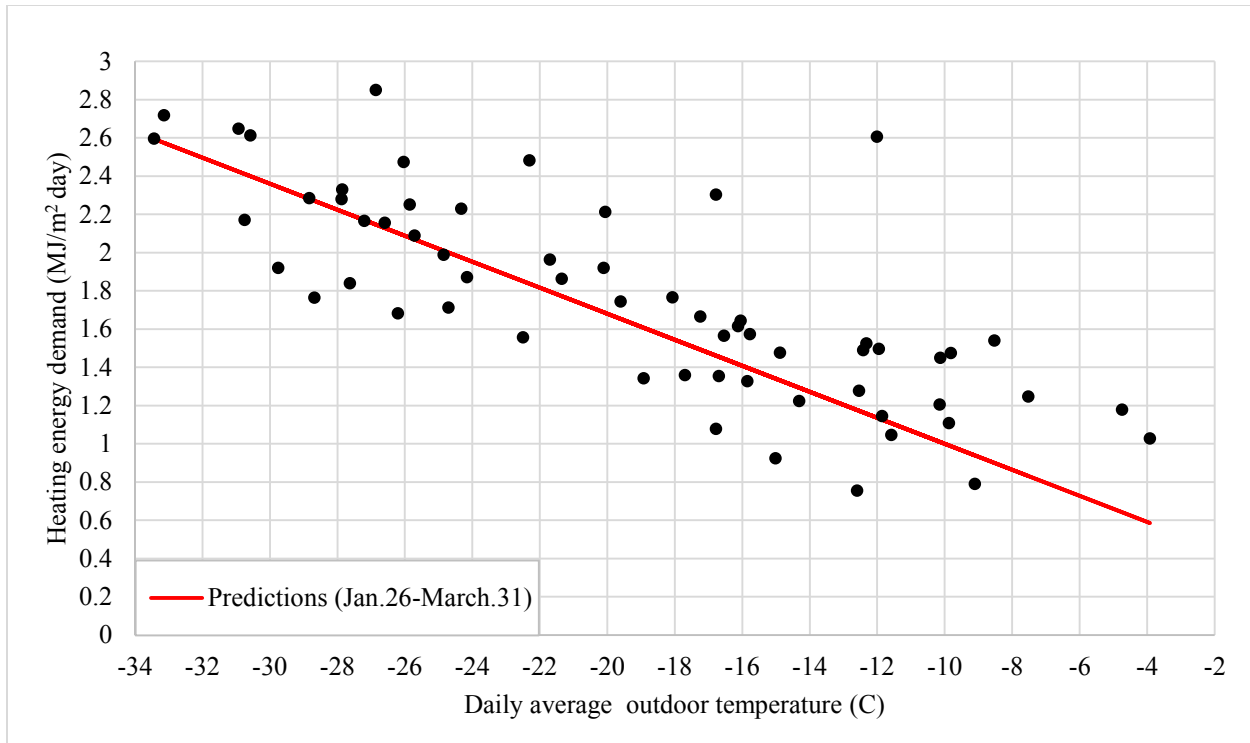
Figure C. 8: Predictions of the daily heating energy demand of house B using seven weeks training data set with augmented window technique, and measurements from Jan.26 to March.31, 2015

Table C. 4: Coefficients of the benchmarking model using augmented window technique with five weeks training data set, and statistical indices of differences between the measurements and models forecasts of daily heating energy demand in house B

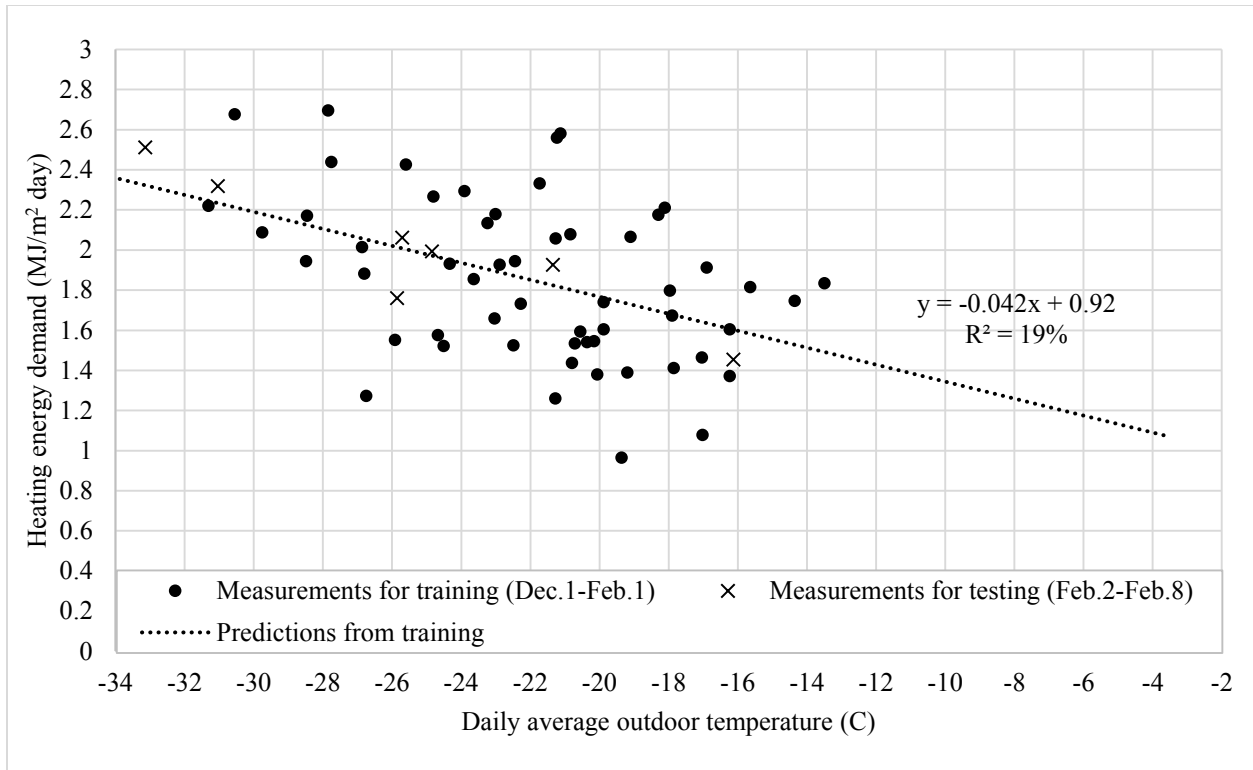| Period	Training period			Testing and prediction periods	
	a (MJ/m^2 °C day)	b (MJ/m^{2}day)	R^2 (%)	RMSE (MJ/m^2 day)	CV(RMSE) (%)
Dec.1-Jan.18 (Training)				-	-
Jan.19-Jan.25 (Testing)	-0.068	0.32	59	0.25	14
Jan.26-March.31 (Prediction)				0.37	21

Figure C. 9: Daily signature of space heating energy demand as a benchmarking model of house A with augmented window technique from nine weeks data set of Dec.1, 2014 to Feb.1, 2015
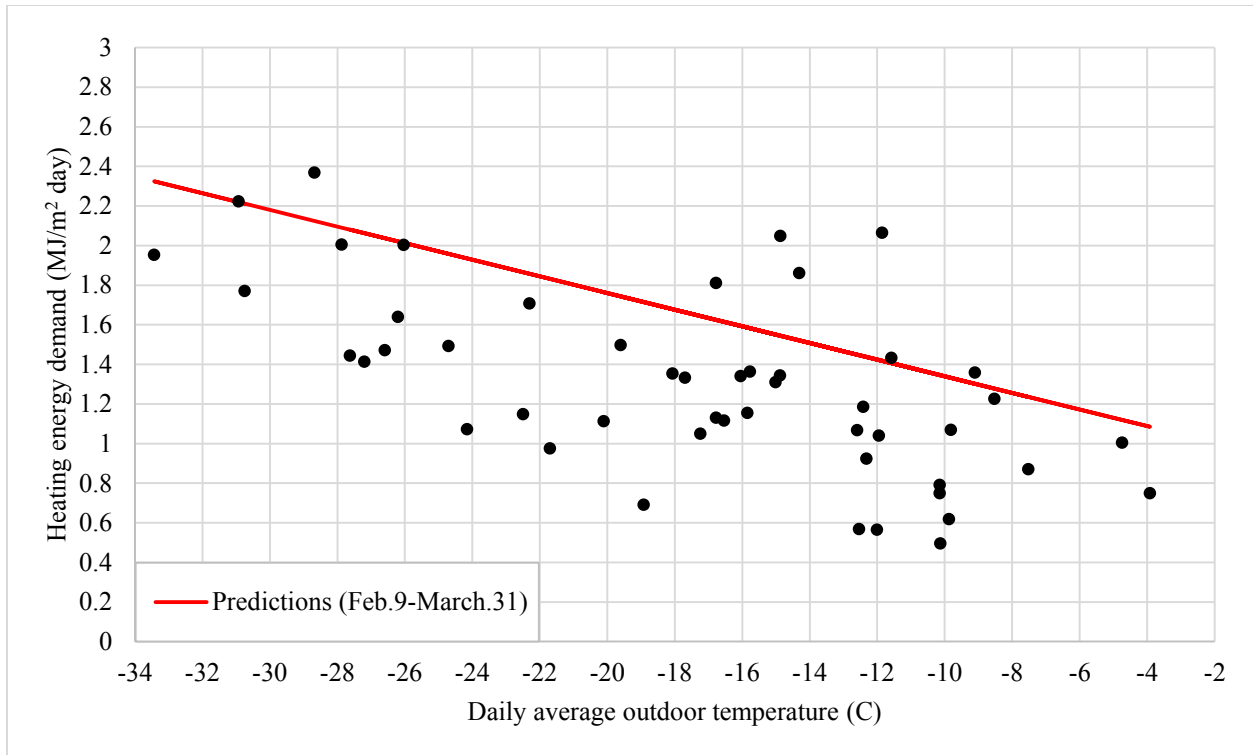
Figure C. 10: Predictions of the daily heating energy demand of house A using nine weeks training data set with augmented window technique, and measurements from Feb.9 to March.31, 2015

Table C. 5: Coefficients of the benchmarking model using augmented window technique with nine weeks training data set, and statistical indices of differences between the measurements and models forecasts of daily heating energy demand in house A

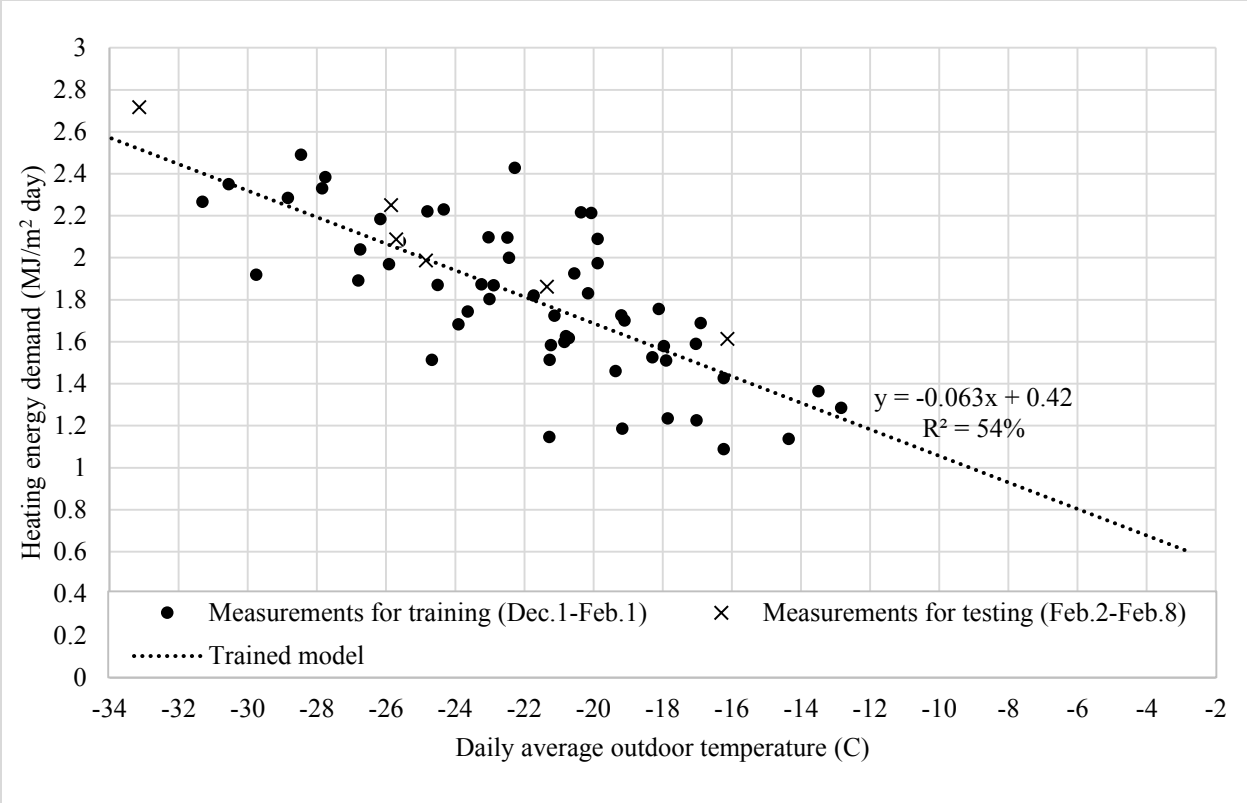| Period	Training period			Testing and prediction periods	
	a (MJ/m² °C day)	b (MJ/m²day)	R^2 (%)	RMSE (MJ/m² day)	CV(RMSE) (%)
Dec.1-Feb.1 (Training)				-	-
Feb.2-Feb.8 (Testing)	-0.042	0.92	19	0.16	8
Feb.9-March.31 (Prediction)				0.5	38

Figure C. 11: Daily signature of space heating energy demand as a benchmarking model of house B with augmented window technique from nine weeks data set of Dec.1, 2014 to Feb.1, 2015
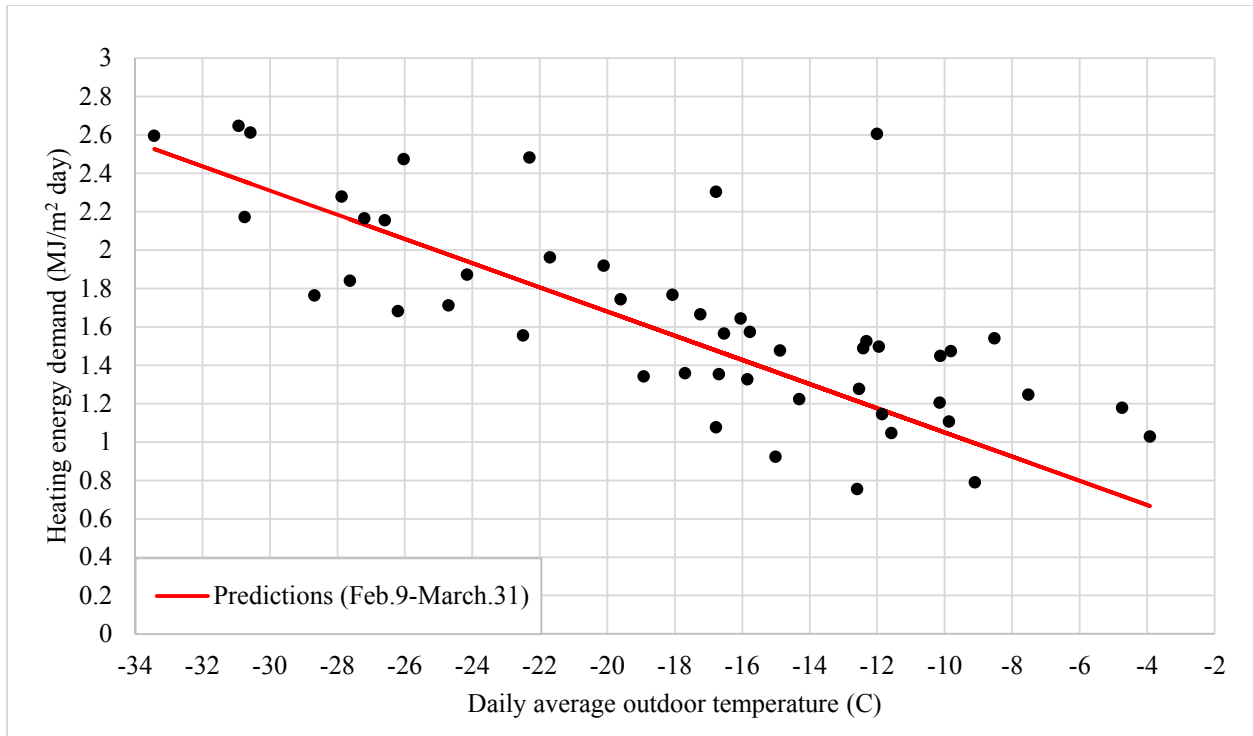
Figure C. 12: Predictions of the daily heating energy demand of house B using nine weeks training data set with augmented window technique, and measurements from Feb.9 to March.31, 2015

Table C. 6: Coefficients of the benchmarking model using augmented window technique with nine weeks training data set, and statistical indices of differences between the measurements and models forecasts of daily heating energy demand in house B

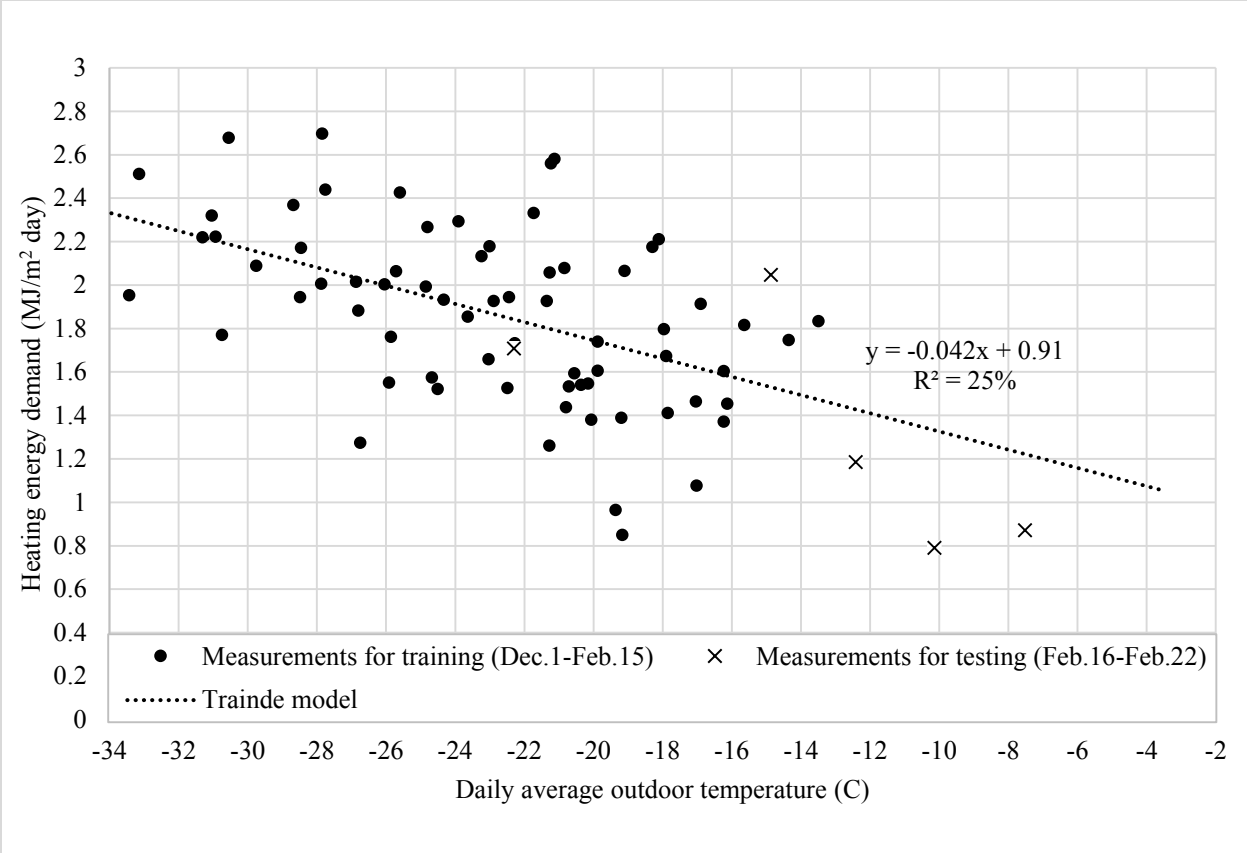| Period	Training period			Testing and prediction periods	
	a (MJ/m² °C day)	b (MJ/m²day)	R² (%)	RMSE (MJ/m² day)	CV(RMSE) (%)
Dec.1-Feb.1 (Training)				-	-
Feb.2-Feb.8 (Testing)	-0.063	0.42	54	0.16	8
Feb.9-March.31 (Prediction)				0.37	23

Figure C. 13: Daily signature of space heating energy demand as a benchmarking model of house A with augmented window technique from eleven weeks data set of Dec.1, 2014 to Feb.15, 2015
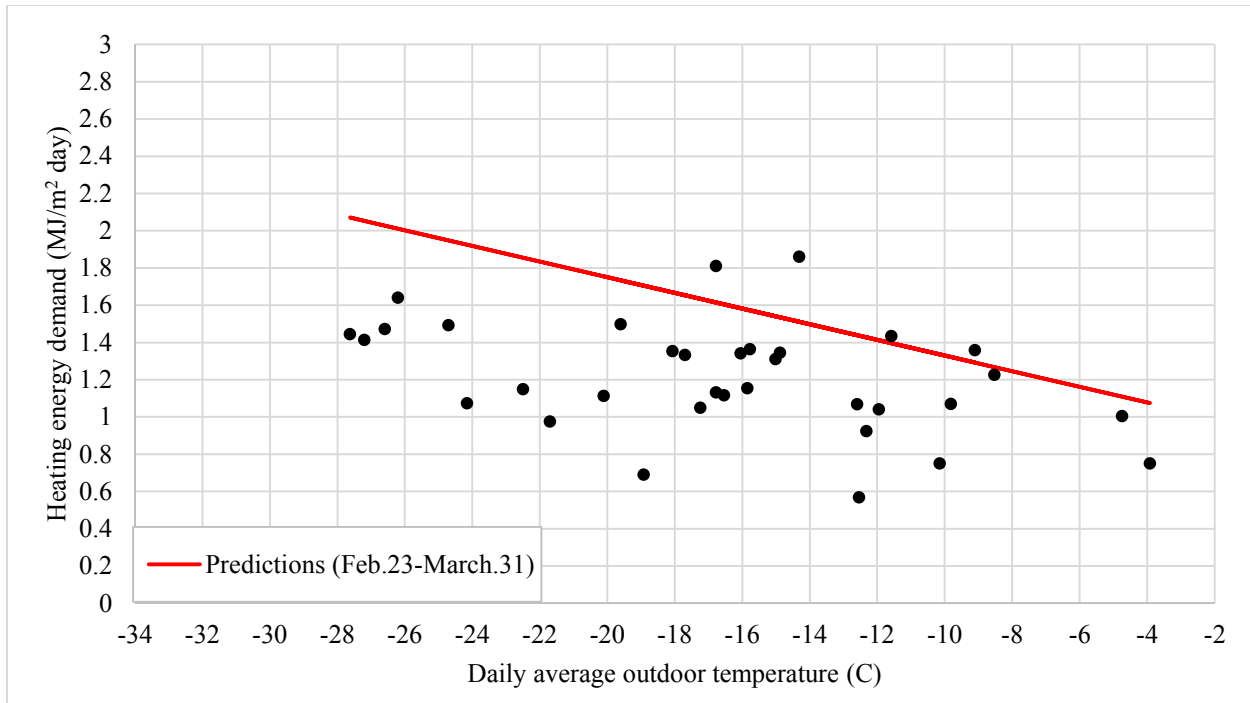
Figure C. 14: Predictions of the daily heating energy demand of house A using eleven weeks training data set with augmented window technique, and measurements from Feb.23 to March.31, 2015

Table C. 7: Coefficients of the benchmarking model using augmented window technique with eleven weeks training data set, and statistical indices of differences between the measurements and models forecasts of daily heating energy demand in house A

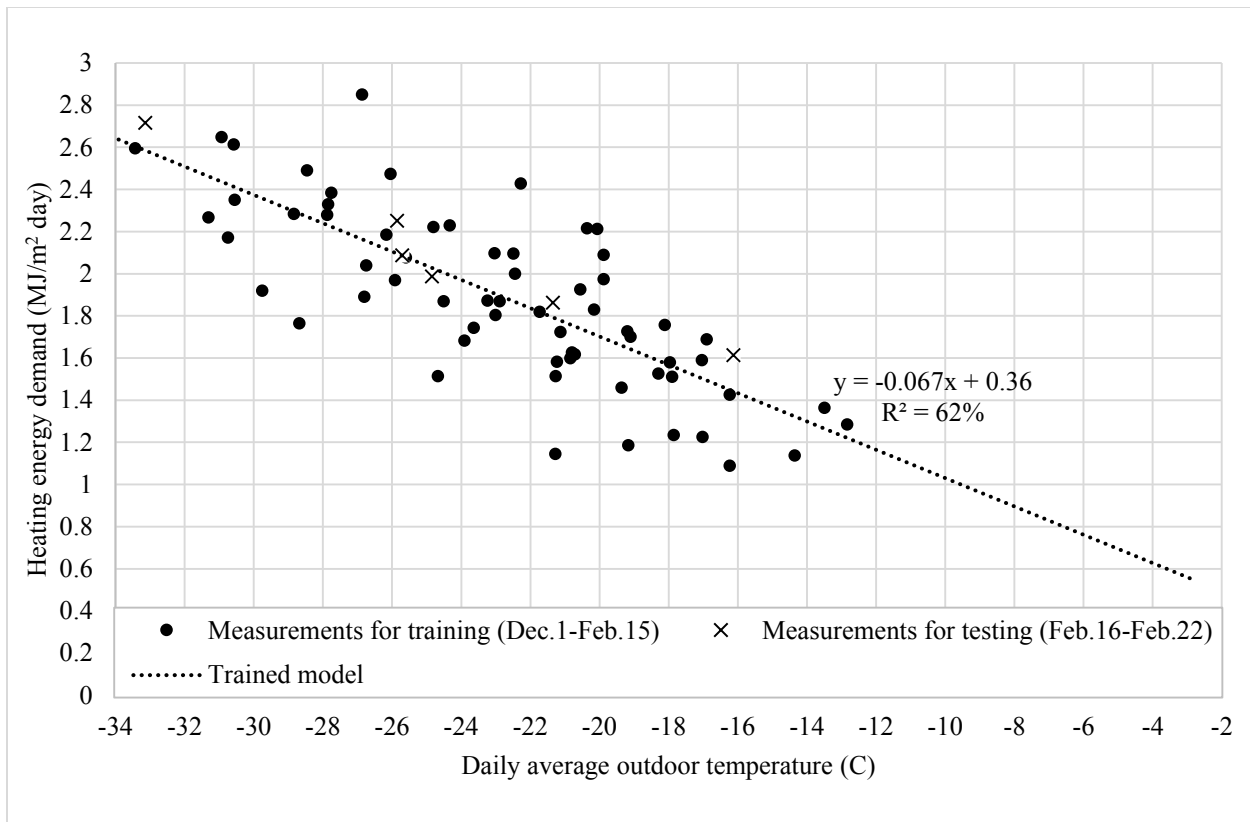| Period	Training period			Testing and prediction periods	
	a (MJ/m^2 ºC day)	b (MJ/m^{2}day)	R^2 (%)	RMSE (MJ/m^2 day)	CV(RMSE) (%)
Dec.1-Feb.15 (Training)	-0.042	0.91	25	-	-
Feb.16-Feb.22 (Testing)				0.44	33
Feb.23-March.31 (Prediction)				0.5	41

Figure C. 15: Daily signature of space heating energy demand as a benchmarking model of house B with augmented window technique from eleven weeks data set of Dec.1, 2014 to Feb.15, 2015
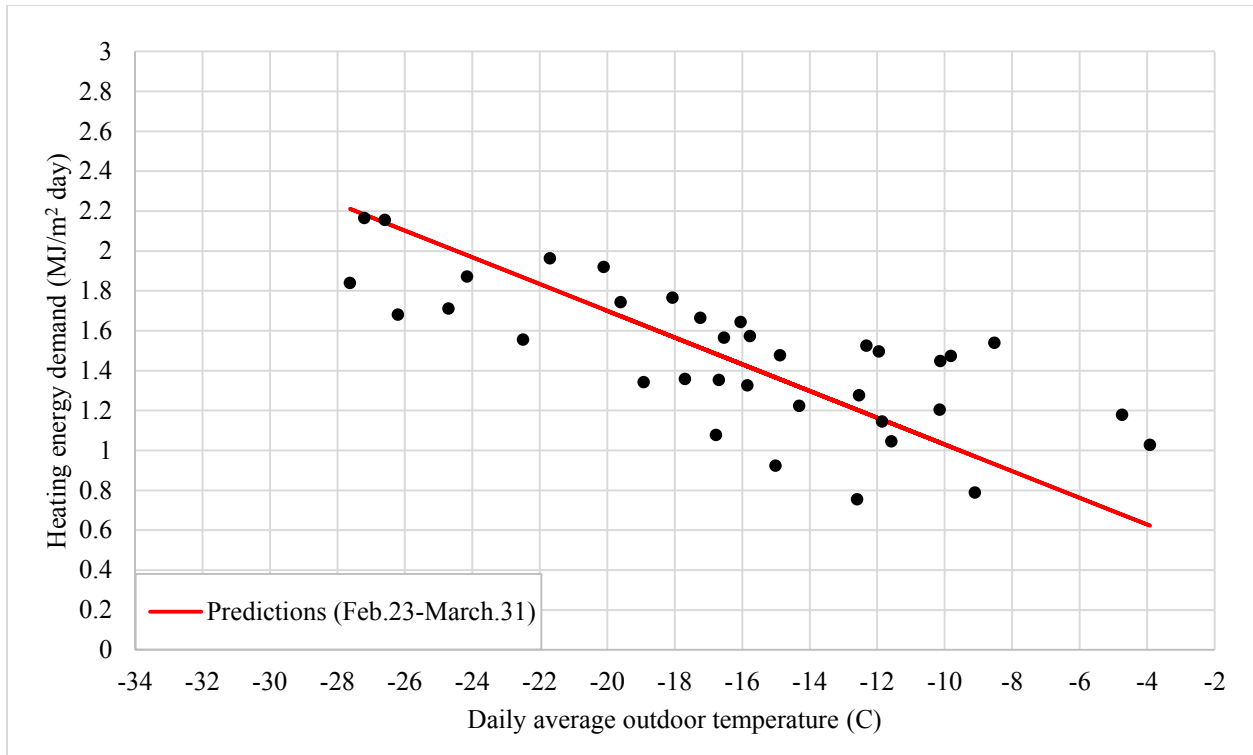
Figure C. 16: Predictions of the daily heating energy demand of house B using eleven weeks training data set with augmented window technique, and measurements from Feb.23 to March.31, 2015

Table C. 8: Coefficients of the benchmarking model using augmented window technique with eleven weeks training data set, and statistical indices of differences between the measurements and models forecasts of daily heating energy demand in house B

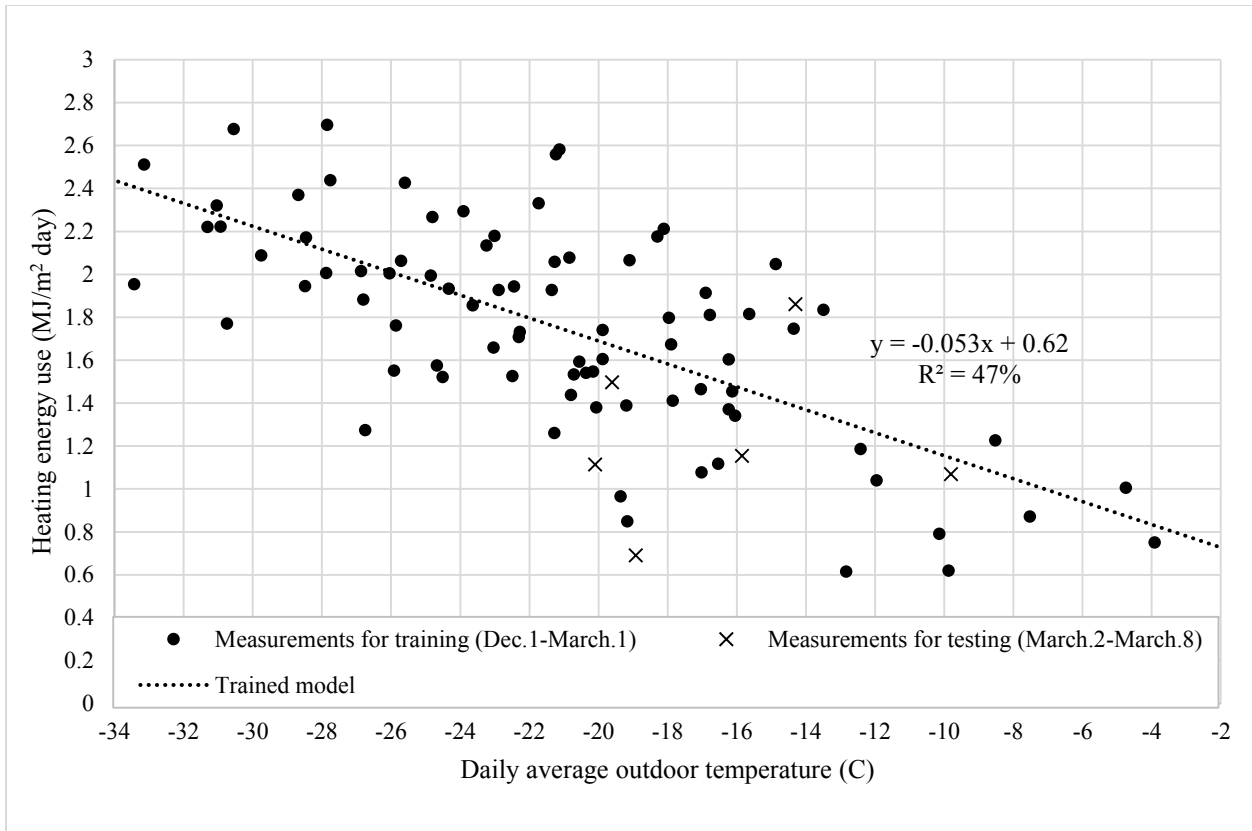|	Training period			Testing and prediction periods	
Period	a (MJ/m² °C day)	b (MJ/m²day)	R^2 (%)	RMSE (MJ/m² day)	CV(RMSE) (%)
Dec.1-Feb.15 (Training)				-	-
Feb.16-Feb.22 (Testing)	-0.067	0.36	62	0.82	46
Feb.23-March.31 (Prediction)				0.29	20

$y = -0.053x + 0.62$
$R^2 = 47\%$

Figure C. 17: Daily signature of space heating energy demand as a benchmarking model of house A with augmented window technique from eleven weeks data set of Dec.1, 2014 to March.1, 2015
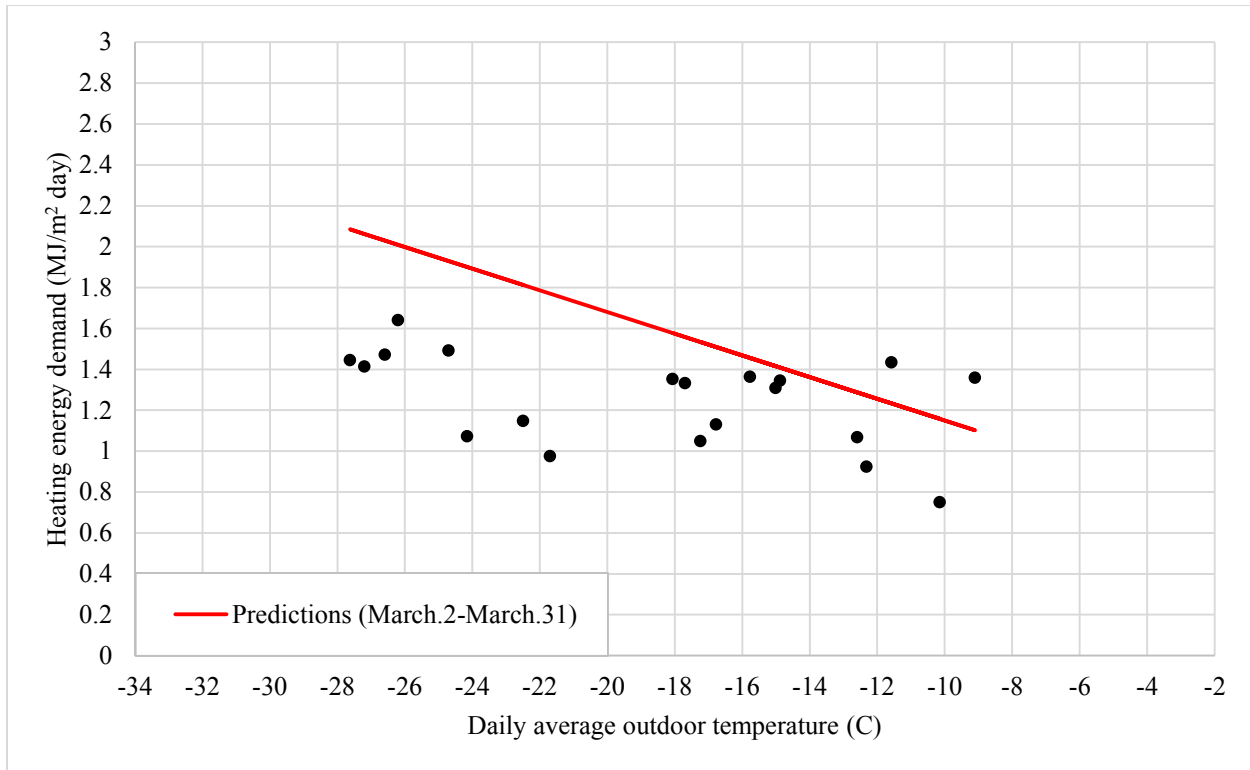
Figure C. 18: Predictions of the daily heating energy demand of house A using thirteen weeks training data set with augmented window technique, and measurements from March 2 to March 31, 2015

Table C. 9: Coefficients of the benchmarking model using augmented window technique with thirteen weeks training data set, and statistical indices of differences between the measurements and models forecasts of daily heating energy demand in house A

Period	Training period			Testing and prediction periods	
	a (MJ/m^2 ^{o}C day)	b (MJ/m^{2}day)	R^2 (%)	RMSE (MJ/m^2 day)	CV(RMSE) (%)
Dec 1-March 1 (Training)				-	-
March 2-8 (Testing)	-0.053	0.62	47	0.56	45
March 9-31 (prediction)				0.47	37

Chart showing y = -0.05x + 0.78, R² = 52%

Legend:
- Measurements for training (Dec.1-March.1)
- × Measurements for testing (March.2-March.8)
- .... Trained model

X-axis: Daily average outdoor temperature (C)
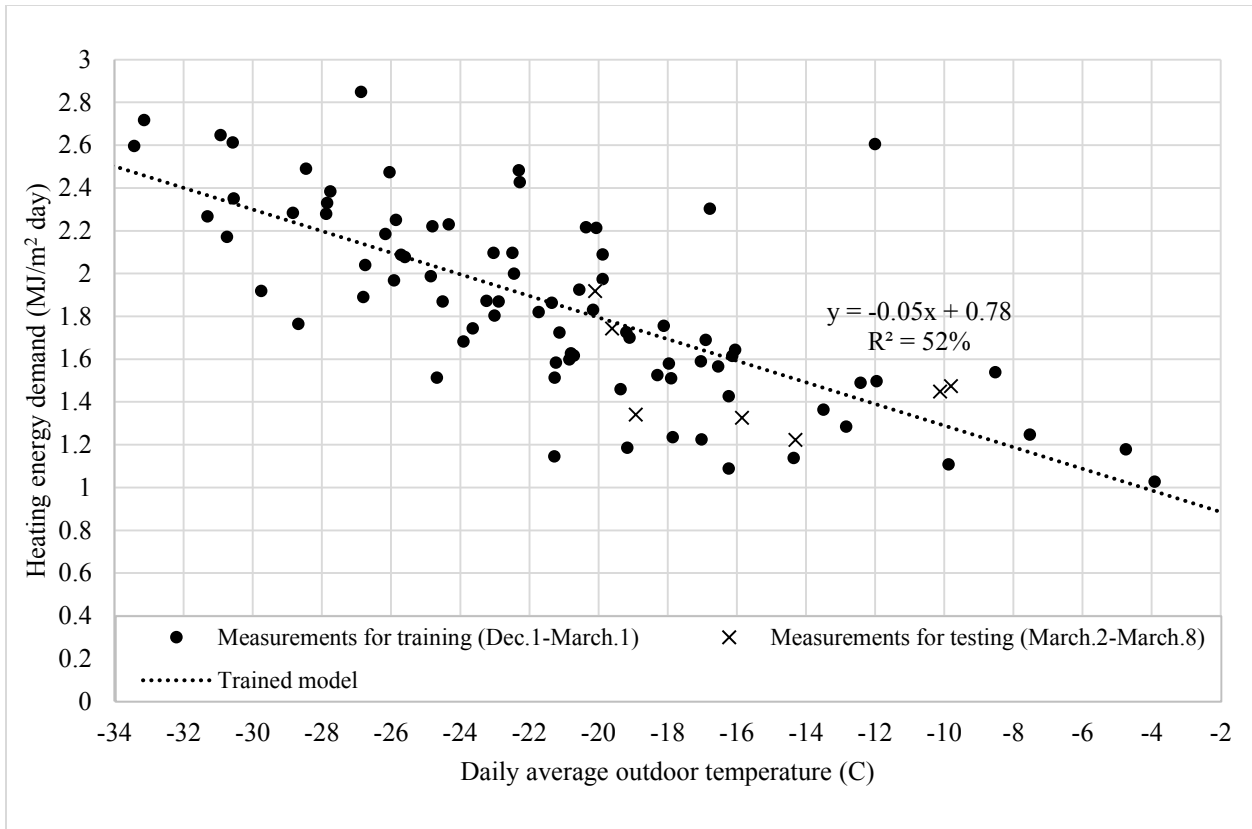Y-axis: Heating energy demand (MJ/m² day)

Figure C. 19: Daily signature of space heating energy demand as a benchmarking model of house B with augmented window technique from eleven weeks data set of Dec.1, 2014 to March.1, 2015
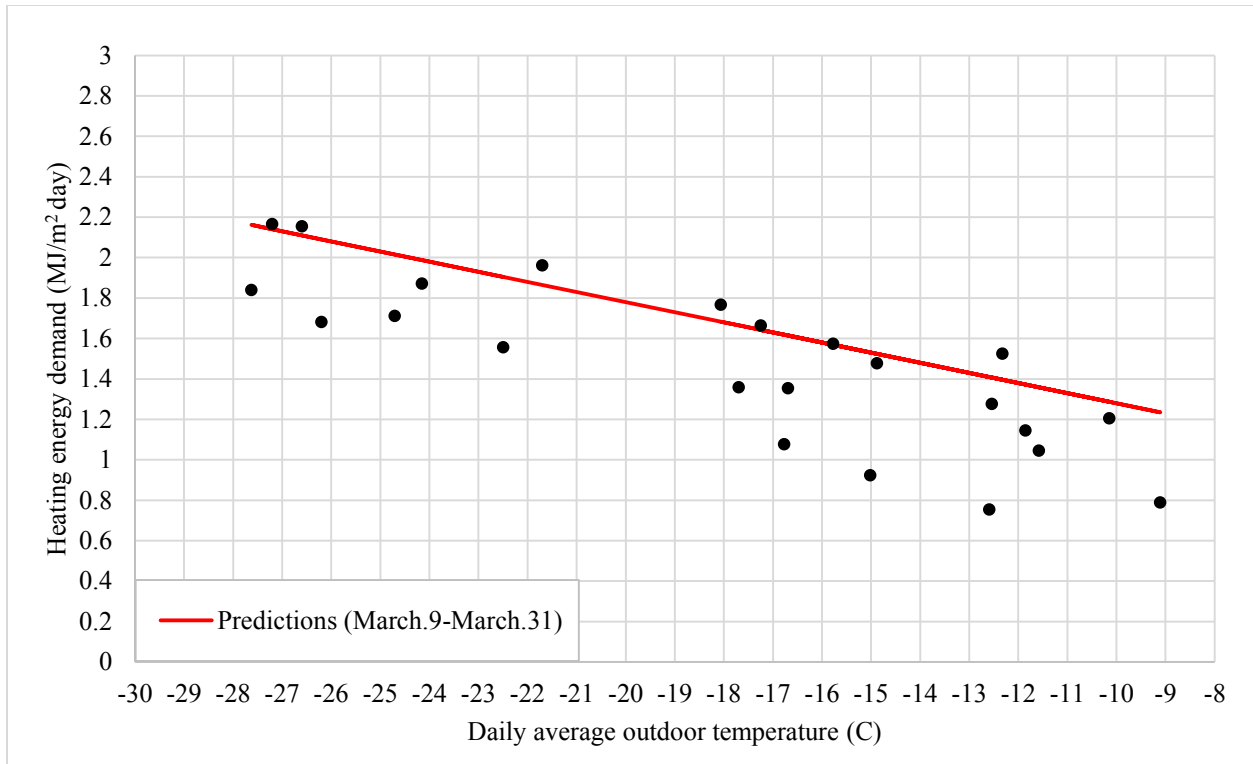
Figure C. 20: Predictions of the daily heating energy demand of house A using thirteen weeks training data set with augmented window technique, and measurements from March 2 to March 31, 2015

Table C. 10: Coefficients of the benchmarking model using augmented window technique with thirteen weeks training data set, and statistical indices of differences between the measurements and models forecasts of daily heating energy demand in house B

Period	Training period			Testing and prediction periods	
	a (MJ/m^2 °C day)	b (MJ/m^2 day)	R^2 (%)	RMSE (MJ/m^{2}day)	CV(RMSE) (%)
Dec 1-March 1 (Training)				-	-
March 2-8 (Testing)	-0.05	0.78	52	0.25	17
March 9-31 (prediction)				0.31	21